Helsinki University of Technology Control Engineering Laboratory

Espoo 2006 Report 150

FAULT DIAGNOSTICS AND VIBRATION CONTROL OF PAPER WINDERS

Timo Virtanen

TEKNILLINEN KORKEAKOULU
TEKNISKA HÖGSKOLAN
HELSINKI UNIVERSITY OF TECHNOLOGY
TECHNISCHE UNIVERSITÄT HELSINKI
UNIVERSITE DE TECHNOLOGIE D´HELSINKI

Helsinki University of Technology Control Engineering Laboratory

Espoo June 2006 Report 150

FAULT DIAGNOSTICS AND VIBRATION CONTROL OF PAPER WINDERS

Timo Virtanen

Dissertation for the degree of Doctor of Science in Technology to be presented with due permission of the Department of Automation and Systems Technology, for public examination and debate in Auditorium AS1 at Helsinki University of Technology (Espoo, Finland) on the 2nd of December, 2006, at 12 noon.

Helsinki University of Technology

Department of Automation and Systems Technology

Control Engineering Laboratory

Distribution:
Helsinki University of Technology
Control Engineering Laboratory
P.O. Box 5500
FI-02015 HUT, Finland
Tel. +358-9-451 5201
Fax. +358-9-451 5208
E-mail: control.engineering@tkk.fi
http://www.control.tkk.fi/

ISBN-13 978-951-22- 8467-2 (printed)
ISBN-10 951-22-8467-7 (printed)
ISBN-13 978-951-22- 8468-9 (pdf)
ISBN-10 951-22- 8468-5 (pdf)
ISSN 0356-0872

Picaset Oy
Helsinki 2006

Available on net at http://lib.tkk.fi/Diss/2006/isbn9512284685

HELSINKI UNIVERSITY OF TECHNOLOGY P. O. BOX 1000, FI-02015 TKK http://www.tkk.fi	ABSTRACT OF DOCTORAL DISSERTATION

Author Timo Virtanen

Name of the dissertation

Fault Diagnostics and Vibration Control of Paper Winders

Date of manuscript June 16, 2006	Date of the dissertation December 2, 2006

☒ Monograph ☐ Article dissertation (summary + original articles)

Department	Automation and Systems Technology
Laboratory	Control Engineering Laboratory
Field of research	Control Engineering
Opponent(s)	Professor Okyay Kaynak, Professor Urpo Kortela
Supervisor	Professor Heikki Koivo, AS-74
(Instructor)	Dr. Kai Zenger, AS-74

Abstract

A Level-to-Level Minimization (LLM) algorithm based on Boolean algebra was developed and compared to the Quine-McCluskey algorithm based on the manipulation of truth tables of logic functions. The minimization with Boolean laws can save much computing time and memory with certain types of logic functions when compared to the methods based on truth tables. A Multilevel Product-Of-Sums net model is introduced as well. A practical example demonstrates the use of the methods in the paper winders.

Two different case studies of model-based fault diagnostics are introduced. The first deals with tension control of a paper web and the latter the hydraulic force control of a rider roll. A very detailed simulation model of a rider roll is used to examine the effects of various types of faults in a hydraulic system.

The theories of the delayed resonators and active resonator absorbers were further developed. The new methods make it possible to control both resonance frequency and damping factor. A cascade-controlled delayed resonator was also developed to broaden the operating range of actively controlled mass dampers. Stability issues were considered as well. An active damping application based on a hydraulic actuator was also developed. This method was tested with a full-scale pilot winder.

Keywords	fault diagnostics, vibration control, paper winding, PLC, Boolean algebra		
ISBN (printed)	951-22-8467-7	ISSN (printed)	0356-0872
ISBN (pdf)	951-22-8468-5	ISSN (pdf)	
ISBN (others)		Number of pages	135
Publisher	Helsinki University of Technology, Control Engineering Laboratory		
Print distribution	Helsinki University of Technology, Control Engineering Laboratory		

☒ The dissertation can be read at http://lib.tkk.fi/Diss/

TEKNILLINEN KORKEAKOULU PL 1000, 02015 TKK http://www.tkk.fi	VÄITÖSKIRJAN TIIVISTELMÄ

Tekijä Timo Virtanen

Väitöskirjan nimi
Pituusleikkurin vikadiagnostiikka ja värähtelyn säätö.

Käsikirjoituksen jättämispäivämäärä 16.6.2006	Väitöstilaisuuden ajankohta 2.12.2006
☒ Monografia	☐ Yhdistelmäväitöskirja (yhteenveto + erillisartikkelit)

Osasto	Automaatio- ja systeemitekniikan osasto
Laboratorio	Systeemitekniikan laboratorio
Tutkimusala	Systeemitekniikka
Vastaväittäjä(t)	Professori Okyay Kaynak, Professori Urpo Kortela
Työn valvoja	Professori Heikki Koivo, AS-74
(Työn ohjaaja)	TkT Kai Zenger, AS-74

Tiivistelmä

Työssä kehitettiin Boolen algebraan perustuva Level-to-Level-Minimization (LLM) algoritmi loogisten funktioiden muuntamiseksi tarkoituksenmukaiseen muotoon vikadiagnostiikkaa varten. Algoritmia verrataan Quine-McCluskey algoritmiin, joka on perinteinen totuustaulun käsittelyyn perustuva menetelmä. Työssä osoitetaan, että tietyntyyppisillä loogisilla funktioilla LLM-menetelmä säästää tietokoneen muistia ja laskenta-aikaa totuustauluun perustuvaan menetelmään verrattuna. Lisäksi esitetään vikadiagnostiikkajärjestelmän rakennetta kuvaava Multilevel-Product-Of-Sums net (MPOS net) -malli. Menetelmän käyttöä pituusleikkurin vikadiagnostiikassa havainnollistetaan käytännön esimerkein.

Analogisten signaalien vikadiagnostiikkaa koskevassa osassa esitetään kaksi mallipohjaiseen vikadiagnostiikkaan perustuvaa menetelmää. Ensimmäinen käsittelee pituusleikkurin rainan kireyden säädön ja jälkimmäinen painotelan hydraulista voimasäädön valvontaa. Jälkimmäinen menetelmä verifioitiin yksityiskohtaisen painotelan simulointimallin avulla.

Työn toisessa, värähtelyn säätöä koskevassa osassa viivästettyyn resonaattoriin ja muihin aktiivisiin massavaimentimiin perustuvaa olemassa olevaa teoriaa kehitetään edelleen. Uudet menetelmät tekevät mahdolliseksi säätää vaimentimen ominaistaajuutta ja vaimennusta toisistaan riippumatta. Kaskadisäätöön perustuvalla menetelmällä pystytään taas laajentamaan vaimentimen toiminta-aluetta ja robustisuutta. Työ sisältää myös eri menetelmien stabilisuustarkasteluja. Hydraulisylinteriin perustuva aktiivivaimennusmenetelmä esitetään ja verifioidaan täysimittaisella pilot-pituusleikkurilla tehdyin kokein.

Asiasanat vikadiagnostiikka, tärinän säätö, pituusleikkuri, PLC, Boolean algebra

ISBN (painettu) 951-22-8467-7	ISSN (painettu) 0356-0872
ISBN (pdf) 951-22-8468-5	ISSN (pdf)
ISBN (muut)	Sivumäärä 135

Julkaisija Teknillinen korkeakoulu, systeemitekniikan laboratorio

Painetun väitöskirjan jakelu Teknillinen korkeakoulu, systeemitekniikan laboratorio

☒ Luettavissa verkossa osoitteessa http://lib.tkk.fi/Diss/

Preface

This thesis was carried out at Metso Paper in Järvenpää and at the Control Engineering Laboratory, Helsinki University of Technology, with Professor Heikki Koivo as supervisor. I would like to thank him for his valuable guidance during this work. I would also like to thank Dr. Kai Zenger for all the effort he put into this project. Luckily he is a better instructor than runner. Professor Antti Niemi is also acknowledged for encouraging me to start my postgraduate studies in the 90s. I would also like to thank all my former colleagues and good friends at the Control Engineering Laboratory. Professor Erno Keskinen, Professor Juha Miettinen, Pekka Salmenperä and Ville Järvinen from Tampere University of Technology are also acknowledged for their support during this project.

I would like to thank the Metso Academy, as well as Pauli Koutonen and Kenneth Åkerlund from Metso Paper for financially supporting this thesis. Pauli Koutonen also encouraged me to apply to join the Metso Academy.

My colleagues in Metso Paper, Dr. Jari Paanasalo and Dr. Marko Jorkama, are gratefully acknowledged for their support and our numerous discussions. Other colleagues who I would like to thank for their help during these years are Timo Åhman and Pertti Pulkkinen, regarding the fault diagnostics of binary signals, and Tuomas Ratilainen, for his co-operation with me in the research into hydraulic active damping methods. I would also like to thank all my other friends and colleagues in Metso Paper who supported me during this work.

I would also like to thank my parents, Pirkko and Veikko, for their support, especially during my school and academic years.

Finally, I would like to thank my family, Sirpa, Tytti, Tommi, and Hippi for their support and encouragement during this project.

Espoo, June 2006

Timo Virtanen

Symbols and abbreviations

The main symbols and abbreviations used in the text are summarized below. The section where they appeared for the first time is also mentioned.

Symbols

ω_0	Natural frequency	4.3
A_c	Effective area of piston side (piston area)	4.3
A_h	Effective area of rod side (piston area-rod area)	4.3
Vc	Total oil volume of piston side between valve and piston	4.3
Vk	Total oil volume of rod side between valve and piston	4.3
m	Mass	4.3
β	Bulk modulus of hydraulic oil	4.3
$\beta_{effective}$	Effective bulk modulus	4.3
β_l	Bulk modulus of hose	4.3
V_H	Oil volume in hose	4.3
F_C	Coulomb friction force	4.4
F_μ	Friction force	4.4
F_S	Static friction force	4.4
v	Signed speed	4.4
v_S	Stribeck velocity	4.4
F_v	Slope of viscous friction	4.4

δ_S	Factor that depends on the geometry of the application	4.4
g_c	Critical gain of delayed resonator	5.3.1
τ_c	Critical delay time of delayed resonator	5.3.1
ω_c	Critical (resonance) frequency of delayed resonator	5.3.1

abbreviations

MTBF	Mean Time Between Failures	1
MTTR	Mean Time To Restoration	1
MTTF	Mean Time To Failure	1
FMS	Flexible Manufacturing System	1
LLM	Level-to-Level Minimization	1
PLC	Programmable logic control	1
POS	Product of sum expression	3.1.1
IL	Instruction list	3.2.1
ST	Structured text	3.2.1
LD	Ladder diagram	3.2.1
FBD	Function block diagram	3.2.1
SFC	Sequential function chart	3.2.1
SOP	Sum-of-product expression	3.3.1
POS	Product-of-sum expression	3.3.1
MPOS-net	Multilevel Product-Of-Sums net	3.4
Maxterm	Sum term of POS expression	3.5
Minterm	Product term of SOP expression	3.5

FDI	Fault Detection and Isolation	4.1
ARX	Autoregressive with exogenous input	4.4
ARMAX	Autoregressive moving average with exogenous input	4.4
MD	Machine direction in a paper machine	5.1
FPP	Free Pole Placement design method	5.4
RMS	Root Mean Square	5.9

Contents

1. Introduction

A paper winder is a machine that is used in the paper industry to produce customer rolls for printing. Its automation and control system is a combination of machine automation and traditional process automation. Modern paper winders have many servo-controlled movements, which have replaced the previous simple movements controlled by directional control valves. The productivity of a paper machine can be increased basically by reducing downtimes or increasing the running speed. Paper winding is a batch process and the paper winder is stopped during a set change when a set of customer rolls is taken away from a paper winder. Therefore, the productivity of a paper winder can be improved by speeding up the machine and the servo-controlled movements of machine parts. Running speed affects the productivity of a paper winder in the same way as in a paper machine. Acceleration and deceleration values are important too, because the paper winder is stopped and started continuously.

A paper winder is one of the main critical components in the paper-making process and therefore it has a major requirement for reliability. In a paper machine, the down time means that period of time when the paper machine does not produce paper. The down time includes planned and unplanned breaks in production. As mentioned, in a paper winder there are breaks in production during the normal operation, too. A failure in a paper machine leads quite soon to a situation where winders need to be stopped because they have run out of paper. The reliability performance describes a machine's ability to perform certain tasks at certain times. Especially in paper winders, the reliability performance is a much better measurable quantity than the down time. Mean Time Between Failures (MTBF) can be used to measure the reliability performance. MTBF includes both Mean Time To Restoration (MTTR) and Mean Time To Failure (MTTF), see, for example, (Kuhmonen, 1997).

The purpose of this thesis is to develop methods to improve the performance and runnability of a paper winder. There are two basic fields of research that can be used to improve the productivity of the paper winder: fault diagnosis and vibration control. The state-of-the-art fault diagnostic system can be used to minimize the down time and

improve the reliability performance of the paper winder. Vibration is one of the main reasons that the running speed of the winder is limited, especially with certain paper grades. The vibration control methods can be used to reduce vibration so that the maximum speed of the winder can be used. Both of these methods also have a positive influence on the quality of the end product. Vibration control can also be considered a fault diagnostic method that not only detects vibration but also reduces it.

Kuhmonen (1997) listed the general features of failure types in Flexible Manufacturing Systems (FMS) and claimed that operational disturbances occurred 70 times more often than technical failures. A similar list of general features of failures can be written for a paper winder as well (see Table 1-1). Of course, the ratio between technical failures and operational disturbances differs between paper mills. Anyway, the trend is congruent with the FMS example above.

Table 1-1: Failure types in paper winders.

Technical failure	**Operational disturbance**
Long down time	Short down time
MTTF is long	MTTF is relative short
Random	Can be removed by operators
Requires a maintenance person	Interrupts automatic operations and sequences
Requires disassembly	
MTTR is quite long	
Spare parts needed	

There is also a gray area between technical failures and operational disturbances. These are disturbance situations where the machine is not broken but the disturbance removal procedure is so complex that it needs help from a maintenance person. There has been continuous development in helping both maintenance people and operators to solve faulty situations. Virtanen and Paanasalo (2000) have contributed to this research, especially in the paper-winder environment, and have developed tools for fault diagnostic purposes. These kinds of tools reduce the gray area between technical failures and operational disturbances and help operators to solve more-complex problems. They also reduce the repair time (MTTR), because the primary reason of the fault can be found faster.

A logic explainer has been developed to help maintenance people and operators to find primary faults, (Huuskonen *et al.*, 1995), (Plomp *et al.*, 1996) and (Plomp, 1997). The logic explainer builds a model of the programmable logic control (PLC) programs of the paper winder or another machine. Maintenance people and operators can then use the user interface to ask the logic explainer why, for example, a certain signal is in a certain state,

(Virtanen and Paanasalo, 2000). A time aspect is involved in the logic explainer, too. Also, the user can ask the logic explainer what caused the change in a signal state. In paper winders, the results were introduced in the form of function block diagrams. There has also been more-general research in this field, see e.g. (Huuskonen, 1997).

Virtanen (2004) has developed another method to modify programmable logic control programs for fault diagnostic systems. The programs are transformed into two-level disjunctive or conjunctive forms. In this form, very complex logic functions can be presented with simple graphical symbols. Especially those operators who are not familiar with function block diagrams prefer this representation. This method also reduces manual work in building up a fault diagnostic system. Manual work is not only time-consuming and expensive, but usually leads on to a situation where updating a system is very difficult in practice. Over a thousand binary signals are used in the PLC programs of the paper winders, so the need for new methods is obvious. The new method described in this thesis has been tested in various industrial projects, and has the following benefits in addition to those of the previous manual configuration of the diagnostic systems.

- The fault diagnostic system work properly from the beginning of start-up.
- Program changes can easily be updated in the system by re-generating the diagnostic system.

The complexity of paper winders and their control systems has been increasing so much that an intelligent automatic generator is needed to produce high-quality fault diagnostic systems with reasonable costs.

A paper winder is the last unit process in a paper line, which affects the quality of the end product. It is well known that process or product faults at the end of the production chain are the most expensive ones. It is possible that customer rolls that are sent to a printing house are returned to the paper mill if there are quality problems in the rolls. This is not only expensive, but it ruins the paper mill's reputation as a reliable supplier. The use of modern process diagnostic methods is still rare in paper winders.

Automatic diagnostic methods started to develop when the first computers were introduced. First model-based methods were presented in the 1970s, and much research has been undertaken in that field during the last two decades. Some of the recent results of the research can be found in (Isermann and Balle, 1997), (Chen and Patton, 1999) and (Simani *et al*., 2003). The car industry is one of the new application areas of the model-based fault diagnosis, see e.g. (Nyberg, 1999). Some of these methods are applied to a paper winder in this thesis.

As mentioned above, quality and capacity are the key factors in paper manufacturing. Vibration is a phenomenon that harms both. Vibration during winding might ruin the whole set of customer rolls. Vibration can also limit the run speed or acceleration of paper winders and limit capacity in that way. Vibration is a common problem in rotating machines. However, a paper winding process has some special features compared to other

unit processes in the paper machine line. A paper winder does not rotate with a constant speed but it accelerates to maximum speed and decelerates down to zero speed during production of every set of customer rolls. Hence a paper winder excites a very wide range of frequencies.

Research into the vibration of structures has been active during the last century, and still is. A traditional method is to design structures that damp the oscillation. Also, damping materials can be used between different machine parts (Beards, 1996).

Passive dampers work without external energy. An impact damper is a typical passive damper. They are used, for example, in bridges, see (Ogava *et. al.*, 1997). It can be used with other types of dampers as well, see (Collette, 1998). A tuned mass absorber is a well-known damper, which consists of a mass and a spring. It is fastened to the vibrating part of a machine and typically has one resonance frequency. When a machine is vibrating with that frequency, the mass damper starts to vibrate, too. However, it oscillates with 180 degrees phase lag and thus absorbs vibration from a machine structure.

Olgac and Holm-Hansen (1995) introduced a new concept, a delayed resonator, as a tunable active vibration absorber. Its basic structure was the same as that in a tuned mass damper. However, an external force element was added to the system. The force was directed to a mass, and was controlled by means of a mass displacement measurement, multiplied and delayed with a gain and a delay element. Advantages of this system were that the excitation frequency could vary over a wide range, and could be tuned in real time. The delayed resonator was implemented also on a flexible beam (Olgac and Jalili, 1998).

Further expansions of the delayed resonator have been introduced as well. Filipovic and Olgac (1997) introduced a delayed speed feedback, separating it from the traditional position or acceleration feedback. It is also possible to damp a range of frequencies instead of one frequency (Filipovic, 1998 and 1999). Filipovic and Schröder (1998) also made a simulated case study of vibration suppression of winding drums with this kind of band pass absorber.

The delay and gain structure is not the only possibility as a controller in a feedback loop. For example, a single transfer function with a gain and time constant can be used for that purpose. Jalili (2004) introduced that kind of active resonator absorber.

In this thesis, a new method is introduced to configure the fault diagnostic system automatically. Before that, the work was performed manually. The manual configuration is very expensive, time-consuming, the quality varies, and it is difficult to change the configuration afterwards. There was one automatic method developed earlier, the logic explainer. However, it was proven to be far too complicated for operators. In the field of machine automation and programmable logic controllers, there has not been anything like that published before. This work covers not only the fault diagnosis of the machine automation, but the fault diagnosis of the process variables, too. This idea of combining these two in the same work is natural in this case because the paper winder contains both the machine automation and the process automation. In addition to the fault diagnosis, the

problems of the vibration control are approached. Both theoretical work and practical tests were carried out. The new theory was developed for delayed resonators, where there was a gap between theory and practice. Experiments were conducted with the actual damper.

The outline of the thesis is as follows. Chapter 2 deals with the unit processes in a paper mill. One unit process, the winding, is discussed in detail. The winding process and the main units of the paper winder and its automation system are described. This chapter supplies the reader with the information that is needed in the following chapters.

Fault diagnostics of binary signals and logic control programs are discussed in Chapter 3. The manipulation and presentation of logic control programs, together with the logic explainer, are discussed to give the reader the basics with which to understand the new methods described in this chapter. The new Level-To-Level Minimization (LLM) algorithm based on Boolean algebra is introduced and compared to the methods based on the manipulation of truth tables of logic functions. It can be shown that, with certain types of logic functions, the minimization with Boolean laws can save much computing time and memory when compared to the methods based on truth tables. A novel Multilevel Product-Of-Sums net model is introduced in Chapter 3 as well.

In Chapter 4, model-based fault diagnosis methods are discussed. There has been a tremendous amount of research carried out in the field of model-based fault diagnosis, but, until now, almost nothing relating to paper winders. Chapter 4 applies the fault diagnostic methods to a paper winder. Two different case studies are introduced. The first deals with tension control of a paper web, while the latter discusses force control of a rider roll. A very detailed simulation model of a rider roll is used to examine the effects of various types of faults in a hydraulic valve. The model-based fault diagnostic system is then applied to detect faulty situations and isolate the faults.

Active vibration control is the topic of Chapter 5. The theories of the delayed resonators and active resonator absorbers are further developed. The idea is to be able to modify both the eigenfrequency and the damping factor. A cascade-controlled delayed resonator is also introduced to broaden the operating range of actively controlled mass dampers. Stability issues are considered as well. In Chapter 5, an active damping application based on a hydraulic actuator is also introduced. This method was tested with a full-scale pilot winder.

Conclusions are given in Chapter 6.

The main contributions of the thesis can be summarized as follows:

- A new Level-To-Level-Minimization (LLM) algorithm is developed to transform logic control programs of paper winders to a representation suitable for a fault diagnostic system. The algorithm changes logic programs into a two-level minimum or near minimum form that can be presented in a graphical format in a user interface of a fault diagnostic system. A novel theoretical Multilevel Product-Of-Sums net (MPOS net) model is developed to present the information of logic programs of a paper winder in a form that is suitable for a fault diagnostic system.

The model contains blocks that are generated with the algorithm mentioned above. The model also includes links between blocks and systems outside of a control system.

- A practical solution is developed for building up automatically the fault diagnostic system of a paper winder. It automatically reads, transforms and minimizes the logic control programs of the paper winder. The result is stored in a database in the form of the model presented in this thesis. These databases have been used in practice in several fault diagnostic systems of paper winders in various paper mills. A limited questionnaire study is conducted to survey experiences of maintenance people concerning fault diagnostic systems and maintenance work in general.

- Model-based fault detection and isolation methods are applied to a paper winder. Only very few studies have been reported before in literature. Two different cases are considered. In the first case, a neural network model is used to supervise the web tension control of a paper winder. In the second case, a very detailed simulation model of one key component of a paper winder, a rider roll, is introduced. The model is used to test and verify the model-based fault detection and isolation system developed for the rider roll.

- A new method is developed for actively controlled mass dampers. This extended version of the delayed resonator enables not only the resonance frequency to be tuned, but the damping factor as well. Both variables can be tuned separately. A new pole placement method is introduced for active resonator absorbers. This method also makes it possible to tune the resonance frequency and the damping factor separately.

- A new method is introduced to shift the resonance frequency of an actively controlled mass damper. The advantages of this method are that its practical implementation is straightforward and it does not need much energy when operating near the actual resonance frequency of a system.

- A cascade controller is introduced for an actively controlled mass damper. This novel method makes it possible to use the delayed resonator and other methods regardless of the mechanical properties of an element that generates an external force into an actively controlled mass damper. The force element has been a part of the damper's dynamic properties in the previous studies (Jalili, 2004).

- A hydraulic active damping method is introduced to the damped vibrations of the rider roll. Experimental runs with a full-scale pilot winder are carried out to prove the efficiency of the method.

2. Paper winding process and control

This chapter describes the unit processes of a paper and pulp mill. It gives the reader an overview of the whole paper-making process and describes the special features of finishing processes and paper winding. This work concentrates on paper finishing and especially on the paper winding process. For more information on the unit processes of a paper machine see e.g. (Leask, 1987), (Thorp, 1991), (Roberts, 1991) and (Smook, 1992). Virtual training tools like KnowPap (see http://www.knowpap.com/english/) provide detailed information about paper machines and paper finishing.

2.1. Unit processes of paper and pulp mills

The main unit processes of a pulp and paper mill are described in Figure 1. Wood handling consists of unit processes, which transport and treat wood material in a paper mill. Logs are first moved to log-intake and slashing stations. Typically, chain conveyers are used to transport logs to bark handling where they are fed to a debarking drum. If they stay too long in the drum it worsens quality and increases energy consumption. De-icing can also take place between log intake and debarking in the paper mills located in the northern region. Bark is transported to storage, while logs are transported to chipping and screening. The objective of the screening is to deliver chips of a size suitable for the following processes. The chips are transported and stored in silos for future use.

Chips are raw material for chemical and mechanical pulping. In chemical pulping, lignin is dissolved from chips into separate fibers. Heating and chemicals perform the dissolving. The major chemical pulping processes are sulfate and sulfite pulping. In mechanical or thermomechanical pulping (TMP), fibers are separated from chips with mechanical forces and heat. The chips are first pre-processed and then handled in refiners. Typically, these are single-disk refiners, or double-disk refiners, in which two disks rotate against each other. Refiners can be pressurized to improve fiber separation. Mechanical pulp is then pumped from refiners to further processes. Another option for the mechanical separation of

fibers is to produce groundwood by grinding. In the grinding process, barked and cut logs (not chips) are pressed sideways against a large grinding stone. The mechanical strain and heat that develops in the grinding process separates the fibers. The grinding process can also be pressurized when pressure groundwood (PGW) is produced. The unit processes described above belong to a pulp mill. The pulp mill can be integrated with the paper mill. The stock preparation process is located between the two.

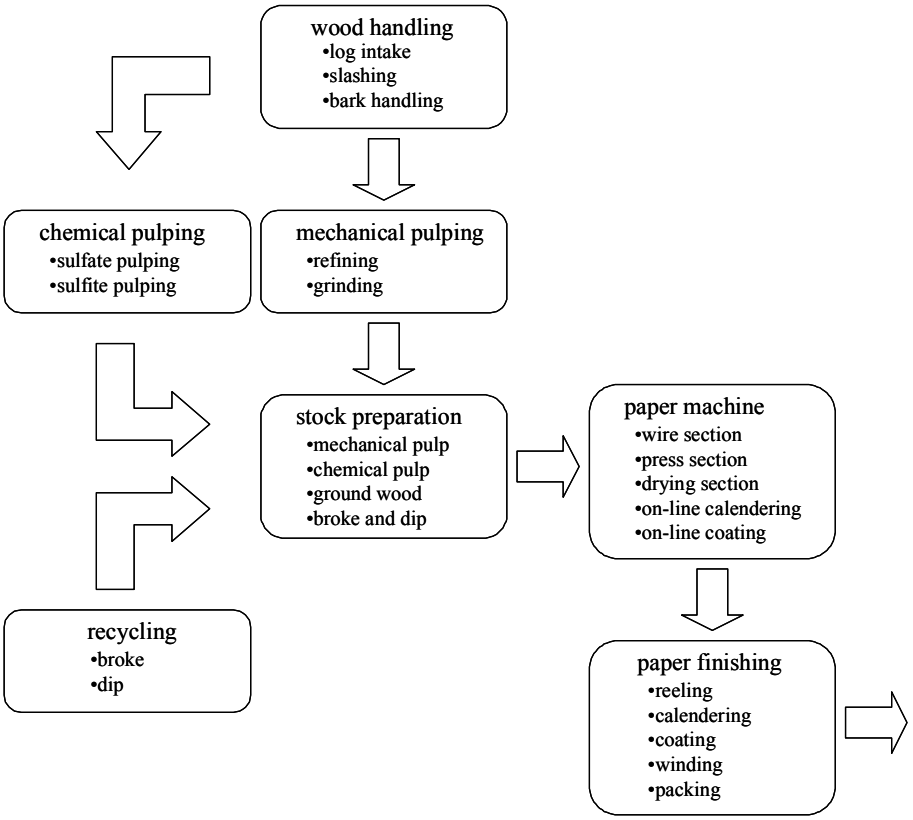

Figure 1: Main unit processes of pulp and paper mill.

Chemical and mechanical pulp, groundwood, broken (waste from the paper machine and finishing machines) and recycled fibers (dip) are transferred into stock preparation. From stock, preparation pulp is pumped into a paper mill.

The first process in a paper mill involves a paper machine. This consists of three main parts: a wire section, a press section and a drying section. In the wire section, stock is fed on a wire from a head box. In the head box, the speed and direction of the stock jet fed into a forming section is controlled. In the forming section, stock suspension changes because of the flow of water through the fabrics. Shear forces are generated in the stock because of the speed differences between the fabric and the different layers of the stock. These shear forces improve the formation of paper and break developing flocs. After formation on the wire section, the web arrives in the press section. Dry content of the stock is roughly 20 %

when the web enters the press section. Then water is removed mechanically from the web by pressing it between a press felt and a roll or between two press felts. The dry content of the web is around 50% when it leaves the press section. It is technically and economically reasonable to dry the web up to 50% dry content by means of mechanical processes. Evaporation is used to dry the web to its final dry content. This is carried out in a drying section. Three different drying methods are used in the drying section: cylinder drying, air-drying and radiation drying. Basically, drying is a simple process, but its energy consumption is high and it should have a good runnability. Drying should not worsen the paper quality either, so proper design of a drying section is very important.

After the paper machine, the web arrives in the paper finishing area. The web coming from the paper machine is reeled on large machine reels. The reeler, which is integrated into the paper machine, is called a machine reeler. However, paper is unreeled and reeled many times before it is a final product, at least in the following processes: coater and calender unwinds and reelers, unwind sections of winders and re-winders, printing machine un-winders, and sheeter unwinds.

Basically, the reeling process does not affect paper properties, but it always impairs paper quality to a certain degree. Smooth reeling on the large-diameter reel spools minimizes that effect and minimizes also the waste on the reel.

Coating is a paper finishing process that improves the printing properties of paper, e.g., smoothness, gloss and brightness. A coating color is applied to one or both sides of the paper. Pigments are the most important components of coating color. The pigments are usually different types of minerals like kaolin clay and calcium carbonate. The coating process can be divided basically into two phases: application of the coating material on the paper, and metering of the coating material to a proper coat weight.

Another important coating method is surface sizing, which is performed with a size-press. Coating machines can be integrated in the paper machine, or they can be off-line machines. For more information on coating technology, see (Lehtinen, 2000).

Calendering is usually the last process where paper properties can still be improved. The paper web is pressed between two or more rolls. The contact area between rolls is called the nip. For example, nip pressure, temperature and length of nip or time that paper stays in the nip area all affect the calendering result. The best calendering result can be achieved in supercalenders. Supercalender is a multi-nip calender consisting of a stack of rolls (see Figure 2). Calenders can also be integrated as a part of the paper machine.

Figure 2: Coater and reel (up-left), multi-nip calender (up-right), paper winder (down-left) and roll handling (down-right). Photos courtesy of Metso Paper.

Large paper reels cannot be delivered to customers. Paper winding is the process where large paper reels are cut and wound to customer rolls. The paper winding process is described in detail in the next section.

After winding, the customer rolls are packed and transported to a warehouse. Roll wrapping and handling processes take care of these procedures. An internal transportation system moves rolls from the winder discharge deck (see Figure 2, down-left) to the wrapping machine and warehouse. The internal transportation system consists typically of conveyers, labeling and weighting machines and identification systems. Winding and roll wrapping and handling are always off-line processes, i.e., they are separated from the paper machine. For detailed information on calendering, winding and roll wrapping and handling, see (Jokio, 1999).

2.2. Paper winding process

A parent reel is a large paper machine wide roll. Its diameter is typically from 2 to 4 meters and its width from 2 to 10 meters; it can weigh over 100 tons. It is not reasonable to transport reels of this size. They are also too large for printing houses. Paper winders cut and wind the large reels coming from the paper machine to customer rolls. From one parent reel, several sets of customer rolls can be made. There are basically two types of paper winders nowadays: two-drum and multi-station. In the two-drum winder, rolls are lying on two drums side by side. The weight of the rolls is directed onto contact points between the rolls and drums. This contact point is called a nip. In multi-station winders, each roll is wound independently in separate stations.

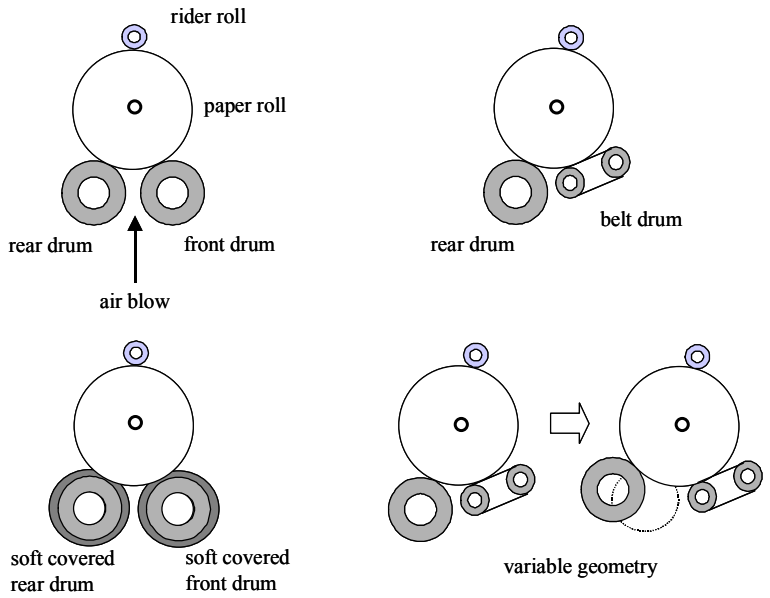

Figure 3: Modified two-drum winders. Air pressure is fed between winding drums (up-left). A rear drum is replaced with a belt drum (up-right). Winding drums are covered with soft material (down-left). Winding geometry is changed with a moving rear drum (down-right).

There are different varieties of two-drum winders. These have been developed mainly to avoid the problems of large diameter rolls (Figure 3). A nip load caused by roll weight itself is so high that it causes quality problems in the rolls. In the following, the most-typical varieties are introduced.

Pressurized air is fed between the winding drums to support rolls and decrease the nip load.

The front drum is replaced with the belt drum. The belt supports rolls more and more when the roll diameter increases. The nip contact is much wider with the belt and the nip pressure per cm^2 is much less compared to a steel drum.

Metal winding drums can be replaced with soft material-covered drums. This widens the nip and decreases maximum pressure.

The position of the rear drum can be controlled in modern two-drum winders. The gap between the winding drums affects the nip load, which can be controlled online during winding. It is also one way to decrease the vibrations in paper winders.

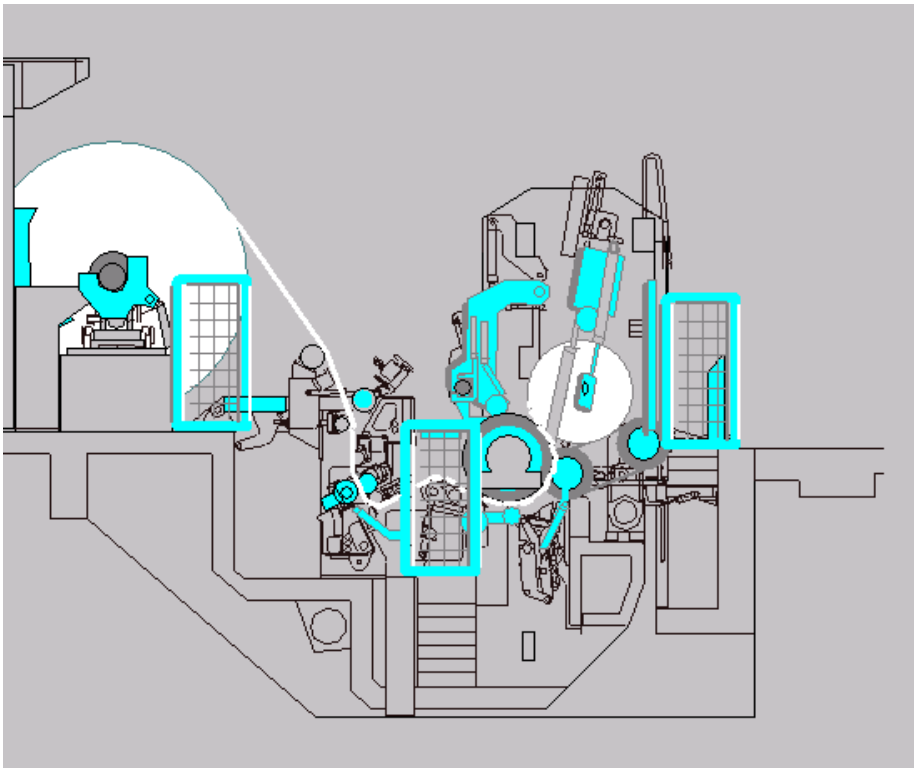

Figure 4: The main parts of the paper winder: the unwind section (left), the slitting section (middle) and the winding section (right). The drawing courtesy of Metso Paper.

The paper winding process can be roughly divided into the following parts (see Figure 4).

The unwind section handles the parent reel. It accelerates and decelerates the large parent reel so that the web tension (unwind tension) stays at the desired level.

In the slitting section, the wide paper web is cut in the machine direction so that the customer rolls of a certain width can be produced.

In the windup section, the customer rolls of a particular width and diameter are wound. Typical windup sections of two-drum winders are described in Figure 3.

In addition to these main winding processes, there are some sub-processes such as machine reel and reel spool handling, which transport the new machine reels to the unwind stand and remove the empty reel spools. An unwind stand is the main part of the unwind section; a large machine reel is located on it. There are electrical drives and brakes to accelerate and decelerate the machine reel. The reel in the unwind stand can be moved sideways to put the web into a correct position. The unwind stand can also be oscillated to decrease the negative effect of local profile variations in the web. The unwind section also controls the unwind tension, which is one of the main controls of paper machines. In Section 4.2, a method is introduced to supervise the unwind tension control.

In the slitting section, the paper web is cut in the machine direction. Cutting is usually performed with shear-cut rotating blades. The customer defines the number of slitters, which depends on the width of customer rolls. A cut paper web needs to be separated after slitting. This is usually performed by D-bars, bowed rolls or sectional spreader rolls. Without spreading, paper sheets will interlock paper rolls together in the winding section (cf. a card deck during a shuffle).

As mentioned above, the winding section consists of winding drums and a rider roll in two-drum winders. In multi-station winders, a winding drum or drums, stations and rider rolls form the winding section. A web is threaded from the unwind section through the slitting section to the winding section. After a set-change, new cores are fed onto the winding drums. Cores are usually glued or taped so that the paper web is stuck to cores when the winding starts. A rider roll is lowered on cores so that they are tightly pressed against winding drums. A rider roll is one of the key components of the winding section. A detailed simulation model of the rider roll is presented in Section 4.3. This simulation model is used to verify the model-based fault diagnostic system developed to monitor the functions of a rider roll (see Section 4.4). Roll diameter first grows very rapidly when a paper winder accelerates to its maximum speed. This puts high demands on the main unwind and winding section controls, i.e., speed and torque controls, of winding drums, unwind tension control and force or pressure controls of the rider roll nip. The rear drum is usually speed controlled, and the front drum, torque controlled. In this way, a proper tightening effect can be applied to the rolls. When the desired roll diameter is achieved, the winder is decelerated and stopped, and the rolls are pushed away from the winding section to the winder discharge deck, and the new cores are loaded into the winder. This set change should be performed as quickly as possible, because it affects the capacity of the winder.

2.3. Paper winder automation

Traditionally, process automation and machine automation are two separate study areas. A paper-winding process is a combination of both. It has very demanding process controls to produce high-quality rolls for customers. There can be independent recipes and trims for

every customer and paper grade. In practice, it is difficult to measure the properties of customer rolls without breaking the structure of a roll. This puts high-quality demands to every part of the process. Quality faults in customer rolls can cause great economic losses to paper mills. Until now, the quality is inspected from outside with, for example, the Smith Needle, or by knocking the rolls with a wooden stick. Recently, Paanasalo (2005) developed new methods to estimate the roll structure by measuring different winding parameters; in the future, these kinds of methods will undoubtedly become more common.

Besides process control loops, there are many high-speed servo-controlled devices in paper winders, which control both position and force. Moveable masses are heavy, and a rider roll, for example, can weigh up to 10-15 tons and a set of rolls easily 20-25 tons. When a rider roll is lowered down to cores, its speed can be 300 mm/s. It nearly stops just before the cores; the position controller is switched to the force controller when the rider roll touches the cores. Cores are made of rather stiff material, so the switching has to be performed very quickly to prevent the force from rising too high. On the other hand, a rider roll has to be very robust against noise and vibration during running.

Besides, the process and servo-controlled loops, many limit switches and other binary-type devices are used in paper winders. These signals are used for safety purposes and to schedule and control different functions. For example, a modern paper winder contains automatic sequences that are scheduled with information coming from sensors. Large electric and hydraulic devices and systems contain a potential risk of severe injures for humans, and machine failures can cause significant economic losses, too. These binary types of sensors and devices are used to minimize the risks mentioned above, but are a complex combination of analog and binary controls, and so put a great demand on the fault diagnostic and control system of a paper winder.

A typical automation system of a paper winder consists of two main parts: programmable logic controllers (see Hackworth and Hackworth, 2004) and control PCs. Devices that have some kind of intelligence and control capabilities by themselves can be considered to act as a third control level.

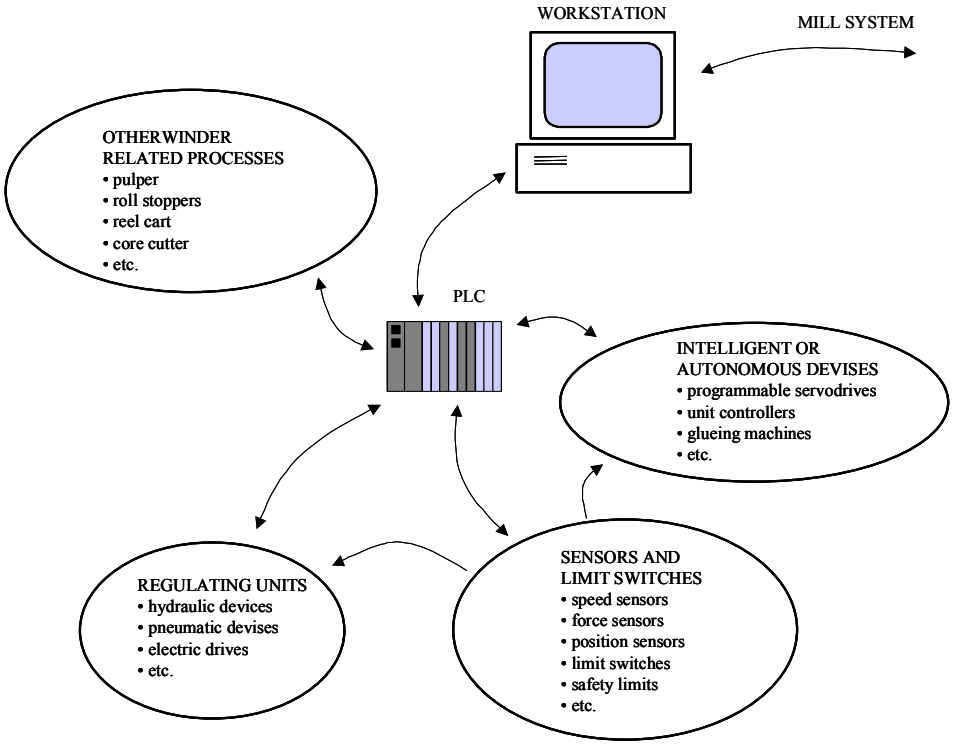

Figure 5: Basic structure of an automation system of a paper winder.

Typically, all time-critical functions are collected to the programmable logic controller PLC, which handles all closed loop controls. The process data are read to the PC through the PLC. Product and recipe information, setpoint values etc. are downloaded from the PC, which is also a user interface to the process. Besides one or several main units, the PLC system consists of several input and output modules and, for example, some control panel units. Input and output units can be distributed to different parts of the winder, or they can be collected into the electrical equipment room. Electrical drives are also controlled with separate PLCs or controllers. A typical structure of an automation system of a paper winder can be seen in Figure 5.

The main controlled process parameters in two-drum winders are tension, nip-load and winding force. The winding force is the tangential force originated from the torque differential generated by a second winding drum or belt. Below are short descriptions of these three process parameters.

(Unwind) tension control – Variation in unwind-tension causes web breaks and defects in the quality, so it plays an important role in winding. Earlier, an unwind tension control system contained only brakes that slowed down the rotation of an unwind reel and generated tension in that way. Nowadays, reels are so large (>100 tons) that electrical drives are needed to rotate the reels at the beginning of winding. Otherwise, tension would rise to a value that was far too high. It would be impossible to run a paper web at high

speed without any tension. Slitting and spreading cannot be performed either without tension. A loose web breaks easily in the cutting blades and the cutting result is poor. An unwind tension affects the end user roll stiffness and structure by generating strain in the web coming in the nip.

Nip load – The force that is directed to a paper roll at contact points with other rolls is called the nip load. The weight of a paper roll itself can create the force, or it can be generated typically with hydraulic or pneumatic actuators in a rider roll. A paper roll has three nips in a two-drum winder: a rear drum, a front drum and a rider roll nip. The stiffness of the paper roll can be controlled with the nip-load. High nip-load increases tension of a web wound on a paper roll and produces a stiffer and harder paper roll. At the beginning of winding, the weight of a core or a small diameter roll is not enough to produce the required nip-load level. A rider roll presses rolls down at the beginning of winding and produces the required nip-load value. When the diameter and weight of paper rolls increase, this extra force is no longer needed and a rider roll just slightly touches the paper rolls to prevent them from bouncing off the winder. For a more detailed study of nip mechanics see (Jorkama, 2001).

Winding force – In two-drum winders, the rear drum is usually speed controlled and the front drum is torque controlled. A torque-controlled front drum can be used to generate a torque difference between rear and front drums. This effect generates strain in the outermost layer of paper wound on a paper roll. High nip-loads can damage paper rolls; by using the winding force, stiff rolls can be produced with a lower nip load level.

Besides the force and position control loops and process automation controls, paper winders have many automatic sequences and functions. The most typical ones are listed in Table 2-1.

Table 2-1: Sequences used in paper winders.

Sequences of paper winders
Web threading sequence
Trim change sequence
Reel change sequences
Set change sequence
Core feeding sequence
Gluing (cores and tail of paper)
Taping (cores and tail of paper)
Splicing (unwind)

In web threading, the paper machine wide web is pulled from the reel in the unwind stand to the cores and winding drums. This can be performed with, for example, ropes, air blows or special felts. In a trim change sequence, slitters are moved to new cross-machine positions according to the desired roll widths. In multi-station winders, stations and rider rolls are also located to new positions. Reel-change sequences take care of removing empty reel spools from an unwind stand and bringing the full reels from the storing places to the unwind stand. When a set of rolls is ready on top of the winding drums, a set change sequence removes paper rolls from the winder and prepares the winder for a new run. A core feeding sequence brings new cores on top of winding drums. It can also be a subsequence for a set change sequence. There are basically two places where gluing or taping are used. Sometimes cores are glued or taped so that a paper web grips on cores properly. There are also devices that glue or tape tails of rolls at the end of winding. When an empty reel spool is replaced with a full one, a new web is taped to the web hanging still in the winder. This is called splicing.

The complex structure of a paper winder makes it reasonable to use special fault diagnostic tools to run paper winders effectively. At least one full-scale fault diagnostic system has been developed for paper winders, see (Virtanen and Paanasalo, 2000) and (Kaistinen, 2001).

This section began with a general description of a paper-machine process, but since then has concentrated more on two-drum winders, because a rider roll of a two-drum winder is chosen as a test bench both in Chapter 4 and Chapter 5. For more information of winding and multi-station winders, see, for example, (Jokio, 1999).

3. Fault diagnostics - binary part

A paper winder has typically more binary type sensors and actuators than other unit processes or machines in a paper mill. The whole paper machine has perhaps more sensors and actuators, but density (the number of sensor and actuators per length of machine) is higher in a paper winder. In a paper machine, the focus of the operation is in process automation and process itself can be defined as a continuous process. The winding process is a batch process; a paper winder has, for example, many servo-controlled movements during normal operation unlike the paper machine. However, a paper winder has still some process-controlled parameters unlike other machines (conveyers, wrapping machine etc.) in the roll finishing area.

The great number of binary signals and devices creates also a need for a fault diagnostic system designed specially for binary signals. Earlier, when a structure of a paper winder was much simpler, a manual configuration of these kinds of diagnostic systems was reasonable. Now the situation is different, and automatic tools are needed to do the work. In this chapter, a new method and an algorithm are introduced to automatically modify and convert PLC programs based on binary signals to a graphical form that is easily interpreted by operators. In Section 3.1, the industrial state-of-the-art methods are covered. Results of a questionnaire are also reported. In Section 3.2, current methods of modifying PLC programs for fault diagnostic systems are introduced. Section 3.3 covers the methods of minimizing logic functions. In Section 3.4, a new model is presented that clarifies the structure of the new fault diagnostic system of the paper winder. A new algorithm, which transforms large logic functions into a form suitable for the fault diagnostic system, is introduced in Section 3.5. A practical example is introduced in Section 3.6.

3.1. Introduction to common methods

In this section, methods are introduced to display binary-type data in fault diagnostic systems. This is a very important human-to-machine interface issue. User profiles and typical problems are also discussed. A short review of results of a questionnaire study carried out in connection with the maintenance people of several paper mills and the start-up people of a paper machine manufacturer are introduced.

3.1.1. Methods

There exist at least the following methods to represent information in fault diagnostic systems of binary signals: sensor state control, sequence charts, mask help, and alarm list.

In sensor state control, actual machine parts like actuators and binary type sensors are typically monitored. Figure 6 shows a typical machine part of a paper winder, a lowering table, where this kind of diagnostic can be used. When a set of paper rolls is ready, these are pushed onto the lowering table. The table is turned with a hydraulic cylinder and rolls are released on a winder discharge deck. To control the movements, and for safety reasons, there are limit switches at both ends of the movement. If the lowering table is controlled in the upper position to wait for the rolls to be released and the upper limit switch is broken, the rolls are not released. A set change is stopped automatically and the winder cannot be used until the broken limit switch is fixed. However, when an operator looks at winder he or she sees that the lowering table is in a correct position. Without a fault diagnostic system, electrical measuring devices or programming devices of a PLC are needed to locate the fault. This is not only time consuming, but a maintenance person is also needed to finish the task. In sensor state control, limit switches are monitored so that when, for example, the lowering table is controlled to the upper position, the upper limit switch has to change its state after a certain time. If that does not happen, an alarm message is generated or an alarm indicator is turned on. Then a mechanical fault can be located immediately without any extra devices or people.

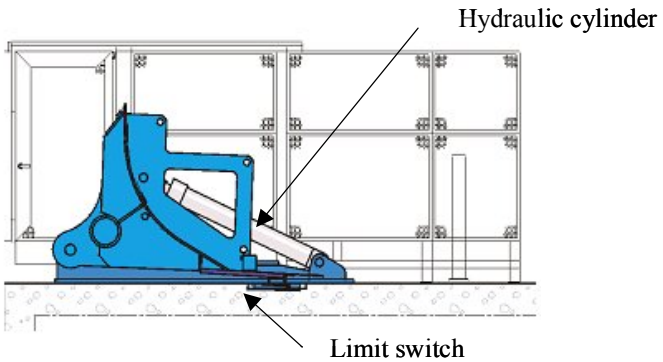

Figure 6: Lowering table of a paper winder where the sensor state control of limit switches is used.

There are some industrial fault diagnostic applications, where this type of diagnostics is performed. In the area of paper winding, see (Virtanen and Paanasalo, 2000).

As mentioned in the previous chapter, paper winders have many sequential tasks. In a sequence program, a set of tasks or sequence steps is carried out so that when one step is ready the second one is started. In a special case, many steps can be on at the same time. Condition signals indicate when a step is ready and a sequence goes on into the next step. A general practice in monitoring the sequences is to use sequence charts. From the sequence chart, it can be seen in which step a sequence is and what the states of the condition signals of that step are. Step times can also be monitored to determine if there are any problems in the sequence. Sequence charts are not only a tool to monitor sequences, but can be used to design and program sequences as well. Figure 7 shows a sequence chart window, where the steps can be seen on the left side and condition signals of the current step on the right side.

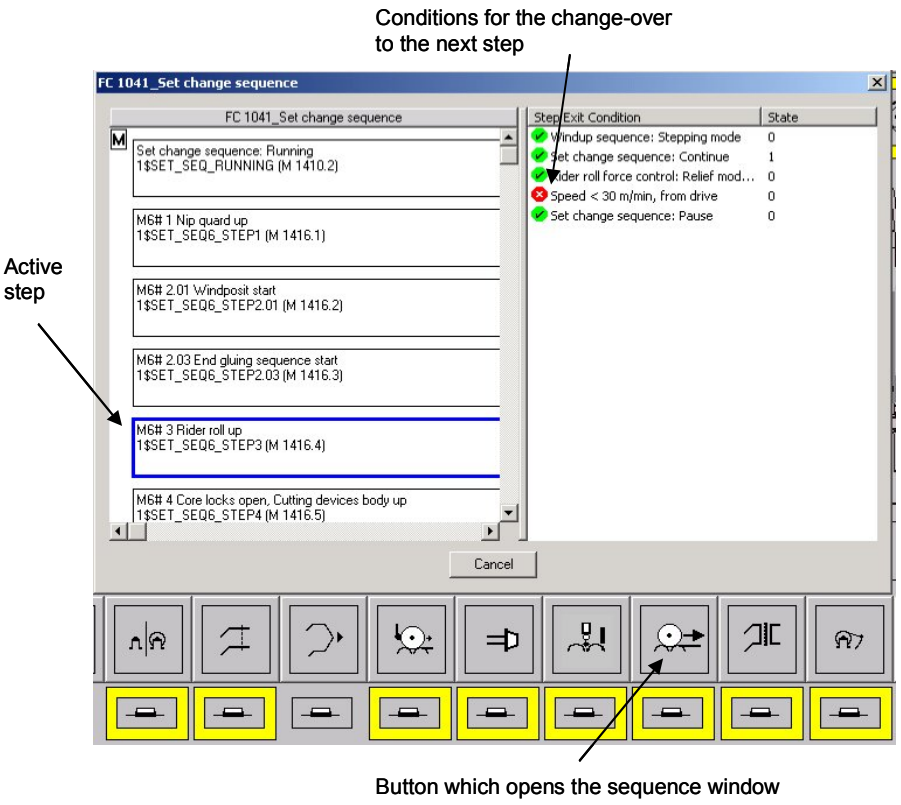

Figure 7: Graphical sequence display. Steps are on the left side and condition signals of the current step on the right side.

Another common way to display diagnostic data of binary signals is the so-called mask help. In the mask help, not only binary data are shown about actuators and sensors but also values of the calculated memory signals. It can be said that the sensor state control

monitors the machine and a mask help both the machine and its functions and programs. Signal states are typically shown with colors in the mask help. Usually a green color means that the signal state is in a correct state and a red color that the signal is in a prohibitive state. The mask help indicates not only machine breaks but also operational faults. Figure 8 shows an example of a simple PLC program network and a mask. Signal "RR_STOP_POS" would generate an alarm indicator, because its value is 1 (TRUE), while, according to mask, its correct value is 0 (FALSE). It must be born in mind that a correct value means a signal value in this network. A correct value of the same signal can be TRUE in another part of a PLC program.

State	Mask	Alarm
1	1	no
0	0	no
0	0	no
1	0	yes

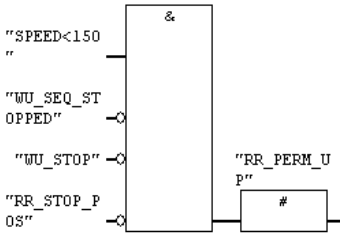

Figure 8: Function of mask help. No alarm is generated while the actual signal value, State, is the same as the mask value. When the values differ, the alarm is generated. In this example, the signal "RR_STOP_POS" would generate the alarm (State=1, Mask=0).

An alarm list (Figure 9) is a traditional way to represent diagnostic data. It looks similar to the alarm printer's output used for decades in the process industry and is a log of alarms.

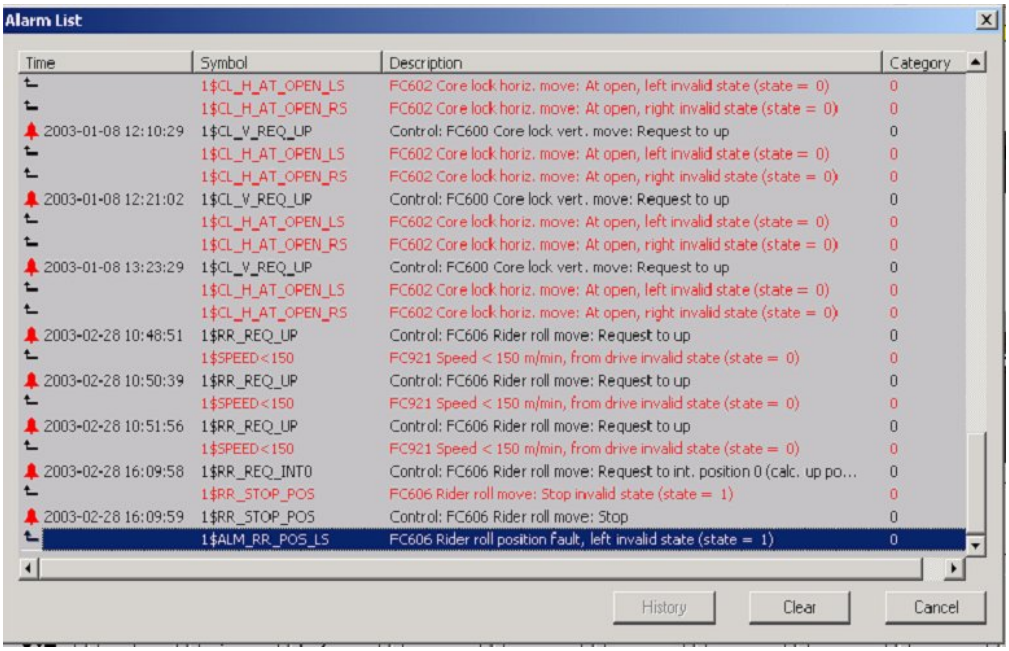

Figure 9: An alarm list of triggers (black) and preventing locking signals (red).

In a binary fault diagnostic system, the states of locking signals are typically monitored only when a control signal of the function in question is on. The control signal is also called a trigger in this context, because it triggers an alarm if one of the locking signals is in an incorrect state. However, such alarm lists do not take full advantage of modern graphical user interfaces. For a detailed study of user interfaces and their usability in automation systems, see (Paunonen, 1997).

3.1.2. Problems

This section deals with problems concerning different types of alarm systems. Some problems are common both to an analog and a binary fault diagnostic system. Undoubtedly demands on fault diagnostic systems have increased, because machines, instrumentation, and control systems have become more complex and downtimes lower (Idhammar, 1997). New machines in a paper industry tend to be more reliable and their downtime lower. Unfortunately, complex machines seem to have complex faults. For example, it has been reported in the steel industry (Parr, 1997) that in a modern production line the downtime tends to be lower, but that it is concentrated in fewer, but more extensive, delays. These complex faults are a challenge for industrial fault diagnostic systems. Unfortunately, they continue to have certain type of drawback.

Below is a list of typical drawbacks of traditional alarm systems (Hasan *et al*., 1994).

- Alarms that are not specific enough
- Alarms that are too specific
- Too many alarms during a system disturbance
- False alarms
- Multiplicity of alarms for the same event
- Alarms changing too fast to be read on the display
- Alarms not in a priority order
- Alarms remaining on the display after being acknowledged

False alarms are usually caused by a defective fault diagnostic system. Either there have been faults from the beginning or the control system has been changed later and the configuration of the diagnostic system hasn't been updated. Traditionally it requires a lot of manual work to build up such a configuration, so changing the system is time-consuming and demanding.

The problem of there being too many alarms during a faulty situation is quite common. Much research has been carried out into avoiding that problem by finding the so-called primary faults, see e.g. (Rollo *et al*., 2004).

The reason for alarms being too specific, or not being specific enough is due to the fact that capabilities of users to utilize such systems and to solve the problems vary a great deal. The users can be roughly divided into three different levels (Figure 10): operators, maintenance people, and experts.

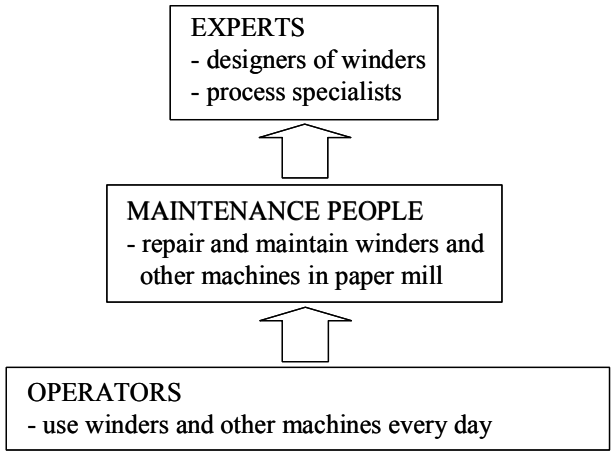

Figure 10: Three basic levels of users of fault diagnostic systems in paper winder area.

Operators are people who use the machine daily. They do not know how to use programming devices and their knowledge of electronics and hydraulics is limited. They usually work only on one machine like a paper winder, but sometimes they are circulated to other machines, too.

Maintenance people are called upon when there are more serious faults in the machine. They know how to change the programs and they are capable of repairing electronic and hydraulic devices. Their problem is that usually they are responsible for the whole paper line or even the whole paper mill. For this reason, their knowledge of a single unit process in a paper mill is limited.

The expert-level user knows one part of a process very precisely. Experts may work in a paper mill, but more often they are outside consultant engineers or representatives of paper machine suppliers. They are needed when complex machine faults or process disturbances have to be solved.

The problem of the alarm list type of diagnostic windows is that they cannot serve all three levels of users. A structure of a modern fault diagnostic system should be like an onion,

with tools for all types of users. The different levels should be arranged so that they do not disturb each other.

3.1.3. Questionnaire study

Questionnaire studies are used to collect tacit knowledge from organizations. They have been used, for example, to evaluate expert systems in nuclear plants (Seong and Kim, 2000). The aim of the study was to survey the users' opinions of the diagnostic systems and their usability. In this research, questioning was directed both to maintenance people working at paper mills and to start-up people of a paper machine supplier; however only the results concerning the paper mills are summarized in this section, because they are the targets of the diagnostic systems.

A set of statements was introduced to participants, who were given the chance to choose from five different categories.

The five different categories were:

-2 = totally disagree

-1 = slightly disagree

0 = no opinion

1 = quite agree

2 = totally agree

Bar diagrams of the results are summarized in Appendix 1. Nine maintenance people from three different paper mills participated in the study. One paper mill had some problems with their diagnostic system and that might have had an effect on results. However, different paper mills were not classified because of privacy protection.

Maintenance people felt that they benefited from the diagnostic systems and that the systems were adequately reliable (see Figure A 1).

On the other hand, false alarms were considered as a problem (see Figure A 2). One mill that took part in this study had a system where false alarms were generated during a normal operation. Because of that, very generalized conclusions cannot be drawn from answers concerning the quality of systems. However, the conclusion that false alarms hinder the use of diagnostic systems can be drawn.

Questions in Figure A 3 were chosen to evaluate how easy the fault diagnostic systems were to use and how maintenance people liked user interfaces. The conclusion was that user interfaces should be simpler to use. Their usability was, however, rated somewhat better than user interfaces.

The quality of information given by the fault diagnostic system was evaluated with two questions (see Figure A 4). The first question dealt with alarm messages and the second with how easy it was to find primary faults with a fault diagnostic system. Answers were distributed quite evenly.

Importance of operating and service manuals was ranked high (see Figure A 5). Electric and hydraulic drawings were also considered to be an important tool in fault detection, and especially in the clearing of faults.

Importance of experience was also evaluated (see Figure A 6) and was considered very important. According to this study, a good knowledge of the machine itself is crucial in fault diagnosis. The observations of the author at different paper mills during the last eight years also support that conclusion. For this reason, it was also quite obvious that maintenance people felt that they needed more training (see Figure A 7).

On the basis of this questionnaire study, the following conclusions can be drawn. Training, experience and good knowledge of machines and systems are the bases for working maintenance organization. If maintenance organization lacks these, undoubtedly the full potential of the fault diagnostic system will not be achieved.

Users find fault diagnostic systems an important tool in fault detection and clearing of faults. At the same time, users suffer from faults in the systems. Systems themselves are working well, but the deficiencies in implementations seem to cause trouble. The method described in Sections 3.4-3.6 is developed to overcome this problem.

Great care must be taken to ensure that the user interfaces are also simple enough to use. The result of this questionnaire was quite positive concerning the user interfaces, but users felt that there were still improvements to be made.

3.2. Methods to modify logic diagrams

3.2.1. Background

First, logic functions in industrial applications were implemented with relays and switches. Later, when microprocessor technology had been developed, the same logic functions were implemented with programmable logic controllers (PLC). In PLCs, there are mainly five different program languages according to standard IEC 61131-3 grouped in text-based languages and graphical languages.

Text based languages

- IL, instruction list

- ST, structured text

Graphical languages

- LD, ladder diagram
- FBD, function block diagram
- SFC, sequential function chart

An instruction list is very close to assembly language as a programming language. A structured text is a higher-level programming language and it is based on the modern programming languages Pascal and C. Ladder diagrams are used to represent basic Boolean functions in the industrial control logic systems. It was basically developed to present relay logic operations. A similar kind of logic is described by function block diagrams, but the functions are now represented as a set of blocks (e.g., OR- and AND-blocks) and connection lines between them. SFC is a graphical representation of sequences with steps and transitions. As in computer programming, higher-level and graphical languages have superseded the instruction list as a programming tool in PLCs. Figure 11 demonstrates the differences between IL, ST, FBD, and LD.

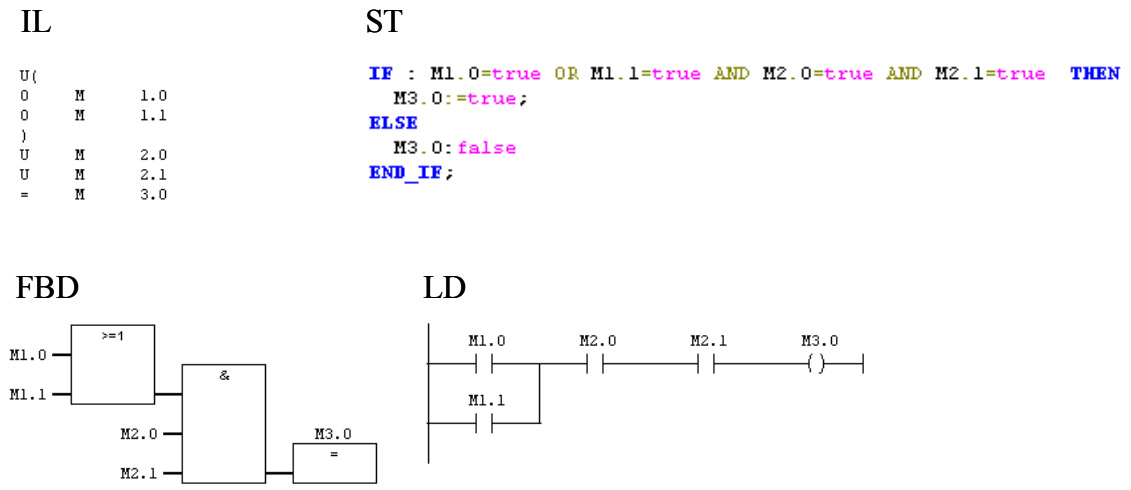

Figure 11: The same logic function represented with four different PLC languages, IL, ST, FBD, and LD.

Boolean functions are usually programmed with FBD and LD, whereas more complex algorithms are written with ST or IL, (Berger, 1998). PLC programs consist of both Boolean functions and higher-level functions, but the following sections deal with Boolean functions only.

3.2.2. Logic explanation

There has been a lot of research in the field of logic analysis and logic minimization in electronic design, see e.g. (Nam *et al*., 2004), (Chang *et al*., 2002) and (Mohamed *et al*., 1997), and in telecommunication technology, see e.g. (Nevalainen, 1988). Web search engines can be mentioned as a new field of technology (Yowono, 1996). Industrial automation applications are still rare but research has been carried out in that field also. The logic explainer described below is based on the methods described in (Brayton *et al*., 1987), (Bartlett *et al*., 1988) and (Colon-Bonet *et al*., 1989).

Huuskonen (1997) divided explanation levels into four different categories: diagnostic level, behavioral level, functional level, and program level.

Program level is the lowest level; the machine code part of the paper winder programs in instruction list format can be mentioned as an example. Functional level is the level represented by the FBD program. For behavioral level, there is no clear analogy in the PLC program environment, but SFC can be considered to belong to this level. Diagnostic level can be considered as the level where PLC code is transformed into a representation that helps operators and maintenance people to solve problems in a machine or a process. A real system can include all levels or only some of them. If a system consists of only the program level, problem solving is very difficult in practice. Debugging assembler code is very demanding even for very skillful programmers. In a normal industrial PLC system, there exists a functional level also. This provides quite a good tool with which to solve problems for maintenance- and expert-level users, but it still demands a good level of knowledge of PLC programming and machine structure.

One practical solution that has been developed is a logic explainer (Plomp, 1997), which is based on research by Huuskonen *et al.* (1995 and 1997) and described in (Plomp *et al.,* 1996) and (Virtanen and Paanasalo, 2000). According to the definition above, the logic explainer belongs to the program, functional and diagnostic level. The logic explainer basically gives an answer to the following questions.

- What caused the observed signal transition?
- What should be done to achieve a transition in a given signal?

To be able to answer the first question, the system needs both a programmable logic code and historic data of previous signal values. To the second question, the answer is given in terms of the signal states that are needed to change in the Boolean function to make the output of the function to change its value. The logic explainer gives that answer in a format called a dependency graph.

In the figures below, an example of a function of the logic explainer is given. Figure 12 shows a typical, but rather complicated, network of a programmable logic code in a function block diagram format. Some input signals are in correct states, but some prevent the output reaching its correct value. The logic explainer filters those signals that are in a

correct state from the network. It then shows the result in a dependency graph format, as in Figure 13, which consists of basic function block diagram commands (AND, OR, NOT) and looks like a typical logic program network. This is, however, pseudo-PLC code and it is not equivalent to the actual logic program code. A dependency graph can be generated from PLC code, but original logic code cannot be generated from a dependency graph. Different kinds of dependency graphs will also be generated from the same logic program, depending on the signal states.

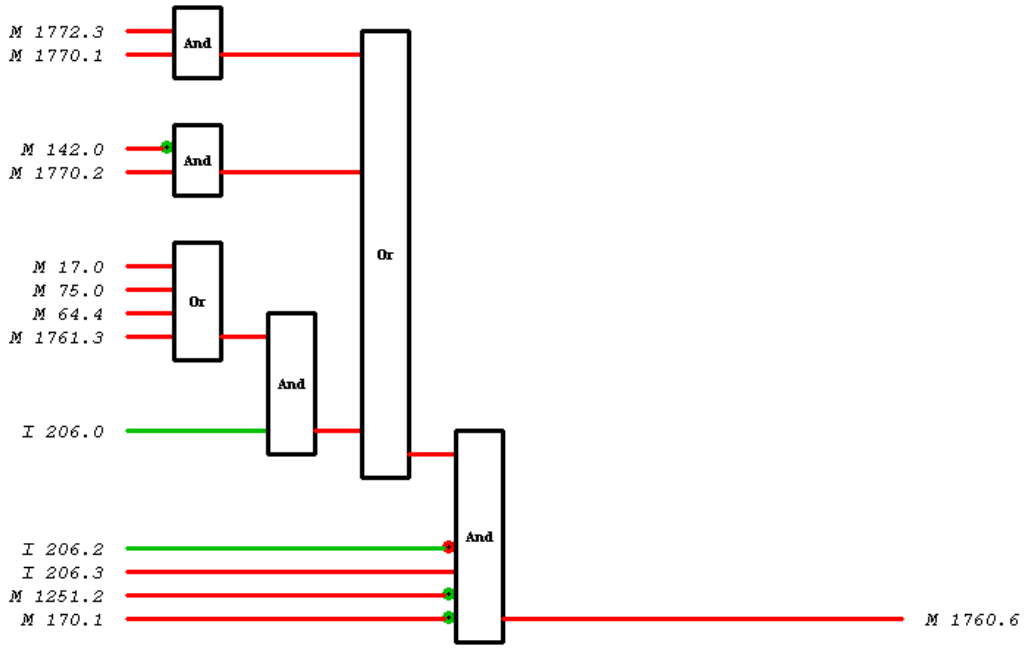

Figure 12: An example of a network presented in a function block diagram format.

Plomp *et al.* (1996) define levels of explanation (see Table 3-1) differently from Huuskonen (1997) and mention that the logic explainer belongs to level three (Dependency level). Plomp *et al.* also claim that the logic explainer is a good basis for natural language explanations for daily operators, but they are not concerned how those natural language explanations are generated from the dependency graphs.

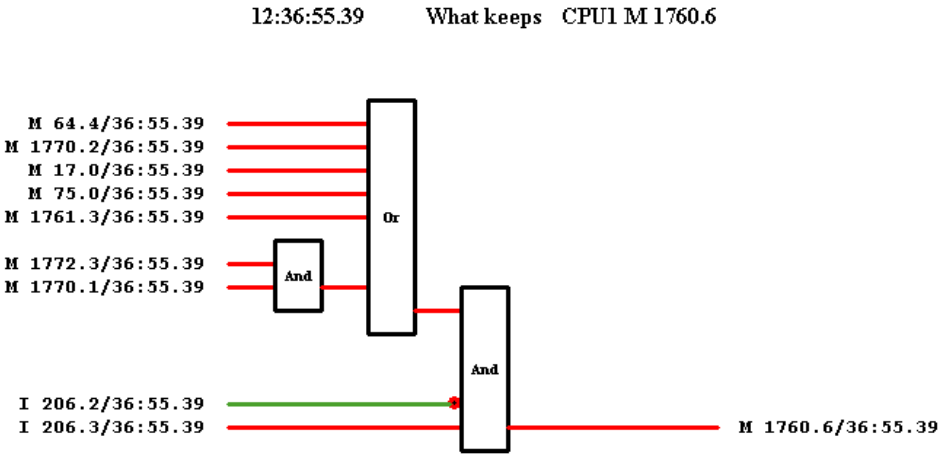

Figure 13: Dependency graph of the network in Figure 12 generated by the logic explainer.

The author has gained a lot of experience of using the logic explainer in practice over several years. The experience certainly supports the fact that the logic explainer is far too complicated for daily operators. It is assumed that Plomp *et al.* mean by *daily operator* the same as thesis calls an operator and mean by *operator* the same as in this work is called a maintenance person. Understanding the dependency graphs clearly requires a basic knowledge of PLC programming.

Table 3-1: Different levels of explanation according to Plomp *et al.* (1996).

Level	Representations	User
Diagnostic level	Machine diagram / Textual	Daily operator
Dependency level	Dependency graphs with timing	Internal/Operator
Logics level	Logic Networks / State machines	Operator
PLC level	Sequential instruction lists (assembly)	Programmer/ Operator

3.3. Transforming logic diagrams to minimal representation

In the previous section, a method was introduced to filter logic programs to be used for fault diagnostic purposes. In the following sections, Boolean algebra and other well-known methods of logic minimization are surveyed. A new method is also developed to transform complex logic programs and networks to a simple form. This can be represented in a graphical format to be used by (daily) operators.

3.3.1. Boolean algebra

Mathematician George Boole introduced Boolean algebra in the middle of the 19th century, see (Boole, 1854). His work created the basis for modern computer science and many of its applications. Boolean algebra, see, for example, (Whitesitt, 1961), is an algebra that deals with binary sets and binary operations: a union, an intersection and a complement. In Appendix 2, basic Boolean laws are summarized (Hill and Peterson, 1968).

A truth table as shown in Figure 14 is a common way to present logical functions. Truth tables are widely used in electrical circuit design. First, the desired logical function of apparatus or circuit is written in a truth table. Then the Boolean function of that truth table can be written. There are two well-known formats of a Boolean function that can be written from the truth table very straightforwardly (Hill and Peterson, 1968). These two basic forms of Boolean function are: Sum Of Products (SOP), and Product Of Sums (POS).

A	B	C	Q
0	0	0	0
0	0	1	0
0	1	0	0
0	1	1	1
1	0	0	0
1	0	1	0
1	1	0	1
1	1	1	1

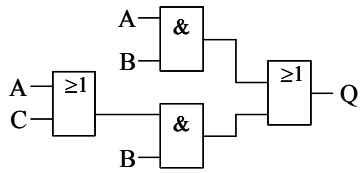

Figure 14: Truth table on the left and the equivalent PLC program in FBD format on the right.

A minterm is a row in the truth table, having the output value 1. A literal is the Boolean variable or its negation. There are three minterms in the truth table shown in Figure 14; every minterm consists of three literals. A SOP form can be written from a truth table by choosing all those rows (minterms) where output has the value true (=1). Then all literals

from a single row are connected with an AND operator and finally all AND circuits are connected with an OR operator (see example below).

In a POS format, all those rows (maxterms) are chosen where output has the value false (=0). Then signals are connected with an OR operator using inverted values of the literals. OR circuits are then connected with an AND operator. In the case of the example in Figure 14, the SOP and POS forms are:

$$Q = \left(\overline{A}\,B\,C\right) + \left(A\,B\,\overline{C}\right) + \left(A\,B\,C\right) \qquad \text{(SOP)}$$

$$Q = \left(A + B + C\right)\left(A + B + \overline{C}\right)\left(A + \overline{B} + C\right)\left(\overline{A} + B + C\right)\left(\overline{A} + B + \overline{C}\right) \qquad \text{(POS)}$$

When the Boolean function of a truth table has been developed it is easy to build, for example, an electrical circuit, which executes that logic function. Boolean functions above are not, however, minimal representations of the truth table.

3.3.2. Logic minimization

In the previous section, a Boolean function was generated from a truth table. As mentioned earlier, these functions were not a minimal representation. Before discussing minimization one must define a minimal logic function. The following definition (Hill and Peterson, 1968) concerns the two-level sum-of-product and product-of-sum type Boolean functions.

> "A second-order sum-of-products expression will be regarded as a *minimal* expression if there exists (1) no other equivalent expression involving fewer products, and (2) no other equivalent expression involving the same number of products but a smaller total number of literals. The minimal product of sums is the same with word *products* replaced by the word *sum*, and vice versa."

Minimization can be started either from the Boolean function itself or from the truth table. For example, if the expression from the above example is minimized with Distributive and Complement laws, the result is $Q = \left(\overline{A}\,B\,C\right) + \left(A\,B\right)$. It can be seen that there are lesser terms on the left but the logical function is the same. A Boolean function can be written also from the PLC program shown in Figure 14 and can be minimized with the laws of Boolean algebra. The result is $Q = \left(AB\right) + \left(B\left(A + C\right)\right) = \left(AB\right) + \left(BC\right)$. The results of the two minimizations were different and there was one literal less in a result after the second minimization. If the expression is minimized with a different procedure, where an actual function is canceled with each product term separately, the result is the minimal representation $Q = \left(AB\right) + \left(BC\right)$. The minimization results are now the same. Another possible way to minimize a Boolean function is to use the truth table itself. That is an

appropriate method especially when a truth table is created first to design electrical circuits, for example.

3.3.3. Quine-McCluskey algorithm

One basic method to find a minimal sum-of-product form from a truth table is the Quine-McCluskey algorithm, (Quine, 1952, McCluskey, 1959). It is an algorithm that does the same type of minimization as Karnaugh Maps, (Karnaugh, 1953). It is not a graphical, but a numerical, method, and the dimensions of the truth table are not limited in theory. However, in practice, computer memory size and the clock frequency of the processor (CPU speed) limit its use. If the Karnaugh Map is suitable for up to 4-6 variables in a Boolean function, the Quine-McCluskey algorithm is adequate for maybe up to 20 variables. The size of the truth table is 2^n lines where n is the number of inputs. Every line can produce a value of 0 or 1 so a 2^n line truth table may have 2^{2^n} different logic functions.

The Quine-McCluskey algorithm consists of two different algorithms. These can be further divided into three different steps assuming that the truth table already exists. This is not obvious in practice unless a design procedure has started from the truth table. The prime implicant is a minimum cover of two or more minterms. For example, the prime implicant for the minterms $\overline{A}BC\overline{D}$ and $ABC\overline{D}$ is $BC\overline{D}$. The essential prime implicants are the minimum cover of the prime implicants that implements the original Boolean function.

The three main steps of the Quine-McCluskey algorithm are:

1. Find all the prime implicants from the truth table's minterms.
2. Build a table where the relevant minterms are in columns and prime implicants in rows.
3. Find a minimum cover of prime implicants (essential prime implicants).

The first algorithm carries out the first step and the second algorithm steps 2 and 3.

Figure 15 shows how the first part of the algorithm functions. The first table in the figure is the truth table for which the minimum SOP representative is sought. The next table shows all the terms in the truth table, which gives an output value one (true) in the truth table. All the terms that differ only by one literal are searched for from those implicants. Character x is put in the position where literals differ and the result is written into the next table. That is continued until no more implicants can be found that differ only by one literal. Now, all the prime implicants of that truth table have been found. The prime implicants are surrounded with a thick black line. The duplicate implicants are dropped away during that procedure.

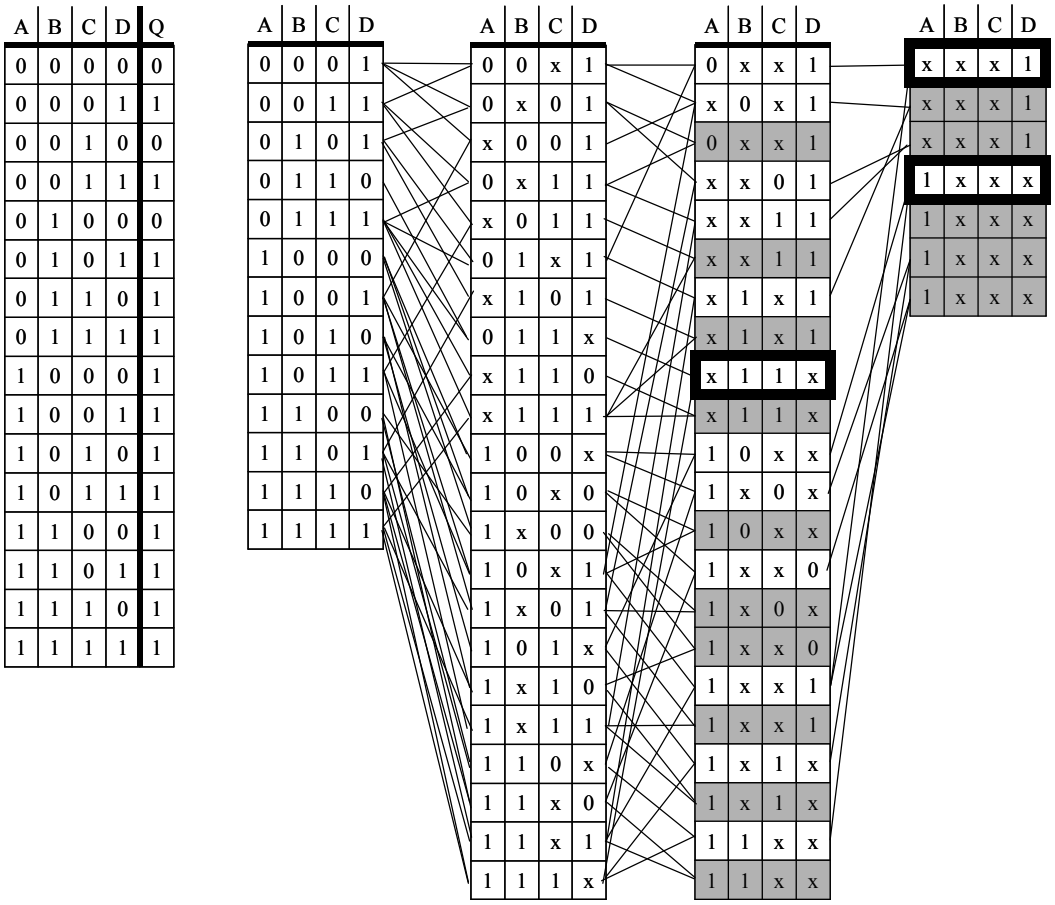

Figure 15: The first part of the Quine-McCluskey algorithm.

The second phase of the Quine-McCluskey algorithm finds the minimum cover of the prime implicants (essential prime implicants) from the result of phase one. In the second part, prime implicants are located in rows and relevant minterms in columns (see Figure 16). Checks are put on those positions where the prime implicants cover minterms. Then the first column is searched for where there exists only one check and a line is drawn down through that column. A line is also drawn horizontally through that row. Then circles are drawn on those indexes where the checks are on that current row. The procedure is repeated for every column where there is only one check and the index of which is not yet circled. In Figure 16, all indexes are circled at that point. If there are still indexes that are not circled, the column, which has the least checks, is chosen. A line is drawn through the row, which covers as many checks as possible. That is continued until all indexes are circled. At that point, all essential prime implicants have been found and they are on those rows through which lines are drawn. The final result is $Q = A + D + BC$.

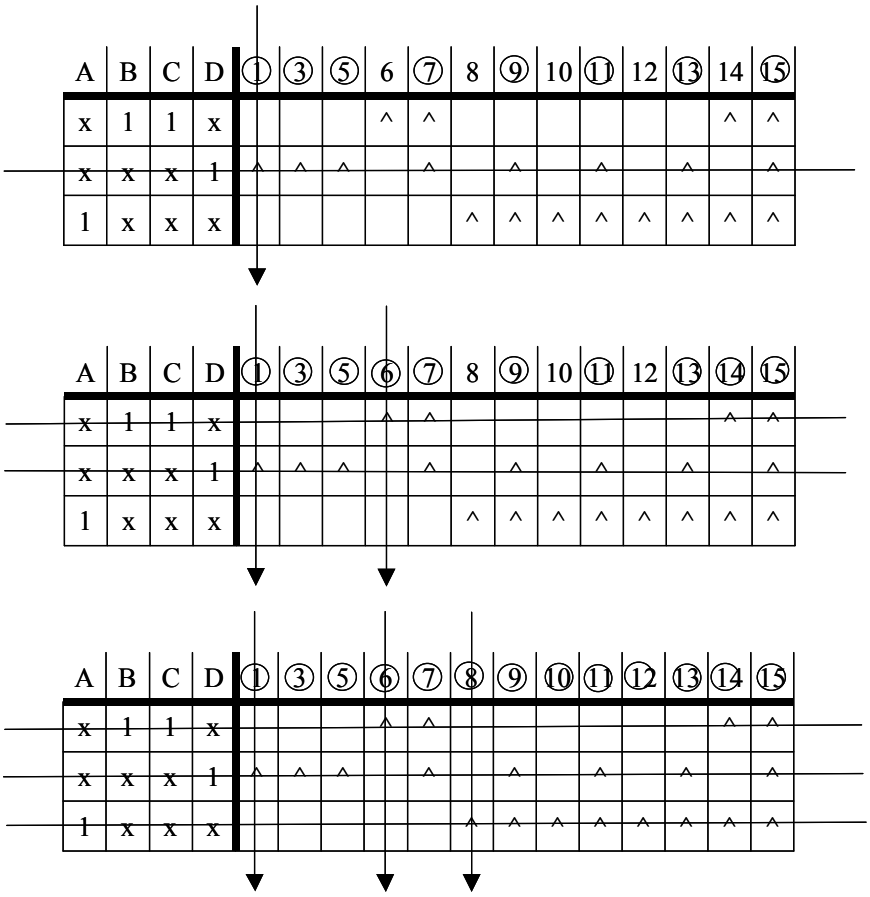

Figure 16: Second part of Quine-McCluskey algorithm finds the essential prime implicants.

3.3.4. Other SOP minimization methods

In the previous sections, two basic methods were introduced to minimize the logic functions. In this section, a survey of other methods is presented. Hong and Muroga (1991) classified the different methods as follows.

- Map, (Karnaugh, 1953)
- Tabular, (McCluskey, 1959) and (Hong *et al.*, 1974)
- Cube reduction, (Brayton *et al.*, 1984)
- Algebraic, (Quine, 1952)

One tabular method was described in Section 3.3.3. The Cube reduction methods are close to the Map methods but are extended to n-dimensions. For large-scale systems, there are,

for example, the Espresso method (McGeer *et al.*, 1993) and the inclusion function method (Hong and Muroga, 1991) and others, e.g., (Rudell and Sangiovanni-Vincentelli, 1987), (Coudert *et al.*, 1993) and (Coudert, 1995). The Espresso method can handle larger systems than the Quine-McCluskey method can, but it does not guarantee the minimum solution and there is a trade-off between the absolute minimum and computing time. There are also other types of methods similar to Espresso, e.g., (Hlavicka, 2001). The issues concerning prime implicants in the tabular methods are treated in, for example, (McMullen and Shearer, 1986) and (Sloan *et al.*, 2005).

3.4. Multilevel Product-Of-Sums net

Methods described in the previous sections are developed basically to design electrical circuits and devices. The use of truth tables is rare in PLC programming. In comparison to typical electrical circuits, PLC programs of paper winders are quite large. Both the number of terms and the number of literals are high. Figure 17 shows that there can be over 25000 different binary signals in use in a modern industrial PLC.

type	abbreviation	number of bits
input	E	4096
output	A	4096
timer	T	512
flag	M	16384
		total 25088 bits

Figure 17: Typical numbers of signals in use in the Siemens S7 400-series PLC.

The number 25000 is only a number of different signals, but the number of literals can be much higher, because the same signal can occur in several places in a PLC program. However, not every bit is in use and it is estimated that there are about 20-40000 literals in a typical PLC program of a paper winder. The estimated number of terms is 5000-10000. The size of a truth table of the whole PLC memory space could be 2^{25088} ($\sim 10^{7552}$) lines, so it would be impossible to generate it in practice.

In a PLC, inputs are measurements that are read with separate input cards and outputs are control signals that are written out through output cards. Those I/O cards are the PLC's

connection interface to a paper winder. Earlier, these cards were the only interface to the PLC but nowadays it is possible to read and write signal values through industrial networks (e.g., Ethernet, Profibus). In PLC programs, output signals can also be inputs in logical functions. Consequently, all types of signals can be regarded as a similar type of literals.

PC applications consist of several computer programs. They are built from smaller functions and procedures. Similarly, a winder control program is not one huge logic function, but consists of several functions and networks. There are typically different types of functions in PLCs (for example, a function (FC), a function block (FB) and an organization block (OB)). Different types of functions are used to clarify the program structure of the PLC, but their logic function is the same. Note that the expression "function" covers all types of PLC programs in this work.

The logic functions are divided further into networks. A network consists of one logical function with inputs and one or several outputs. In the networks of paper winder PLC programs (see Figure 18), the number of literals is typically ranges from 2 to 50, but it is possible to write networks larger than that.

However, networks are not totally separated from each other. An input signal in one network can also be output or input signal in another network. In fact, one large logic function could cover the whole control logic of a paper winder, but it is undoubtedly clearer to handle the program in pieces.

The logic program can be considered as a net where a single network models a block and connections between them are called nodes. Notation of blocks and nodes has been used also in (Plomp, 1997), where a general description of a PLC logic model was presented. The Multilevel Product-Of-Sums net (MPOS-net) model (Virtanen, 2004) described below differs from the PLC logic model in some details. There are at least three types of blocks in the PLC logic model (functions, function blocks and programs). The MPOS-net model contains only one type of block.

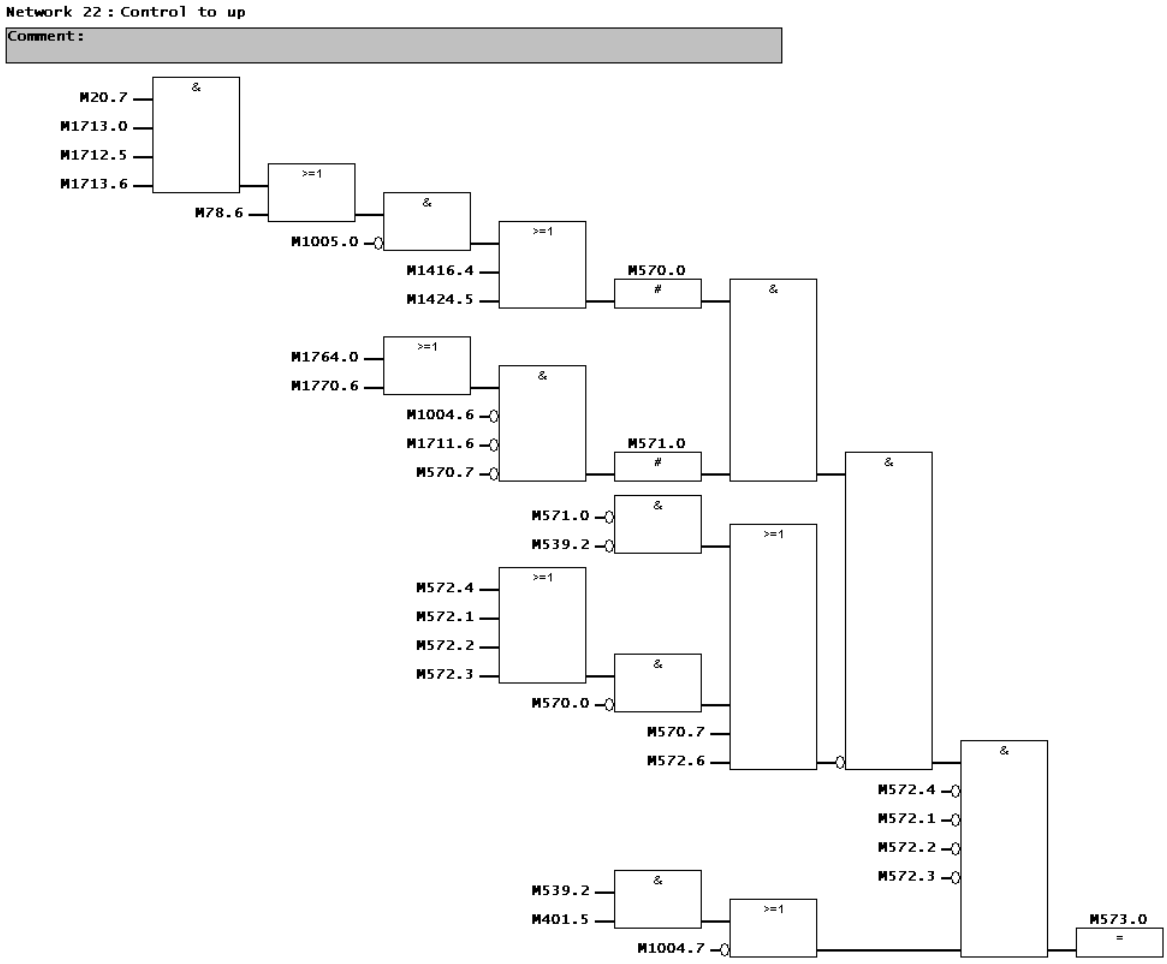

Figure 18: Structure of a network of a paper winder (31 literals).

Blocks in a PLC logic model are multilevel logic functions, the structures of which vary a great deal. In the MPOS-net model, all the blocks are transformed into a POS format; hence it enables their use in graphical format in fault diagnostic systems.

From Figure 19 it can be seen that the number of terms (3) is the same in both models. However, the number of literals in the PLC logic model is four, and in the MPOS-net model, five. Actually, that is true even though the MPOS-net model is in a minimum POS format according to the definition in Section 3.3.2. It can be seen that there is one level more in the PLC logic model, which explains why there can be fewer literals than in the minimum POS representation. This same phenomenon is studied in, for instance, (Perkowski *et al.*, 1992). Basically, logic minimization can be performed in terms of at least the following three variables: terms, literals and levels, and their combinations.

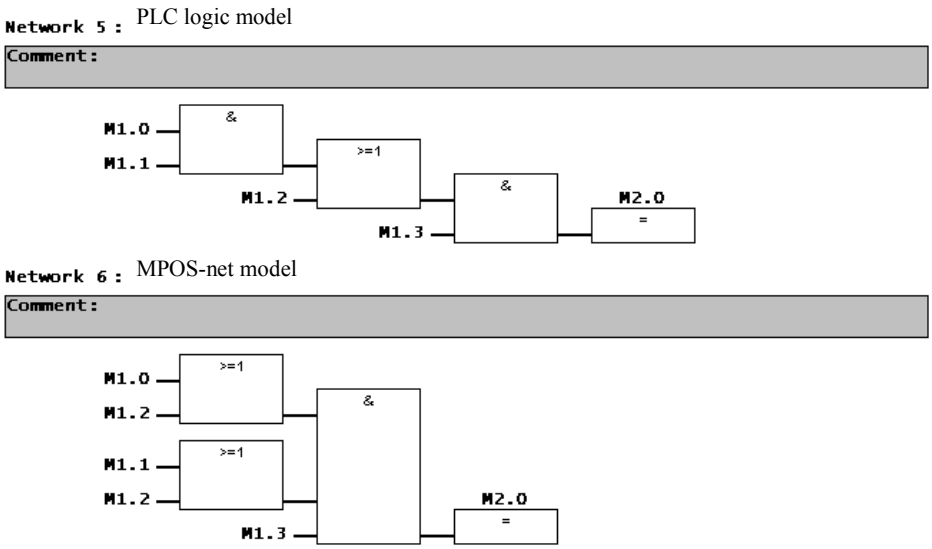

Figure 19: Networks in a PLC logic model, above, and MPOS-net model format, below. The logic function of both representations is the same.

Figure 20 demonstrates the structure of the MPOS-net. Primary inputs and outputs are the only signal types that exist in the model. Intermediate signals (see M570.0 and M571.0 in Figure 18) are either removed or made into separate blocks. It is important to point out also that every node between the blocks is also an output of the net, because it is possible to read out every signal value out from the PLC.

Blocks are transformed to a POS format, which enables their use in fault diagnostic systems. Logic functions in POS format can be converted into a graphical format. That enables searching through PLC code without basic knowledge of PLC programming. Signal states are indicated with colors as mentioned earlier. A red color means a prohibitive signal that prevents the winder from executing a certain function and a green color means that signal is in a correct state. Different OR-terms are separated with indexes and colors. Single signals are also drawn with a different symbol. The user can choose either to look at all signals or only prohibitive ones. When the user studies only prohibitive signals, an OR-term is shown only if all its literals are in a prohibitive state. Figure 21 points out the difference between those two graphical representatives. In comparison to the logic explainer described in Section 3.2.2, the basic difference is the use of graphical symbols instead of function block diagrams.

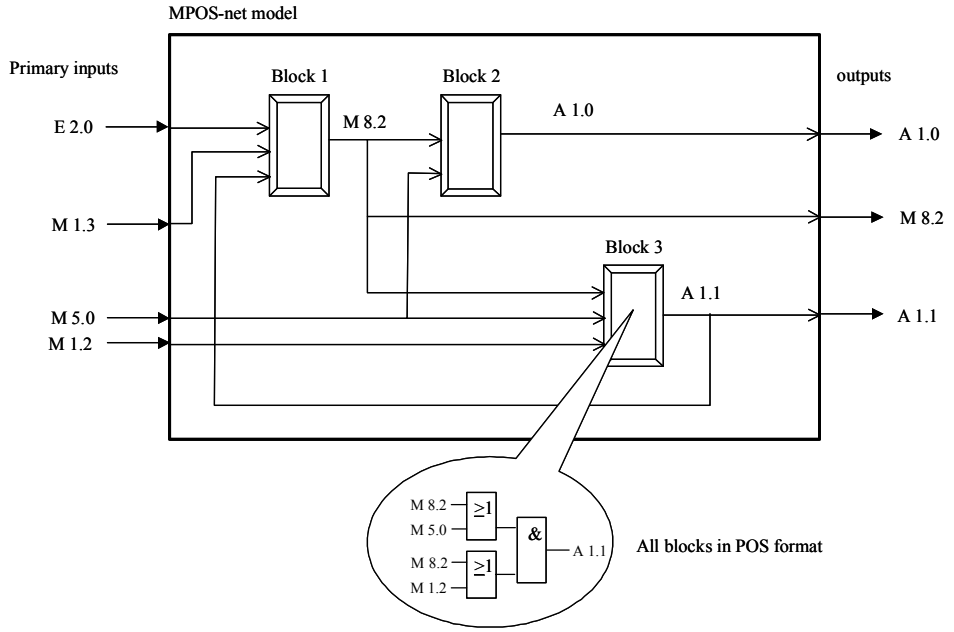

Figure 20: The Multilevel Product-Of-Sums models consist of inputs, outputs, nodes and blocks in POS format (Virtanen, 2004).

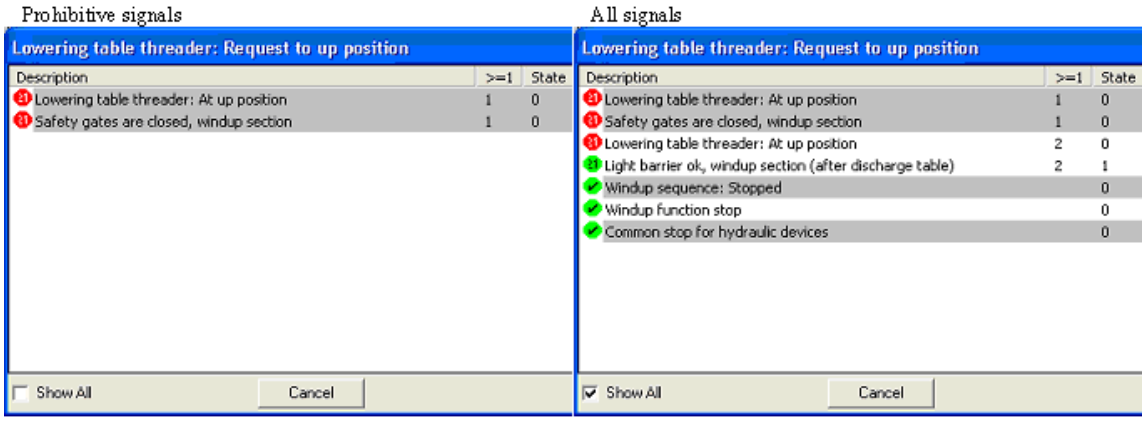

Figure 21: Fault diagnostic window showing only prohibitive signals and all signals (Virtanen, 2004). OR circuits (>=1) are separated with numbered indexes and colors.

3.5. Level-to-Level-Minimization algorithm

In the previous section, the MPOS-net model for PLC programs was introduced. In this model, all blocks are in product-of-sum format. In this section, a method is introduced to transform large logic functions into POS format.

The basis for the transformation is, however, different from that in the methods described in Section 3.3.3. Minimization does not start from the truth table but from the PLC program written by a programmer. The reader is also asked to bear in mind that PLC programs and programming is limited here to paper winders and their control systems. Logic programs written by programmers are usually near minimum representation regarding the number of literals or number of terms (logic gates). On the other hand, the number of levels is usually higher than in the POS format (two levels).

In other words, if Quine-McCluskey algorithm is designed to generate minimum SOP (sum-of-products) representation from a truth table of a small- or medium-size logic function, the Level-to-Level-Minimization algorithm (LLM-algorithm) described in this section is designed to generate the minimum or near-minimum POS (product-of-sums) representation from small to large size near-minimum multilevel (see Figure 22) logic Boolean functions.

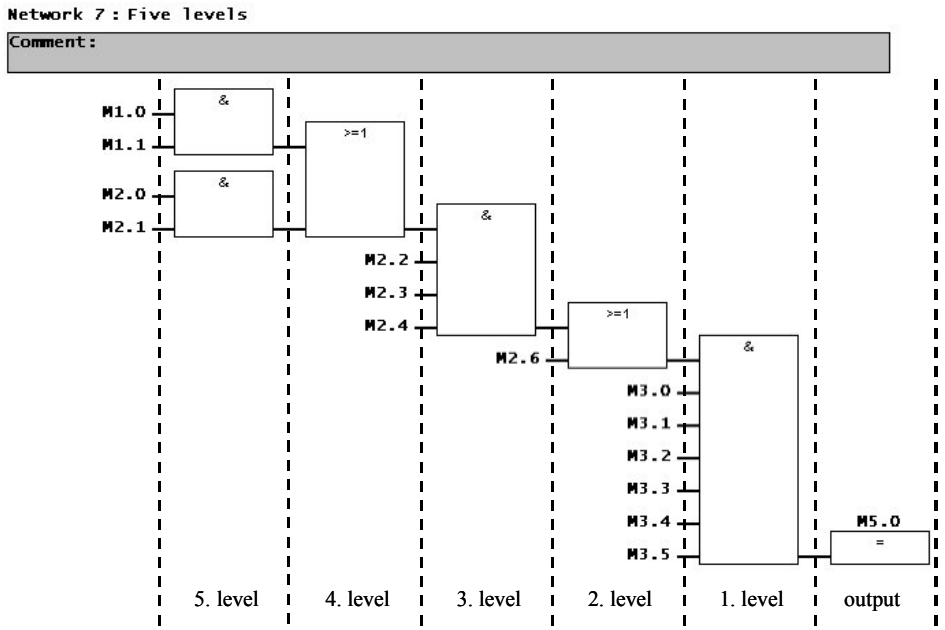

Figure 22: Multilevel logic function in FBD (Function Block Diagram) format.

The basic principle of the LLM-algorithm is to transform a logic function to a two-level POS format level by level. Minimization is performed every time the level is removed until only two levels are left. A result can be, however, in SOP format at this time and conversion from SOP to POS format is performed in that case. Furthermore, if there exist several branches, minimization is performed similarly and separately for every branch. The algorithm is summarized in Figure 23.

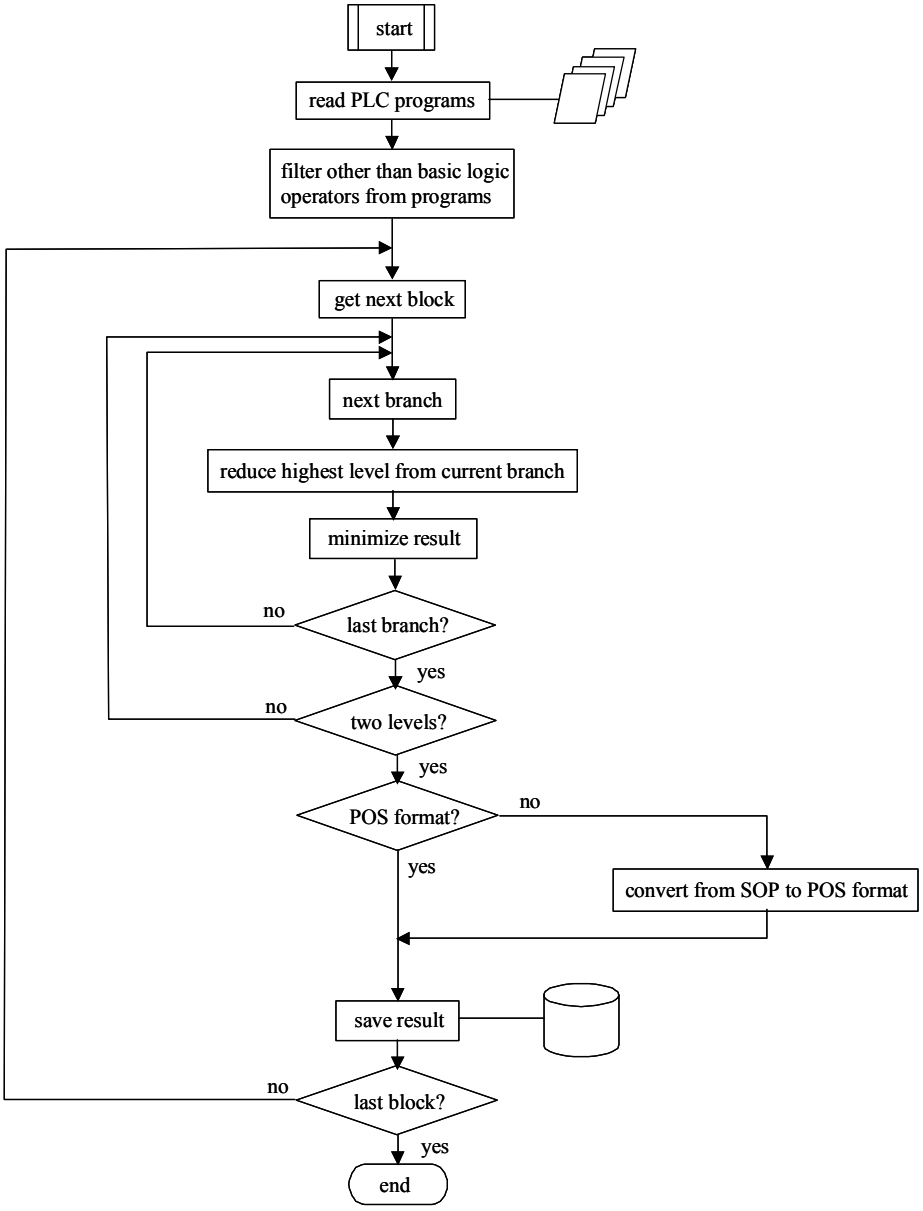

Figure 23: Basic functions of Level-to-Level-Minimization algorithm.

Minimization is based on the following Boolean laws: Complement, Idempotent, Absorption, DeMorgan's, and Distributive laws.

As mentioned earlier, LLM-algorithm does not guarantee absolute minimum, but for those types of logic functions used in paper winders the result is, in practice, a minimum representation. Next, the differences between LLM-algorithm and Quine-McCluskey algorithm are evaluated more precisely.

Let F be a Boolean function consisting of n maxterms X_i, $i=1,...,n$

$$F(X_i) = \sum_{i=1}^{n} X_i \tag{3.1}$$

where maxterm X_n includes k_n literals a_{ni}, $n_i=n_1,...,n_{kn}$

$$X_n(a_{nk_n}) = \underbrace{a_{n1} + a_{n2} + ... + a_{nk_n}}_{k_n} \tag{3.2}$$

Every literal is unique, so $a_{ij} = a_{km}$ if and only if $i = k, \quad j = m$.

Quine-McCluskey algorithm

For function $F(X_i)$ in (3.1), the number of lines N_{LN} in the truth table is

$$N_{LN} = 2^{(k_1+k_2+...+k_n)} \tag{3.3}$$

where k_i, $k_i = k_1,...,k_n$, is the number of literals in maxterm X_i and N_{LN} the number of maxterms and minterms. The number of binary digits N_{QM} is

$$N_{QM} = N_{LN} \underbrace{(k_1 + k_2 + ... + k_n)}_{number\ of\ literals} \tag{3.4}$$

LLM algorithm

For function $F(X_i)$ in (3.1), the number of minterms N_T after conversion from POS -> SOP is

$$N_T = k_1 \cdot k_2 \cdot ... \cdot k_n \tag{3.5}$$

and the number of binary digits N_{LLM}

$$N_{LLM} = n \cdot N_T \tag{3.6}$$

Example 3.1: Let F be a Boolean function $F = (A + B) \cdot (C + D)$ so that k_1=2 and k_2=2.

For the Quine-McCluskey algorithm, $N_{LN} = 2^{(2+2)} = 16$ and the number of digits in the truth table $N_{QM} = 16 \cdot 4 = 64$.

For LLM algorithm $N_T = 2 \cdot 2 = 4$ and number of digits in minterms $N_{LLM} = 2 \cdot 4 = 8$.

Function F after conversion from POS->SOP is $F = (A \cdot C) + (B \cdot C) + (A \cdot D) + (B \cdot D)$

To study the memory requirements of these two algorithms, a few test cases were generated with different types of logic functions. The first test function was a two-term POS-type Boolean function where the number of literals in both terms was increased from 1 to 15. The maximum number of different literals was therefore 30. Results are presented in Figures 24 and 25.

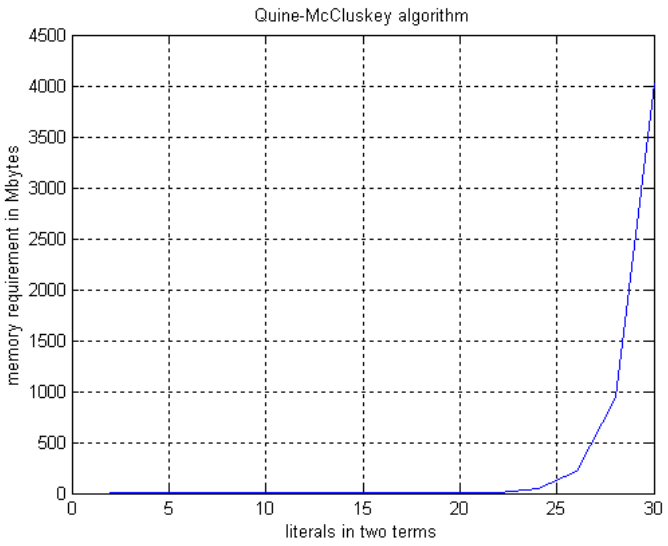

Figure 24: Memory requirement of Quine-McCluskey algorithm's truth table with a different number of literals.

With a maximum number of 15 literals in both OR-gates (totaling 30), the truth table requires a memory of 4000 Mbytes. The LLM algorithm, however, can produce a SOP format of the function with only a memory of 56 bytes, so the difference is remarkable.

The benefits of the LLM algorithm nevertheless bring out just the best with this type of functions. For that reason, other types of function were also tested.

In the second test, a similar type of function was used but the number of terms was increased and the number of literals (2) in each term was constant. The result for the Quine-McCluskey algorithm was the same, because only the number of literals affects the memory requirements of the truth table, not the structure of the Boolean function. In comparison to the LLM algorithm, the result was different.

In contrast to the Quine-McCluskey algorithm, the structure of a function has a significant influence on the memory requirement of the LLM algorithm. Figure 26 shows the result of a second study of memory requirements. In the first case, the memory need was only 450 bytes, but in the second case it was already 60 Kbytes. Still much less than 4000 Mbytes was needed for the truth table, but it shows how strongly the memory requirement can vary.

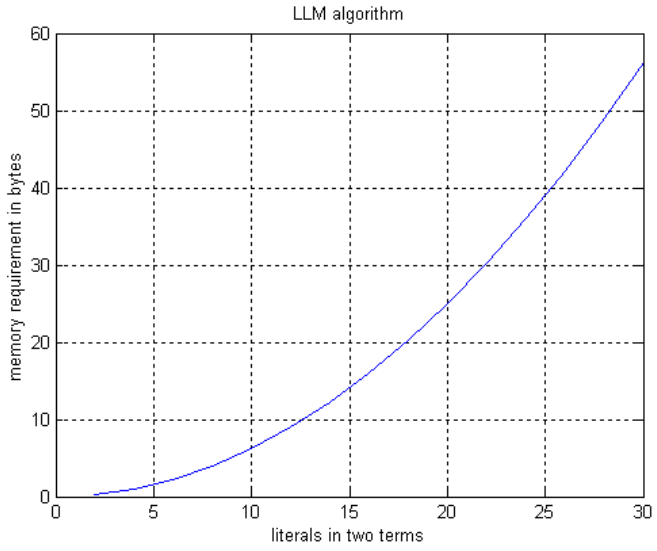

Figure 25: Memory requirement of the LLM algorithm after POS->SOP conversion as a function of number of literals in terms.

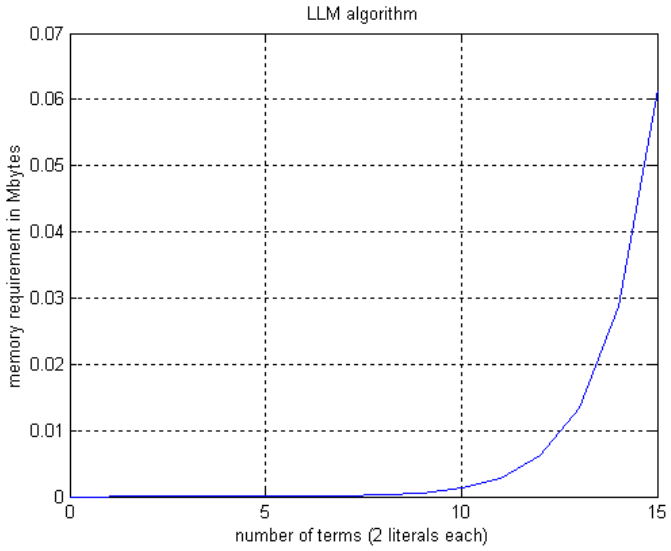

Figure 26: Memory requirement of the LLM algorithm as a function of number of terms with two literals each.

Minimization of different types of logic functions was also studied (see Appendix 3). The results are collected in Table 3-2.

Table 3-2: Results of logic function minimization with Quine-McCluskey (QM) and LLM algorithm.

Non-minimized logic function	QM-algorithm	LLM-algorithm
Q=D+(C(AB+AC))	Q=(A+D)(C+D)	Q=(A+D)(C+D)
Q=D(ABC+~ABC+~AB~C+~A~BC+~A~B~C)	Q=D(~A+B)(~A+C)	Q=D(~A+B)(~A+C)
Q=(D+AB~C)(D+BC+ABC)	Q=D	Q=D
Q=D(BC+~AC+AB)	Q=D(~A+B)(A+C)	Q=D(~A+B)(A+C)(B+C)
Q=DC(B+(A~B))	Q=DC(A+B)	Q=DC(A+B)

Basically, the Quine-McCluskey algorithm gives its result in an SOP format. Even so, minimizing the maxterms instead of the minterms and converting the result with De Morgan Laws can produce the minimum POS format. Results were similar in every other case, except in Case 4, where the LLM algorithm did not minimize the function as much as the Quine-McCluskey algorithm. The reason is that the minimization rule (A+B)(~A+C)(B+C)= (A+B)(~A+C) is not included in the LLM algorithm at the moment.

Actually this is not a problem in this particular winder case, because this type of logic functions is very rare in a winder control logic program; on the other hand, this type of near-minimum representative is almost as useful as the minimum form in fault diagnostic systems. The rule mentioned above was left out mainly to save computation time and to simplify the program.

3.6. Practical example

In the previous sections, a model was introduced to represent PLC functions in the POS format and the links between them and also the LLM algorithm were used to convert the original functions into that format. In this section, a practical example of using these tools in actual customer projects is discussed.

The control program of a paper winder consists of several functions and every function consists of several networks. The single network shown in Figure 27 models one Boolean function. The first step is to download the required programs from a PLC project of a paper winder such as that shown in Figure 28. Downloaded source code is then read to a configuration program, which converts the Boolean functions in the networks into POS format with the Level-to-Level-Minimization algorithm presented in Figure 23.

The result is stored in a database, which can be examined with a special tool developed for that purpose. The user interface of that tool is shown in Figure 29, and the signals of a splicing permit can be seen on the left side of that window.

However, the aim of this procedure was to represent PLC programs in a graphical format without any numerical data. The transformation of networks to POS format makes that possible.

Another kind of user interface is used to show the fault diagnostic data to operators and maintenance people (see Figure 30). In that system, basically three levels of indicators can be seen. The simplest one shows, for example, the states of the safety gates and photocells. Such safety equipment, though simple, prevents the operation of many devices in a paper winder. With these indicators, an operator can see the states of the safety equipment at a glance.

A second type of indicator shows the states of different kinds of permits. This indicator does not necessarily mean that there is a fault in a paper winder, but it does indicate that a certain control action cannot proceed at that time.

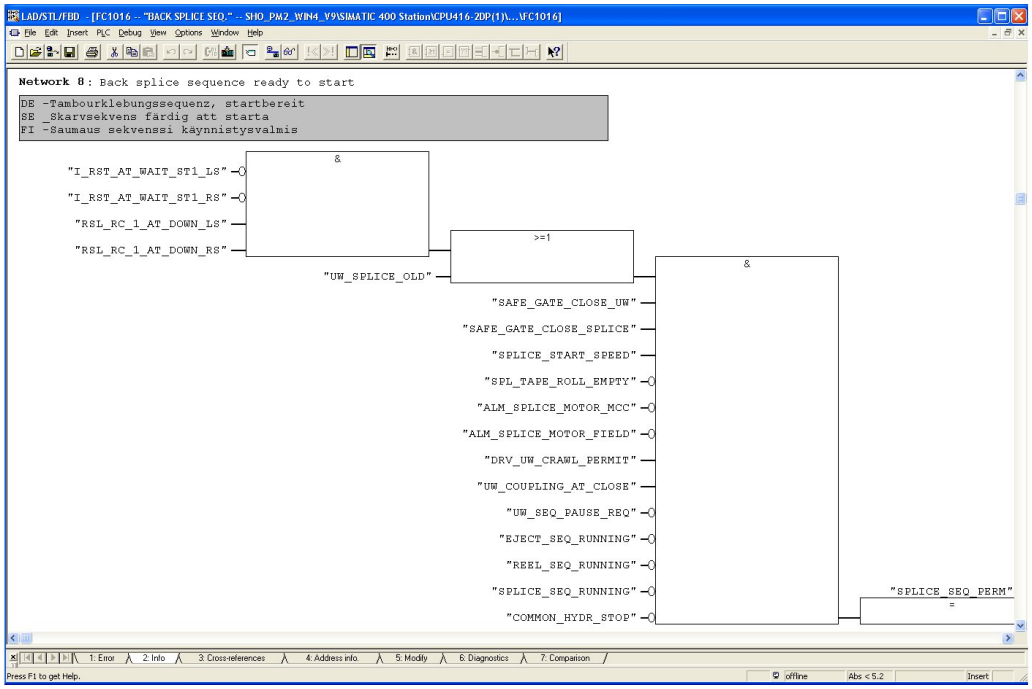

Figure 27: A typical network of a PLC program. An output of a network is a permit to execute a splicing sequence.

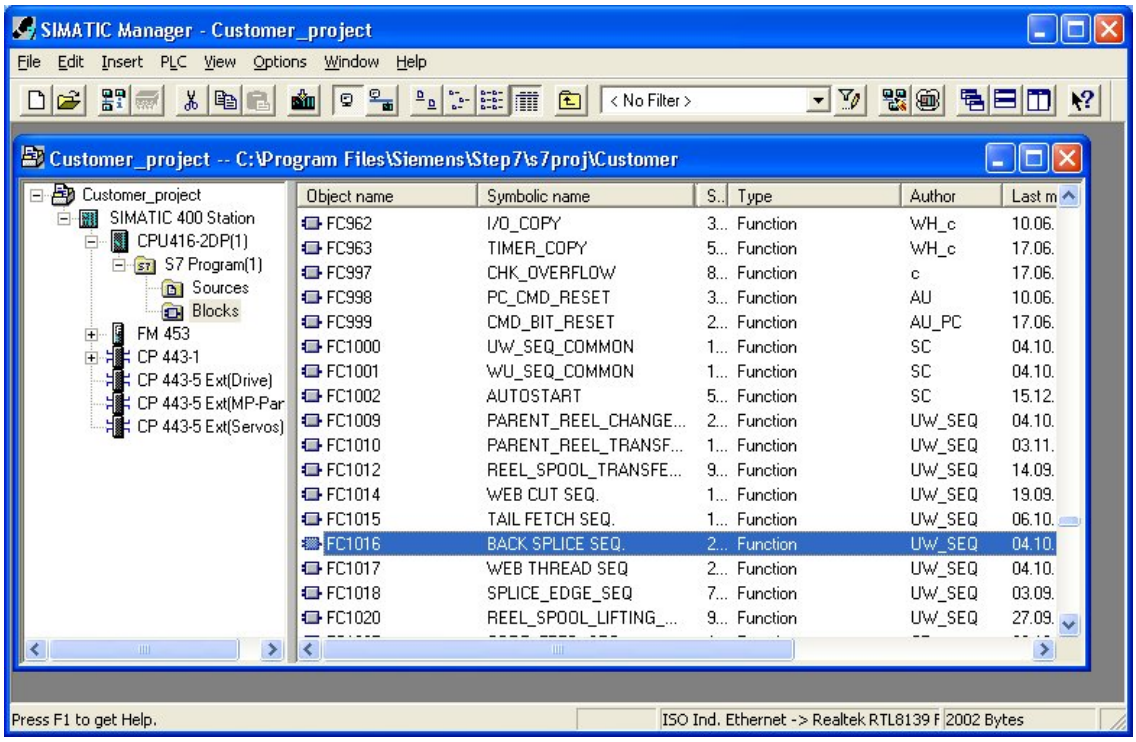

Figure 28: User interface of the programming tool for programming logic controllers. Programs that are to be converted to a fault diagnostic system are downloaded with these kinds of standard tools.

A third kind of indicator alarms when a certain control action is attempted but some locking signal prevents that action. This kind of alarm usually demands some corrective actions from operators.

In the example shown in Figure 30, the unwind crawl permit is missing and that is why it is not possible to proceed with the splicing sequence. However, this unwind crawl permit is an output of another network. As can be seen in the Multilevel Product-Of-Sums model in Figure 20, there are links between different nodes, i.e., networks, in POS format. These links can be used to find the primary cause of the fault. In practice, the operator can go through those links in the alarm windows graphically with a computer mouse. The primary reason for this fault was that the unwind gearbox oil pressure was too low. It can be seen from the actual program code shown in Figure 27 that the primary cause (gearbox oil pressure too low -signal) of this fault cannot be found from the locking signals of the splicing permit. It can be seen from Figure 30 that the unwind crawl permit (DRV_UW_CRAWL_PERMIT) prevents the control action. Now, by clicking the unwind crawl permit signal with a computer mouse in the fault diagnostic window, an operator can open the locking signals of the unwind crawl permit and find the primary reason of the fault.

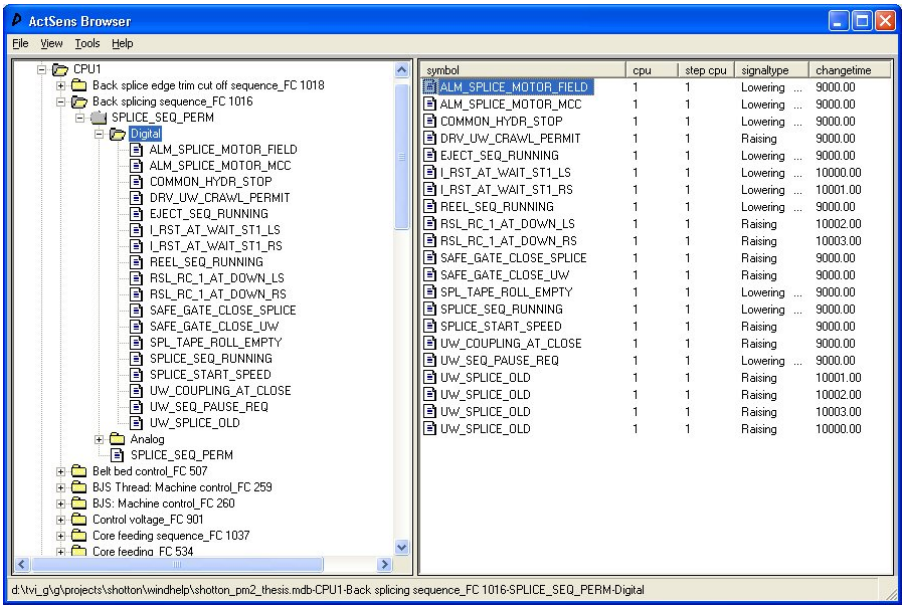

Figure 29: A special tool to examine the fault diagnostic database. The structure of a database can be seen on the left side and correct values of single signals on the right side of the window.

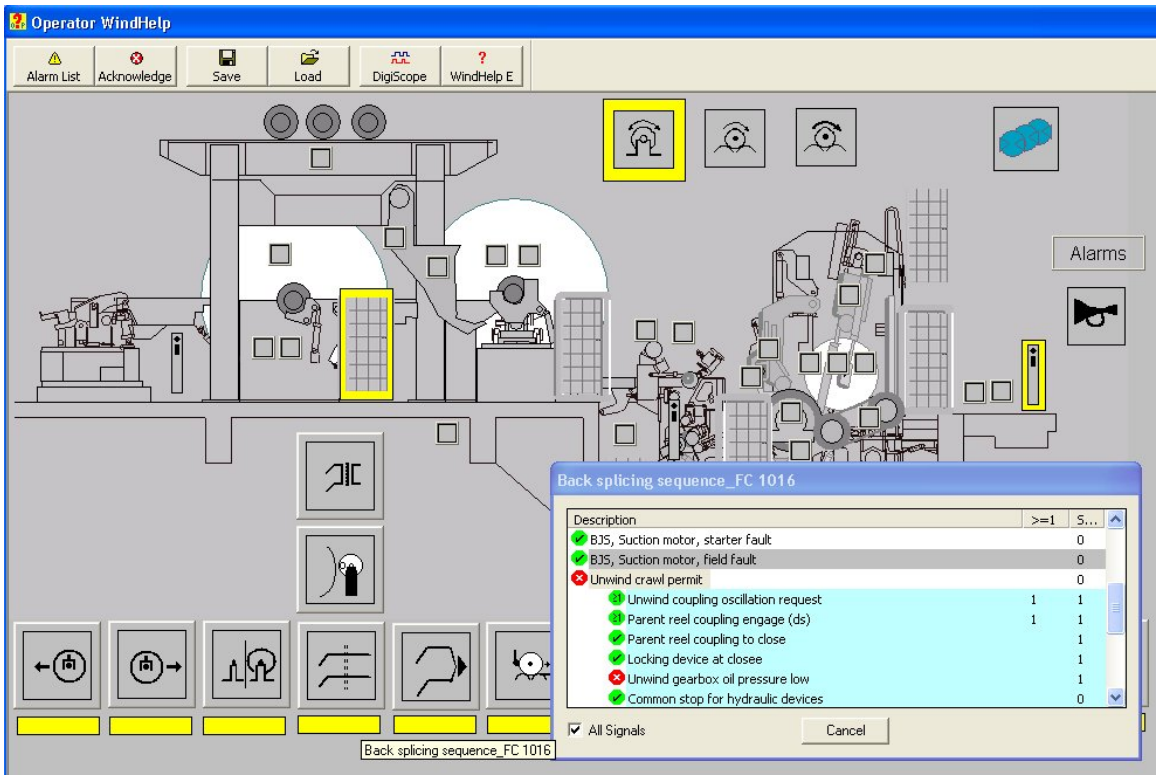

Figure 30: User interface of the fault diagnostic system developed for the operators and maintenance people. Yellow is an indication of a fault or that a certain permit is in prohibited state.

4. Fault diagnostics - analog part

4.1. Introduction to common methods

The methods for fault diagnostics of binary signals described in Chapter 3 are only one part of the field of the fault diagnostic research in the area of paper winders. Much research has been carried out concerning analog signals and systems. The Fault Detection and Isolation (FDI) methods have been researched actively during the last decade. In large and complicated systems it is difficult to observe single faults without some systematic methods. The worst case is that the process seems to continue normally after a fault but there are still some quality problems in the end product. In the paper winder case, there are certain quality parameters and defects in a paper roll that cannot be measured without breaking a paper roll. The most typical ones are listed below.

- Radial tension profile
- Tension profile at lateral direction
- Crepe wrinkles (see Figure 31) and corrugation
- Puckers

These kinds of defects in rolls can cause significant economic losses for paper mills. If the defective rolls are not noticed until at the printing house, the rolls are returned back to the paper mill. It is not only expensive, but it lowers the paper mill's reputation as a reliable deliverer, too. For economic reasons, printing houses keep a very small store of paper rolls, so defective rolls cause problems in their production very rapidly.

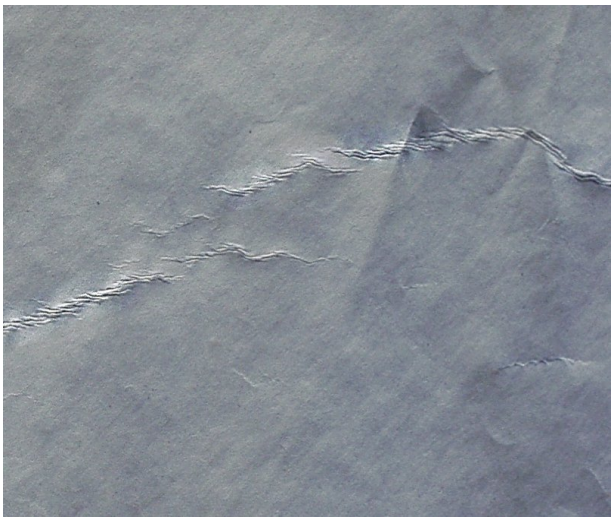

Figure 31: Crepe wrinkles in paper web (photo courtesy of Metso Paper).

When articles written about fault detection and diagnosis are studied, it can be seen that the terminology used is far from uniform. The IFAC Technical Committee SAFEPROCESS has tried to define commonly accepted terms. Some basic terms are represented below, (Isermann and Balle, 1997).

States and signals

- Fault – An unpermitted deviation of at least one characteristic property or parameter of the system from acceptable / usual / standard condition
- Failure – A permanent interruption of the system's ability to perform a required function under specified operating conditions
- Error – A deviation between a measured or computed value and the true, specified or theoretically correct, value
- Residual – A fault indicator, based on the deviation between measurements and model-equation-based computations

Functions

- Fault detection – Determination of the faults present in a system and the time detection
- Fault isolation – Determination of the kind, location and time of the detection of a fault. Follows fault detection

System properties

- Reliability – Ability of a system to perform the required function under stated conditions, within a given scope, during a given period of time.

- Availability – Probability that a system or equipment will operate satisfactorily and effectively at any point in time.

Reliability and Availability seem very straightforward to calculate, but in practice their calculation is not so clear. In continuous processes like those of paper machines, a situation is simpler than in batch processes. The paper winding process can be considered as a batch process, because a set of rolls is produced from a large paper reel. Two examples are listed below where the availability of a paper winder is not so well defined.

1. There is always spare time between the reel changes, so if the winder is repaired during that time, is it available or not?

2. There will be a shutdown on a paper machine and winders are not needed to run for that reason. The paper mill decides to do some maintenance and repair work on the winders during that shutdown. Now the winders are not available; they are shut down in any case.

Automatic calculations of Reliability and Availability are difficult, too, because winders are standing idle for many reasons. The author of the thesis has developed one semi-automatic system for a paper mill. Some alternative downtime reasons were:

- Normal set change
- No paper
- Control voltage problem
- Instrument Air problem
- Hydraulic problem

The system was installed into a re-winder, i.e., a small winder that can be used to rewind small rolls coming from the normal winders. A pop-up window was opened every time a re-winder was started. The system automatically suggested some choices or operator could choose reasons manually. Operators could also add comments manually on downtime data messages.

4.2. Monitoring of tension control

One basic FDI method is to use a process model to estimate the system output and compare it to the measured value. Basics on the use of neural networks in process fault diagnosis can be found in (Sorsa *et al.*, 1991), for example. A case study of web tension measurement is treated here. Different types of faults in paper winders cause different types of errors between the actual and estimated tension. A multilayer feedforward network was used as a process model/output estimator (see Figure 32). It consists of one hidden layer with 50 nodes and an output layer of one node. The number of 50 nodes was selected by trial and error and gave a satisfactory result. The training of the network was achieved with a backpropagation algorithm. There are, of course, more sophisticated algorithms, but the scope of this study was to determine whether these kinds of methods are suited for FDI in paper winders in general. A tan-sigmoid function was used in the hidden layer and a linear transfer function in the output layer. The measurement data consisted of five different test runs. The tests carried out with the full-scale pilot winder located in the Winding Technology Center in Järvenpää (see Figure 33). Every set of data consisted of five measured parameters, roughly 400 data-points in each.

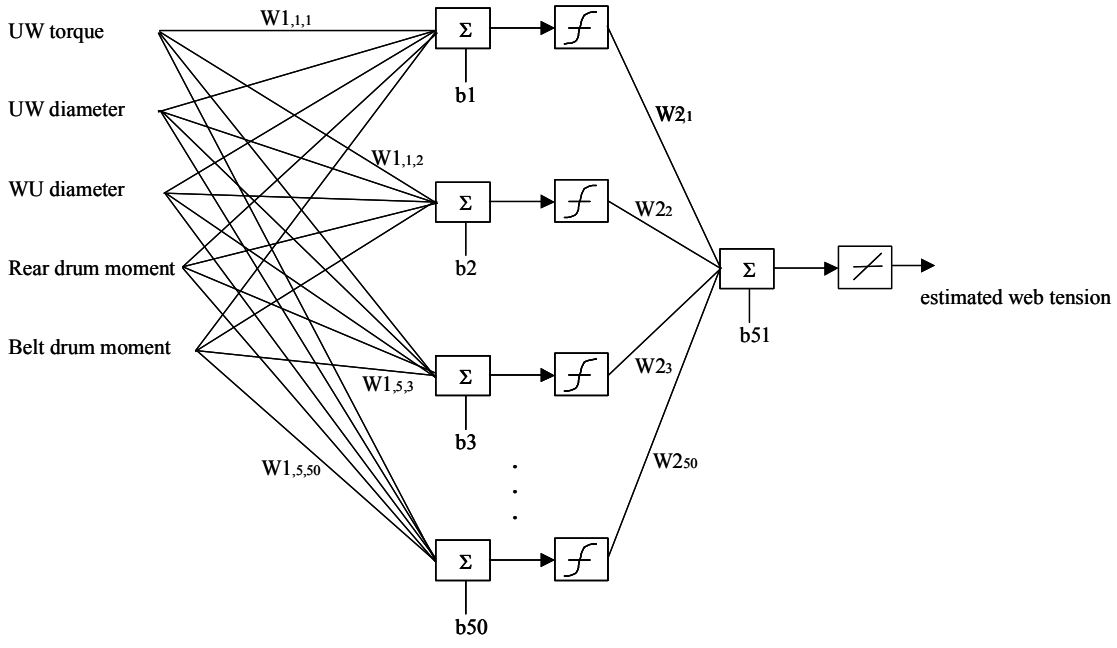

Figure 32: Structure of multilayer feedforward network used in web tension estimation.

Figure 33: The Winding Technology Center. The multi-station winder in front and two-drum winder used in tests in back (photo courtesy of Metso Paper).

Figure 34 (down-right) demonstrates a simulation result of the web tension estimator. The most demanding task was to adjust the estimator to work during the acceleration and deceleration of a paper winder. The different defects in the measurements or in the machine itself were simulated. Faults can be divided into two basic categories (Simani *et al.*, 2003). Additive faults affect the system by summation and multiplicative faults by multiplication. Summation types of errors were generated in unwind, rear drum and belt drum torques in the following simulations. Results of these three simulations are shown in Figure 34 and corresponding estimation errors in Figure 35.

When belt drum torque measurement is 500 Nm/m higher than the actual value (Figure 34, up-left), the estimated web tension is higher than measured web tension. Extra friction in the belt drums, for example, can be the reason for this kind of phenomenon. On the other hand, if unwind torque measurement is 1000 Nm/m higher, the estimated web tension is lower than the actual measurement (Figure 34, up-right). Also, when the measured rear drum torque is 500 Nm/m higher than the actual value, the estimated web tension is lower than measured value (Figure 34, left-down). The estimated web tension without any faults is shown in (Figure 34, down-right). It can be seen that there are disturbances in the estimated tension value during acceleration and deceleration of the winder. All three estimation errors, i.e., the differences between estimated and measured values, are shown together in Figure 35. The unit of measurement Nm/m is the torque per width of the paper web.

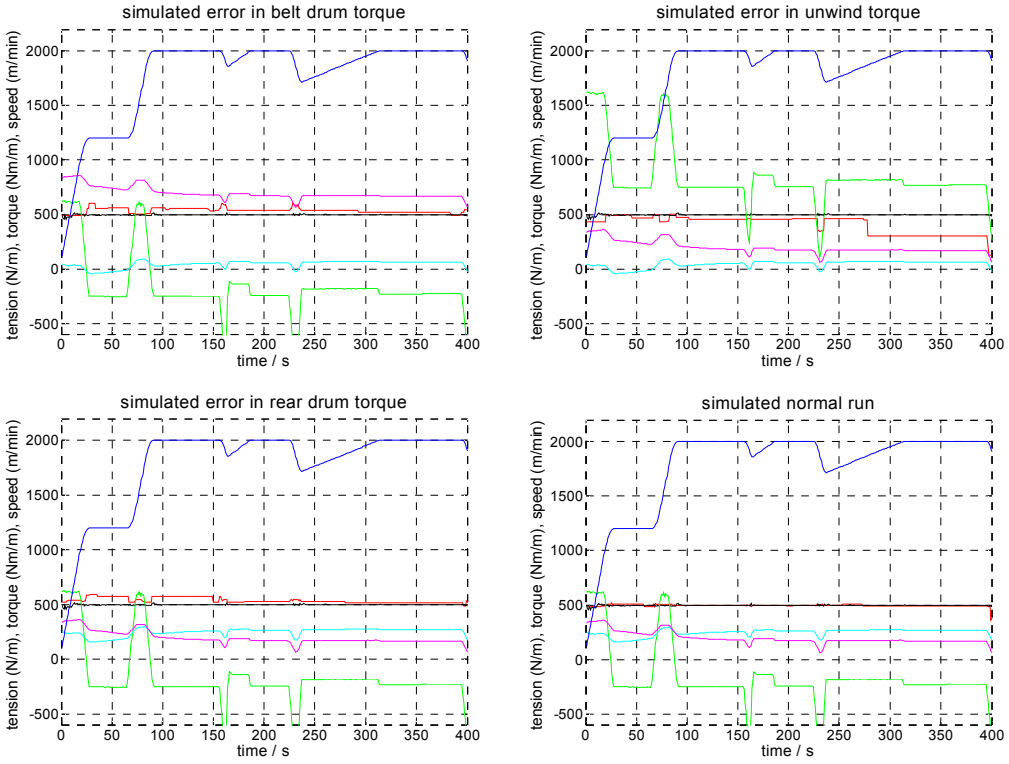

Figure 34: Differences between the actual and estimated tensions, when simulated faults are in belt drum torque (up-left), unwind torque (up-right) and rear drum (down-left). Estimated tension without any fault can be seen in the down-right figure. Measured web tension (N/m, black), simulated web tension (N/m, red), unwind torque (Nm/m, green), rear drum torque (Nm/m, cyan), belt drum torque (Nm/m, magenta/pink) and web speed (m/min, blue).

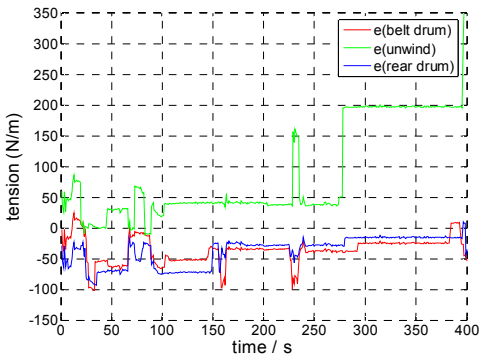

Figure 35: Estimation errors in different simulated fault situations (belt drum error – red, unwind error – green and rear drum error – blue).

In this example, estimation error is calculated from the measured and estimated outputs.

$$e(k) = y(k) - \hat{y}(k) \tag{4.7}$$

This error vector is used for fault detection by calculating residuals from it. The basic structure of the model-based FDI of tension control is shown in Figure 36. Residuals are variables or vectors as in this case, which are calculated as a function of error vector

$$r = f_i e(k) \tag{4.8}$$

f_1 = mean value of e(k) during initial acceleration

f_2 = mean value of e(k) between initial acceleration and deceleration at the end

f_3 = standard deviation of e(k) during initial acceleration

f_4 = standard deviation of e(k) between initial acceleration and deceleration at end

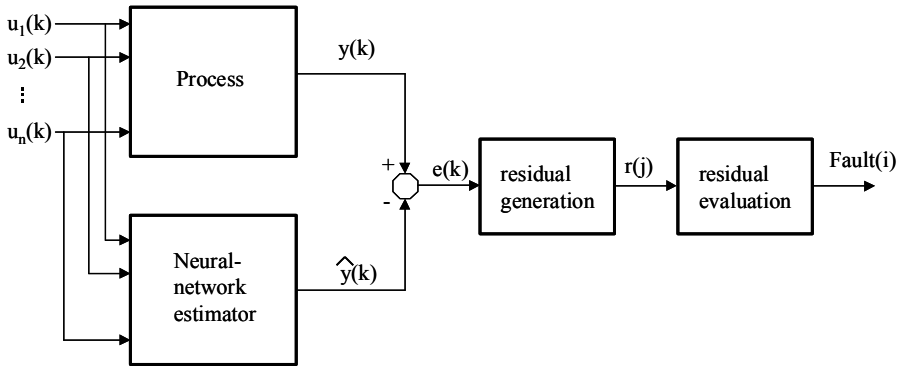

Figure 36: Scheme for a model-based FDI for the tension control of the paper winder.

After residual values are calculated (see Table 4-1), the values are thresholded so that the final residuals are signed binary vectors. Examples of binary residual vectors are shown in Table 4-2. The threshold value was 20 for the first two columns and 40 for the last two.

Table 4-1: Actual values of residuals.

	mean acc.	mean steady	std. dev. acc.	std. dev. steady
r1	3.2078	0.4534	16.404	10.6525
r2	-3.455	-37.9153	18.2181	19.6096
r3	55.7911	90.1354	21.5492	82.9839
r4	-44.4121	-37.4404	14.4584	23.7921

Table 4-2: Threshold binary residual values and equivalent fault types.

	mean acc.	mean steady	std. dev. acc.	std. dev. steady	
r1	0	0	0	0	no fault
r2	0	-1	0	0	fault in belt drum
r3	1	1	0	1	fault at unwind st.
r4	-1	-1	0	0	fault in rear drum

It is straightforward to mask different faults from the binary residual table. In a practical application, the main issues are the robustness of the system and the chosen threshold limit values. Fuzzy reasoning algorithms could be one solution to the threshold problem. By these simulations it can be said that it is possible to detect and isolate faults in the web tension control system with the system based on neural networks. Long-term tests in the paper mills were not possible within this research, so it cannot be said how difficult it would be to apply this method to practical problems.

4.3. Simulation model of rider roll

Simulation is a widely used tool in the field of control engineering. It has been used to test new control algorithms and simulate different types of processes and their controls. At first, simulation was used mainly in the process industry. Simulation has also spread into the field of mechanical and servo-mechanical systems. In modern simulation systems, it is quite straightforward to model different types of nonlinearities and discontinuities, which are typical in servo-mechanical systems.

Plant-wise simulation is, in addition, used to examine flexible manufacturing systems, for example. There are also simulation tools for studying factory-level conditioning monitoring and maintenance, see e.g. (Honkanen, 2004). A model-based FDI system for the rider roll is introduced in Section 4.4.

A rider roll presses paper rolls during winding. At the beginning of winding, it can press the cores and the small diameter rolls quite hard to generate the required nip load. At the end of winding, it presses high-diameter rolls lightly and just prevents them coming out of a winder. Rider rolls might have electrical drives to make it possible to control the torque and/or rotation speed. Rider rolls have an important role in the winding process; this is one of the main reasons it was selected as a target of simulation. The simulation model does not contain only mechanical parts of the rider roll, but it contains also its contact with paper rolls, hydraulic parts, electrical parts and software components. For general information of systems such as these, see (Norvelle, 2000).

Figure 37: Main parts of the rider roll that presses paper rolls during winding (1=rider roll, 2=rider roll beam and 3=hydraulic cylinder).

4.3.1. Spool

There are various kinds of hydraulic valves, but when fast and accurate control of speed, position and/or force is needed, high-response servo valves are usually selected. Response frequencies of proportional valves are typically less than 10 Hz, although they can be as high as 400 Hz in servo valves. A spool is the part in a hydraulic valve that guides oil flow into the hydraulic cylinder. Characteristics of a spool and its control electronics very much affect the valve properties.

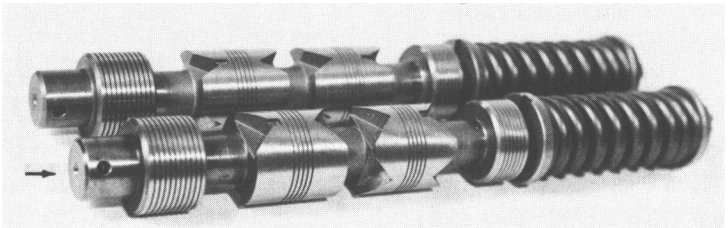

Figure 38: Example of a hydraulic valve spool (Tonyan, 1985).

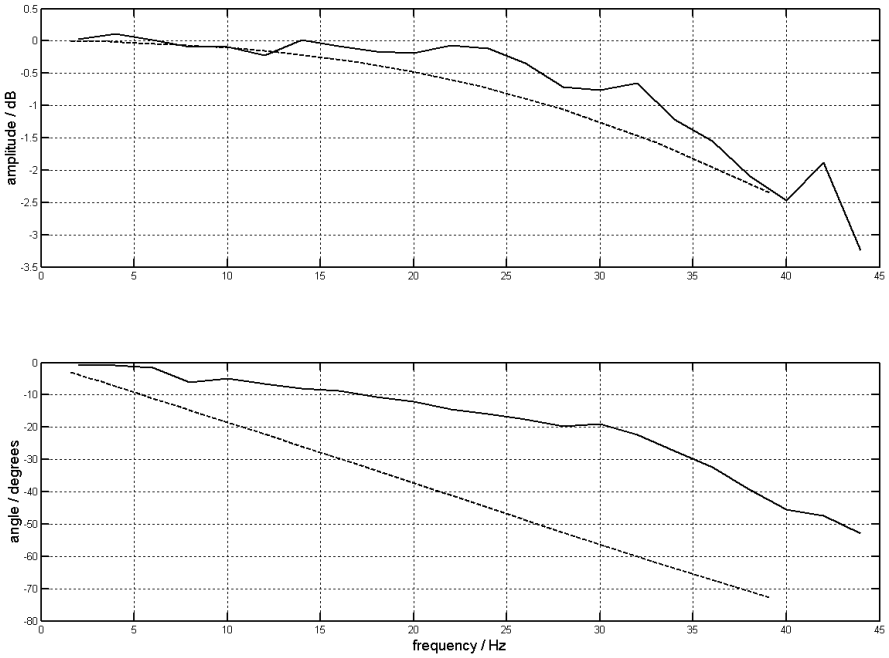

Figure 39: Frequency responses of the spool of a hydraulic valve (measured data – solid line, spool model – dashed line).

A typical frequency response curve of a hydraulic valve is shown Figure A 13 in Appendix 4. The amplitude curve reaches a –3 dB level at 70 Hz with a full valve opening (U_E=+/-100%). A frequency response of the spool was also measured at the Winding Research Center, Järvenpää. A chirp signal from 2 to 45 Hz was fed to the valve. The spool position was measured with a frequency of 512 Hz. A measured phase curve was quite similar to the manufacturer's data, but the amplitude curve did reach the –3 dB level at a lower frequency.

In the simulation model, the spool characteristic was modeled with a second-order transfer function. The frequency response of the spool model is also shown in Figure 39.

4.3.2. Valve

The basic structure of a hydraulic valve is shown in Figure 40. A spool is in the middle of the valve and it controls the flows to lines A and B from pressure line P. From lines A and B, the flow continues into a tank line T. When a spool is in the zero position in the middle, there are small leakage flows from P to A and B. When A and B are blocked, there is the same amount of oil leakage into the tank line T from A and B. Pressure is divided so that if P is 100 bar there will be 50 bar pressure in both lines A and B. Pressure in the tank line T is then 0 bar. In practice, there is usually a small pressure also in the tank line. If the spool is moved to the left, the pressure starts to grow in line A. At the same time, pressure in line B starts to drop, because that side opens more in the tank line T. The valve characteristics

can be presented with a pressure gain curve. Both leakage and pressure gain curves of a valve are usually presented in the data sheet of the valve.

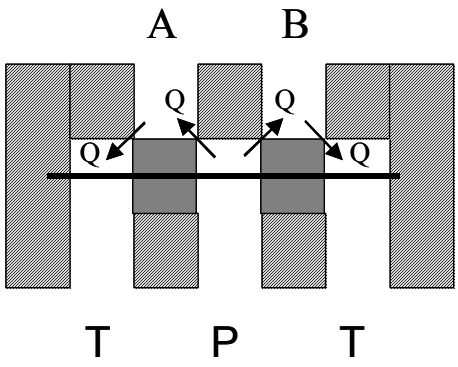

Figure 40: Basic structure of a servo valve (Q = leakage flow).

The valve used in the simulation has the following pressure gain according to the valve manufacturer. When a spool is 4% open, there should be a full pressure in line A or B. Measurements have shown, however, that, in practice, the pressure shown by the gain curve is not as optimal as in Figure 41, but varies between different valves.

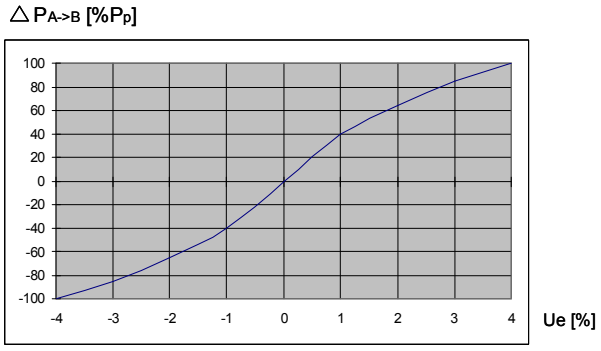

Figure 41: Pressure gain curve of the hydraulic valve.

4.3.3. Hydraulic cylinder

A hydraulic cylinder is often presented as an integrator in simple simulation models. This is a good approximation if the system's dynamic behavior does not need to be examined more precisely. In a rider roll simulation, a relatively large mass is moved with hydraulic cylinders, and the frequency response of the system is an important topic to be considered. Therefore, a more specific model is required. A hydraulic cylinder consists of three basic elements: the cylinder, piston, and piston rod.

A hydraulic cylinder is a nonlinear actuator, the natural frequency and characteristics of which depend on the cylinder length, the cap side area (A_c), the head side area (A_h), the length and the diameter of pipes and hoses, the bulk modulus of hydraulic oil (β) and hoses (β_H), the position of piston, and the moving mass *m*. The bulk modulus of pipes and cylinder casings also play a significant role with high pressures, see, for example, (Rivin, 1987).

The natural frequency of a hydraulic cylinder is basically a function of the mass and the volume of the oil in the cylinder and between the cylinder and a valve. It is calculated with the following equation (Merrit, 1967). V_c is the oil volume in the cap side of the cylinder and V_h in the head side.

$$\omega_0 = \sqrt{\left[\left(A_c^2\beta\right)/\left(V_c m\right)\right] + \left[\left(A_h^2\beta\right)/\left(V_h m\right)\right]} \tag{4.1}$$

The volume includes the volume in a cylinder and the volume of pipes and hoses between a valve and a cylinder. The volume of pipes and hoses has a remarkable effect on the natural frequency (hydraulic) of a rider roll. The simulated natural frequency of the rider roll with and without pipes and hoses is shown in Figure 42. The difference between the respective results of the hoses being used and not being used arises from the fact that the effective bulk modulus depends on the bulk modulus of the hose also. The calculus of the effective bulk modulus is shown in Merrit (1967).

Effective bulk modulus is given by the equation

$$\frac{1}{\beta_{effective}} = \frac{1}{\beta} + \frac{V_H}{V_{total}}\frac{1}{\beta_H} \tag{4.2}$$

When hoses exist in the system, the effective bulk modulus must be used instead of the bulk modulus of the hydraulic oil. Here β is the bulk modulus of the hydraulic oil, β_H is the bulk modulus of the hoses, V_{total} is the total oil volume in the system (cylinder + hoses) and V_H is the oil volume in the hoses. The length of the hoses is relatively short in a rider roll case, so its effect on the natural frequency is rather small. Kajaste *et al.* (2005) and Nykänen *et al.* (2000) have shown that the air in the hydraulic cylinder also has an effect on the bulk modulus, especially with small pressures.

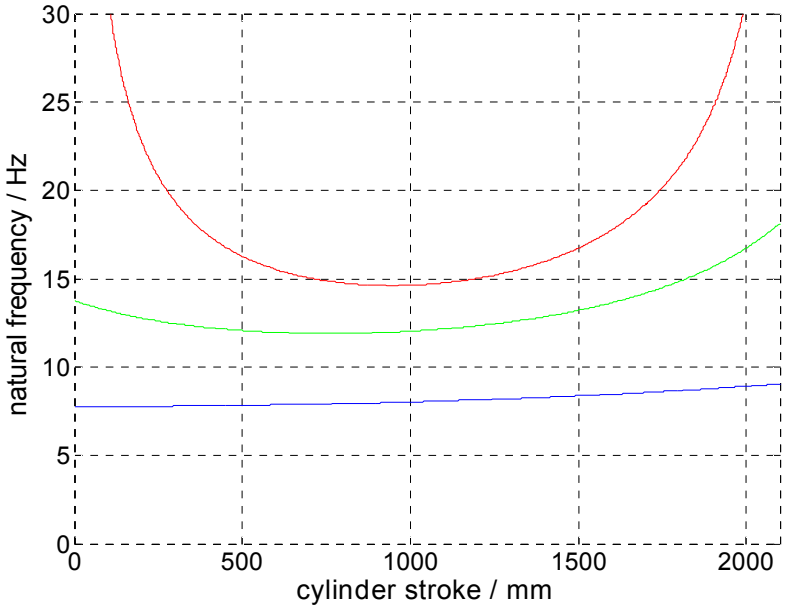

Figure 42: Natural frequencies (hydraulic) of a rider roll with (green line) and without (red line) volume of pipes. The natural frequency when pipes are replaced with hoses (blue line) is also shown in the figure.

Friction of the cylinder is modeled as a pressure-resisting movement that is proportional to the cylinder speed.

4.3.4. Rider roll contact with paper roll

A rider roll nip is modeled as a spring constant. This work does not concern detailed nip models; the simulation model is used to test the fault diagnostic system of the rider roll. The nip and paper rolls generate disturbances in the rider roll but the roll structure and winding process itself is not a subject of this work. That subject is examined in, for instance, (Jorkama, 2001) and (Paanasalo, 2005). In a winding process, paper is first wound around a core. The hardness of the core affects its spring constant. When roll diameter increases, paper quality and winding parameters affect roll hardness and its spring constant. Usually, the spring constant decreases when roll diameter increases. It is quite difficult to define the spring constant for different diameters and different rolls, so a static spring constant value was used in the simulation. There cannot be any negative forces in the nip. Therefore the nip force is limited to zero if a rider roll rises above the surface of the paper roll.

Figure 43 shows all the spring constants of the winding section. The spring constants of the rider roll nip and the hydraulic cylinder are included in the simulation model. This model is two-dimensional; dynamic phenomena of the third dimension, such as deflection of a rider

roll in cross direction, are not included. The fastening of a hydraulic cylinder is also assumed be infinitely rigid.

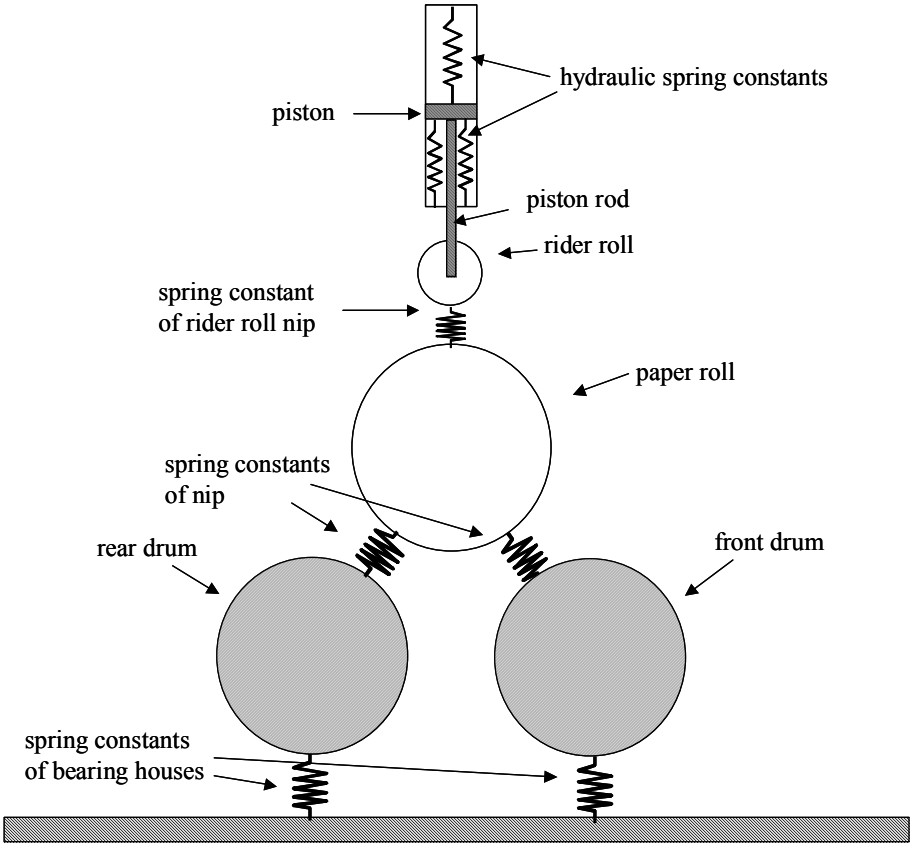

Figure 43: Spring constants of simulated rider roll system.

4.3.5. Programmable Logic Controller

The automation system that controls the rider roll is included in the simulation model. The rider roll is controlled with a PLC. Control programs are called in time to interrupt programs of the PLC, so the logic part of the simulation model is in discrete time format, which corresponds to the cycle time of a PLC. The discrete PI controller is used as a force controller.

The output signal is quantized to be equivalent to the resolution of the analog output card. A cyclic disturbance can be seen in the controlled force, if resolution is insufficient. That phenomenon can be seen both in practice and with the simulation model (see Figure 47).

These kinds of hybrid models, which consist of both continuous and discrete parts, are useful when fast servo systems are simulated, because the cycle time of the control system

is one limiting factor in the control. The flowchart that presents different modules and signals between them is shown in Figure 44.

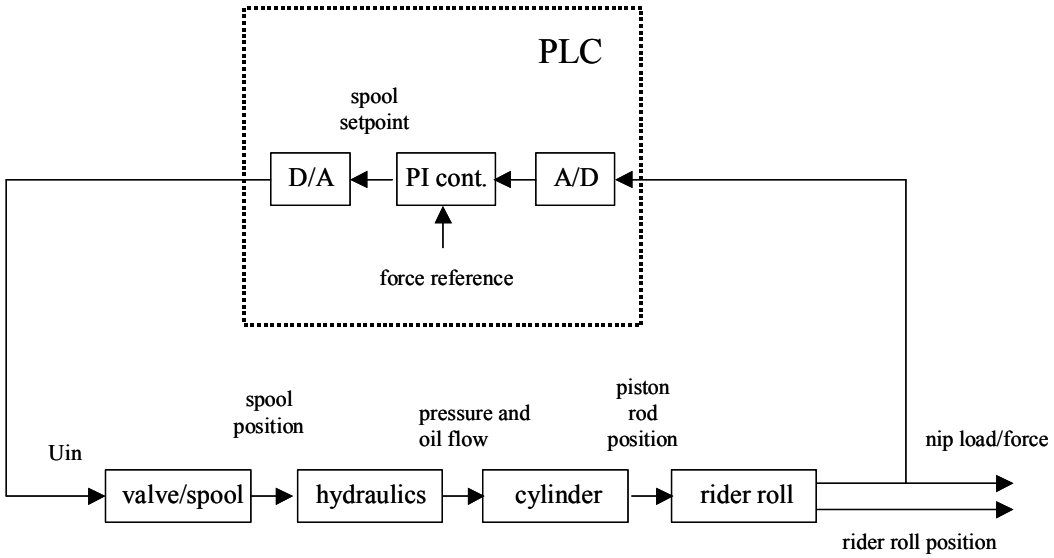

Figure 44: A flowchart of different modules and signals included in the simulation model.

4.3.6. Model validation

Real data from a paper winder were used to validate the model. The rider roll model described above was built from models of physical machine parts. Measured data and data sheets were used to set parameters of those model parts. The whole rider roll model was then built from these parts, basically in the same way as in a real machine. The weight of the rider roll was 2800 kg and the diameter of the hydraulic cylinders was 80 mm (rod diameter 40 mm and length 2100 mm). Measured data were only used to verify the model validity. Some figures, where actual measurements and simulation results are compared, are presented below. Actual and simulated forces and force references are shown in Figure 45. Simulation started from 105 mm cores and was continued to a roll diameter of 1150 mm. At first, the diameter of the paper roll increases rapidly, because the winder is accelerating, and because, with the same paper web speed, more layers wrap round the roll with the small diameter than with the larger one. Some overshooting exists when the roll diameter is growing fast. Force reference is also higher at the beginning of winding, because stiff bottoms of paper rolls are usually preferred. When roll diameter increases, rolls start to generate nip load between the winding drums and the roll, so less rider roll force is needed.

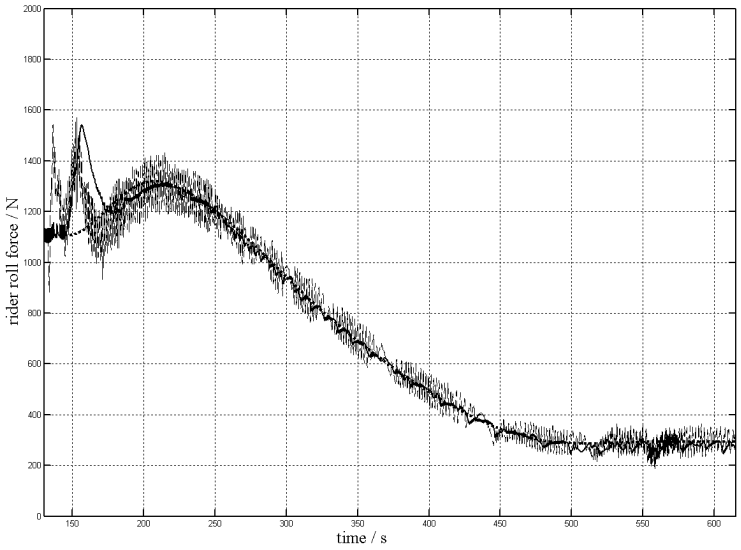

Figure 45: Actual rider roll force (dashed line), force reference (dotted line) and simulated rider roll force (solid line).

Actual and simulated valve spools opening are shown in Figure 46. At the end of the simulation, the difference is increasing. On the other hand, there are a lot of differences between different valves, even if they are of the same brand and type. At the beginning of the winding, the valve opening is larger because the roll diameter increases faster and also because the force reference is higher.

The output resolution effect on the adjustment error of the controller can be seen in Figure 47. The amplitude of the force vibration increases when output card resolution decreases. That phenomenon was first discovered in a real winder. With the simulation model, it was possible to find the primary cause to this low frequency oscillation. The tuning of the controller also affects this oscillation and these simulations were performed with the tuning used in the real winder.

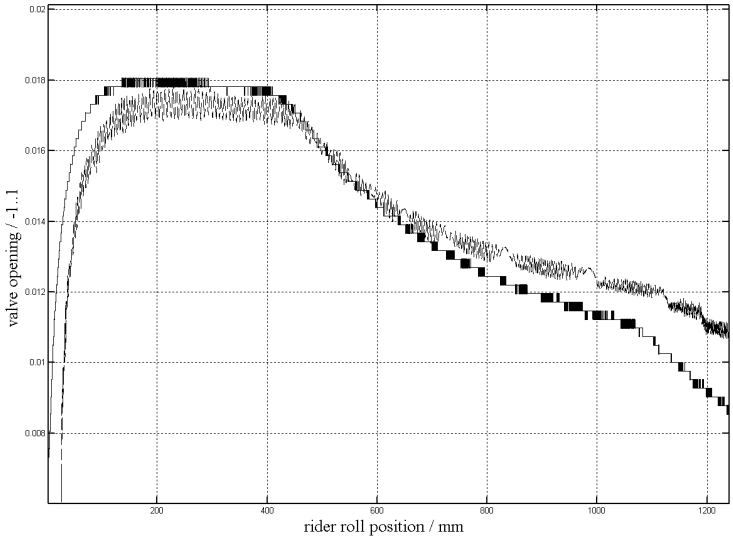

Figure 46: Actual (dashed) and simulated (solid) valve spool position during winding.

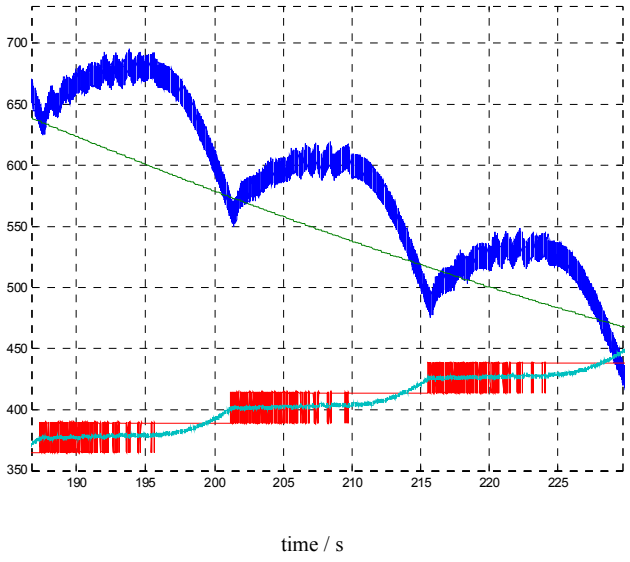

Figure 47: Analog output card's resolution has an effect on accuracy of regulation. (actual force (N) – dark blue, force setpoint value (N) – green, controller output (+/- 32768) – light blue and quantized (13 bit) output signal (+/- 32768) - red).

4.4. Fault diagnostics of the rider roll

The following faults are selected as simulated test cases:

- Stick and slip of valve spool
- Electrical disturbances in valve spool control
- Wearing of hydraulic valve spool
- Abnormal friction in cylinder piston
- White noise measurement disturbance in force measurement
- Process disturbance (vibrating rolls)

Sometimes dirt, foreign particles in hydraulic oil or other faults in hydraulic valves might cause the stick and slip of a valve spool. The effect of this phenomenon on the force control of a rider roll is simulated. Two different types of sticking are tested (see Figures 48 and 49). In the first test, there is sticking lasting 0.1 s once every second and, in the other, there is sticking of 1 s once in every 10 s (Figure 50). Shorter, but more frequent, sticking disturbs the force control less than the longer, but not so frequent, one. The estimated force is also presented in figures; its calculation is shown later in this section.

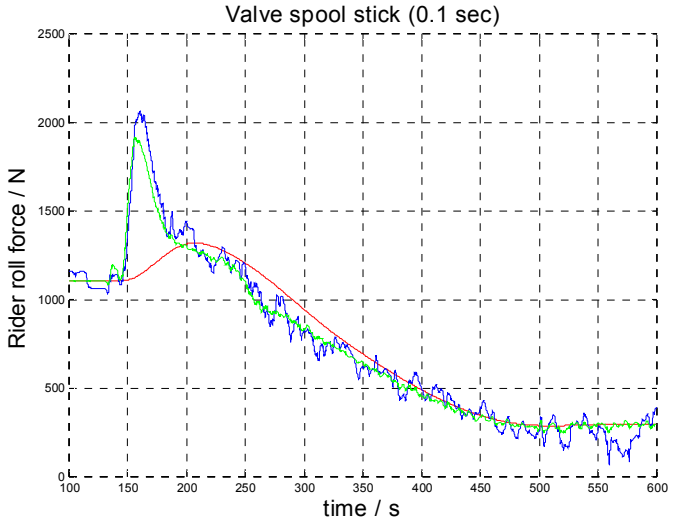

Figure 48: Valve spool sticks lasting 0.1 s within a one-second period (force reference – red, simulated force measurement – blue and estimated force – green).

In modern servo-controlled valves, the spool has its own control electronics, which positions the spool according to the position reference given as a setpoint for the valve. Fast electrical disturbances are possible (but rare) in these circuits. The effect of a 50 ms long and 10 V high disturbance is simulated. It disturbs the force control very seriously and makes the rider roll push against rolls with its full power. This kind of force will cause paper rolls to break and make hard demands on the rider roll mechanics as well.

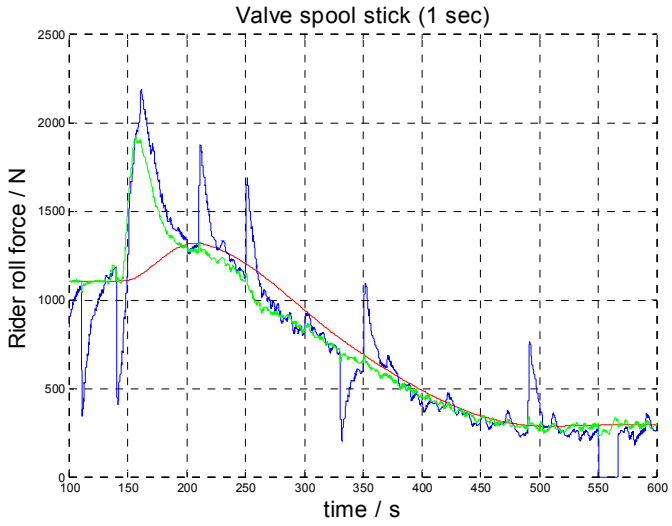

Figure 49: Valve spool sticks lasting 1.0 s with a period of 10 s (force reference – red, simulated force measurement – blue and estimated force – green).

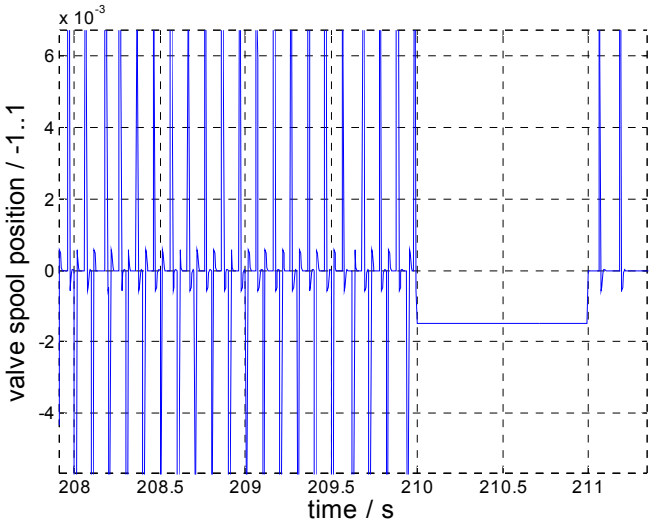

Figure 50: The valve spool is sticking for 1 s (210->211 s).

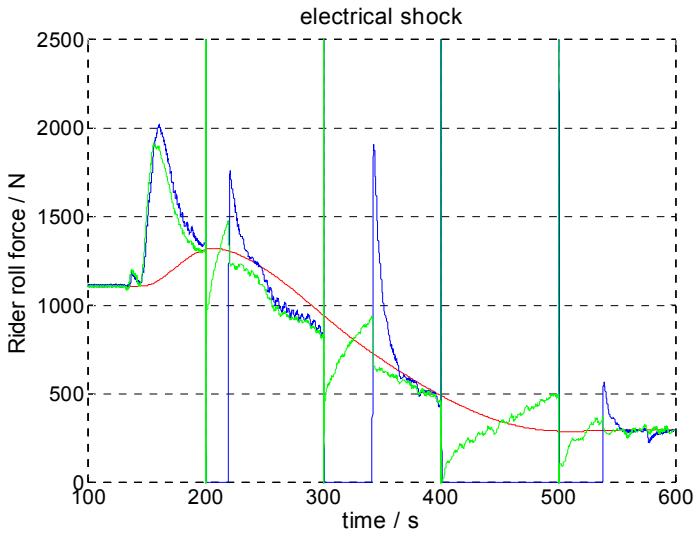

Figure 51: Electrical shock, having an amplitude of 10V and lasting 50ms, affected the valve spool control electronics every 100 seconds starting at t=200 s. (force reference – red, simulated force measurement – blue and estimated force – green).

It is seen in Figure 51 that an electrical shock in valve electronics has serious effects on the rider roll force control. Hydraulic valves also have some safety functions and it is possible to choose the kind of a valve that controls its spool to zero position in case of a fault such as power failure. This kind of safety feature causes smaller force peaks in comparison with electrical shocks (Figure 52). For this reason, it would not damage paper rolls that much. The fact that it can still harm the structure of the rolls even if the machine seems to run trouble-free justifies alarming in this situation.

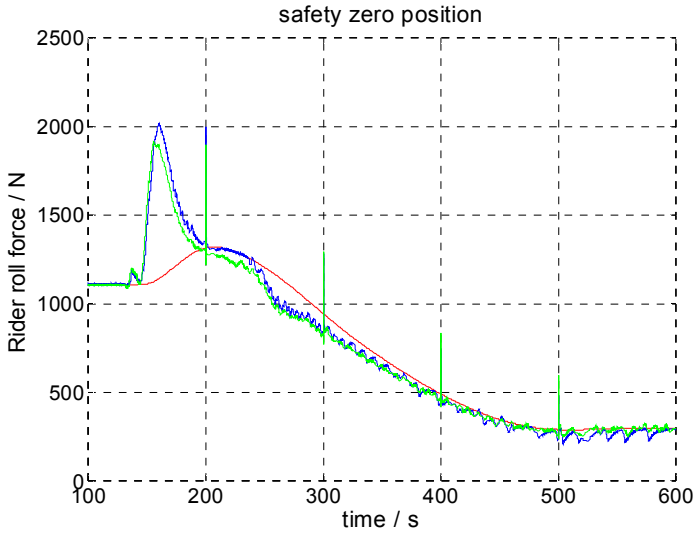

Figure 52: Valve spool positions itself to safety zero position every 200 s (force reference – red, simulated force measurement – blue and estimated force – green).

When a valve has been in use for several years its spindle and valve enclosure wear out. That will change the pressure gain curve of the valve. The result of the wearing is shown in Figure 53. It can be seen that the force control still works quite normally. In the acceleration phase starting at t=150 s, the used valve responds slower. The average difference between the valve spool openings was 0.7%. This will be seen as quite a large difference if one bears in mind that the normal pressure gain curve varies within +/- 4% of the valve opening.

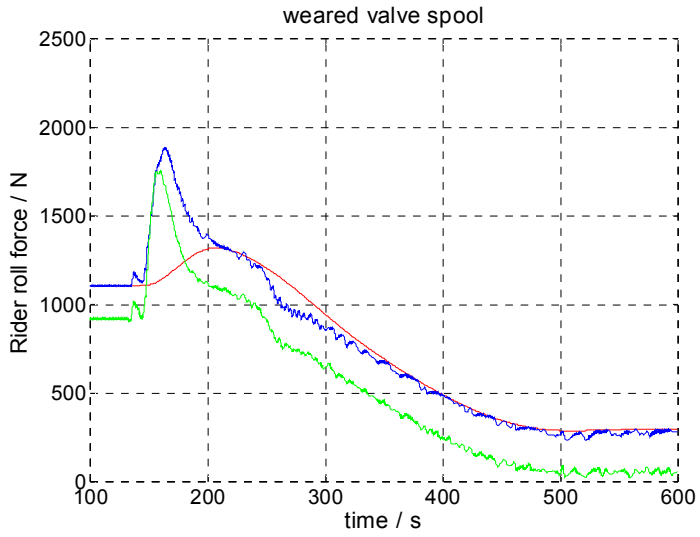

Figure 53: Valve spool with severe wear (spool opening average difference 0.7%) (force reference – red, simulated force measurement – blue and estimated force – green).

The measurement and process disturbances also have an influence on the force control; the simulation results are shown in Figure 54.

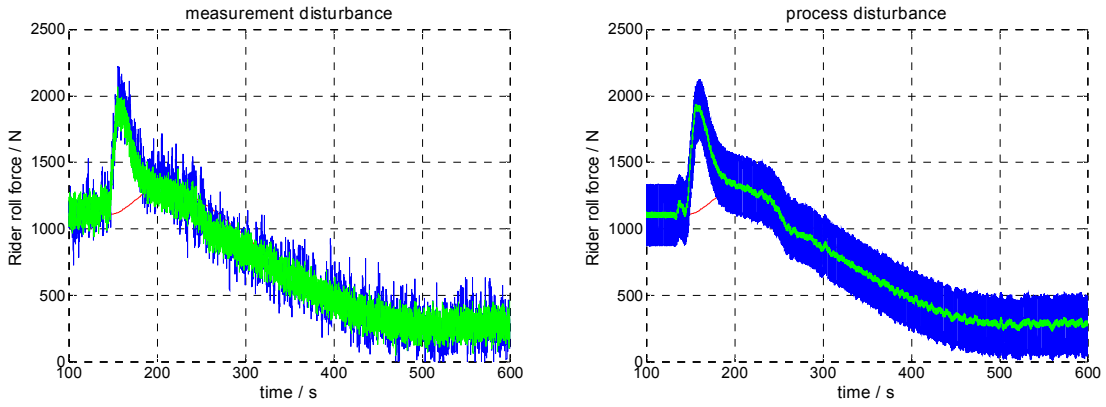

Figure 54: Measurement disturbance (left figure) and process disturbance (right figure) effect on actual and estimated forces (force reference – red, simulated force measurement – blue and estimated force – green).

The measurement disturbance was white noise with amplitude of 250 N and it was added to the force measurement. The process disturbance was vibration of the rider roll with a frequency of 12 Hz. The vibration amplitude was 0.1 mm.

The effect of the cylinder friction is also simulated. A common model for cylinder friction (Olsson *et al.*, 1998) is shown in the following equation. Keskinen *et al.* (1993) have also studied the effect of the seal friction in the hydraulic cylinders. The friction force in the graphical format can also be seen in Figure A 14 in Appendix 4. The friction force is a function of Coulomb friction (F_C), static friction force (F_S), signed speed (v), Stribeck velocity (v_S), the factor that depends on the geometry of the application (δ_S), and viscous friction force ($F_v \upsilon$).

$$F(v) = F_C + (F_S - F_C)e^{-|\upsilon/\upsilon_S|^{\delta_S}} + F_v v \tag{4.3}$$

The effect of the friction can be seen in Figure 55. A very strong stick and slip phenomenon occurs in the steady state situation before winding starts.

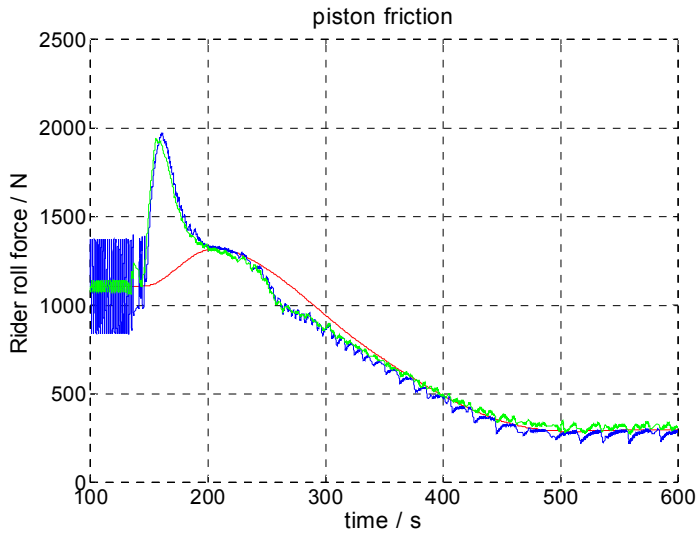

Figure 55: Simulation result with piston friction force (force reference – red, simulated force measurement – blue and estimated force – green).

A model-based fault diagnostic system is developed to distinguish the different faulty situations. A flow chart demonstrating the structure of the system is shown in Figure 56. Process disturbances can occur in different places. There might be problems in a hydraulic valve, in a hydraulic cylinder or in the winding process like bouncing or vibration. Measurement disturbances can also be found in the force measurement.

As the process model, the ARX (autoregressive with exogenous input) model shown in (4.4) is used. The ARMAX model was also evaluated, but the ARX model was chosen eventually. The structure of the ARX model is quite simple and can be used when the system has only one output signal. The weakness of the ARX model is that the disturbances are part of the system dynamics in contrast to, for example, the Bob-Jenkins model. However, in this case, the simplest model that gave an acceptable simulation result is selected. Parameters of the model are estimated with Identification toolbox of Matlab-Simulink. The identification data are generated with the detailed model of the rider roll introduced in Section 4.3.

$$A(q)y(n) = \begin{bmatrix} B_1(q) & B_2(q) \end{bmatrix} \begin{bmatrix} u_1(n) \\ u_2(n) \end{bmatrix} + e(n) \tag{4.4}$$

where u_1 is the setpoint value of the spool, u_2 is the increase in speed of the roll diameter, y is estimated nip load/force, e is the disturbance signal, and q^{-1} is the shift operator backwards in time; the sampling period was 20 ms.

$$A(q) = 1 - 3.701q^{-1} + 5.226q^{-2} - 3.339q^{-3} + 0.8146q^{-4} \tag{4.5}$$

$$B_1(q) = 520.6q^{-1} - 661.7q^{-2} + 197.2q^{-3} - 55.91q^{-4} \tag{4.6}$$

$$B_2(q) = -1.814 \cdot 10^5 q^{-1} + 1.843 \cdot 10^5 q^{-2} + 1.828 \cdot 10^5 q^{-3} - 1.857 \cdot 10^5 q^{-4} \tag{4.7}$$

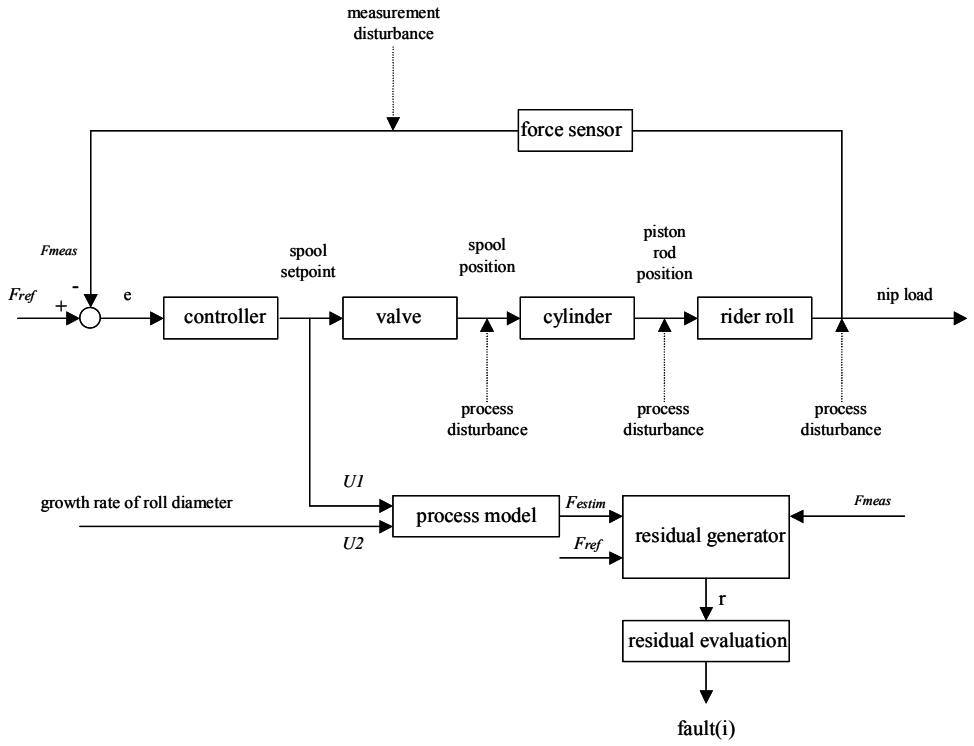

Figure 56: A Basic structure of FDI system for rider roll.

The model has two input signals, a spool setpoint and increase speed of roll diameter. Output is the estimated force. In a steady-state situation, the spool setpoint is the only variable that affects the force in the nip between the paper roll and drum or drums. During winding, however, growing paper rolls push the rider roll upwards. Depending on the roll diameter, the paper thickness and the speed of the paper web, the rolls push the rider roll upwards with different speeds. This creates a situation in which the required nip load or force needs a different valve opening. The model is tested with different nip load levels (force reference) and with different winder speeds (speed factor). Simulation results are introduced in Figure 57.

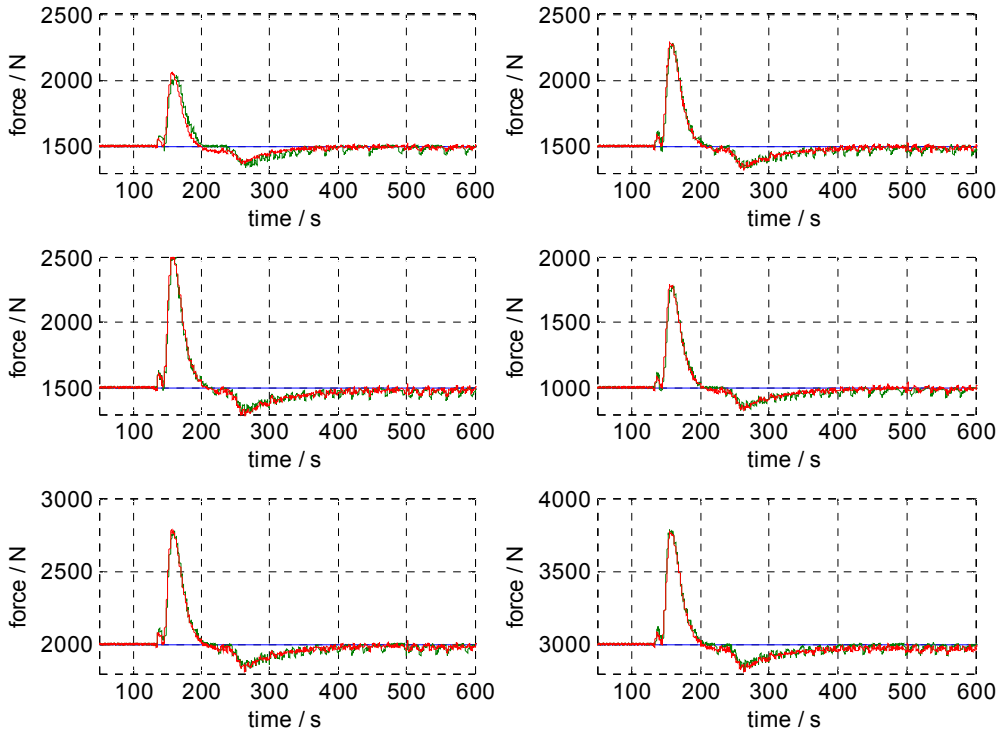

Figure 57: Simulation results with different running parameters (force setpoint – blue, simulated force measurement – green, estimated force – red). Force reference 500 N and speed factor 0.7 (up-left), force reference 1500 N and speed factor 1.0 (top-right), force reference 1500 N and speed factor 1.3 (middle-left), force reference 1000 N and speed factor 1.0 (middle-right), force reference 2000 N and speed factor 1.0 (down-left), and force reference 3000 N and speed factor 1.0 (down-right).

A setpoint error and an estimation error are parameters that are used to calculate residual values. Calculations were performed with six different functions that were based on basic statistical functions like minimum, maximum, mean value and standard deviation.

$$e(k) = y(k) - r(k)$$

$$f_1(e(k)) = \min(e(k))$$

$$f_2(e(k)) = \max(e(k))$$

$$f_3(e(k)) = \frac{1}{n}\sum_{k=1}^{n} e(k)$$

$$f_4(e(k)) = \left| \frac{1}{n} \sum_{k=1}^{n} e(k) \right|$$

$$f_5(e(k)) = \sqrt{\frac{1}{n-1} \sum_{k=1}^{n} \left(e(k) - \bar{e}\right)^2} \quad , \quad where\ \bar{e} = \frac{1}{n} \sum e(k)$$

$$f_6(e(k)) = \max \left\{ \left| e(k+1) - e(k) \right| \right\}$$

and with

$$\tilde{y}(k) = y(k) - \hat{y}(k)$$

$$f_1(\tilde{y}(k)) = \min(\tilde{y}(k)) \text{ etc.}$$

In other words, twelve different key figures are calculated after a produced set of paper rolls. Those key figures formed thresholds to the binary values where zero meant a normal situation. A fault threshold value is set at a 20% difference from normal values. A single fault threshold is used in this experiment, but it is, of course, possible to use individual threshold values for every key figure. From the practical point of view, it is, however, an advantage if a single value is sufficient, because it is a proof of the robustness of the system.

Table 4-3: Binary residual values of different type of faults.

	$f_1(e)$	$f_2(e)$	$f_3(e)$	$f_4(e)$	$f_5(e)$	$f_6(e)$	$f_1(\tilde{y})$	$f_2(\tilde{y})$	$f_3(\tilde{y})$	$f_4(\tilde{y})$	$f_5(\tilde{y})$	$f_6(\tilde{y})$
No error	0	0	0	0	0	0	0	0	0	0	0	0
Sticking spool	0	1	0	0	0	0	1	1	0	0	1	0
Flat pressure gain	0	0	1	1	0	0	1	1	1	1	0	0
Piston friction	0	1	1	1	0	1	1	1	1	1	1	1
Safety zero	0	0	0	0	0	1	0	1	0	0	0	1
Electrical shock	1	1	0	0	1	1	1	1	1	1	1	1
Measurement dist.	1	1	1	1	1	1	1	1	1	1	1	1
Process dist.	1	1	0	0	1	1	1	1	1	1	1	1

A residual evaluation block is used to classify the faults. Table 4-3 shows the residuals that are calculated for different types of fault situations. This table forms the mask that can be used to classify the faults.

4.5. Summary

The use of a model-based or other type of fault diagnostic method is still rare in the paper industry, especially in the paper finishing area. However, in this chapter, two different methods that can be used in paper winders were introduced. The ARX model and the neural network model are used as a model and statistical methods were used for residual generation. The thresholded key figures formed the table of the binary values that is used for the fault isolation.

The multilayer feedforward network of one hidden layer with 50 nodes and an output layer of one node is used to monitor the tension control of the paper winder. The simulated faults are used to verify the system.

The model-based FDI method is introduced. The method is based on the ARX model and is tested with the detailed simulation model of the rider roll. The system is capable of detecting and isolating different types of faults. A statistical residual generation method is used to classify the faults. The basic idea of statistical residual generation is quite simple and is one of the main reasons for its being used in this context. This simple method is chosen to narrow the gap between theoretical research and practical applications.

There are pros and cons to both methods, i.e., the neural network and ARX model, being used in fault diagnostic systems. The structure of the neural network is more complicated, but it is suitable for systems with multiple inputs (and outputs). The ARX model is more intelligible to non-experts than the neural networks and it is easier to use with small-scale systems, i.e., 1-2 inputs and 1 output. The neural network and model-based methods were applied to two different cases and it is difficult to say anything about the order of superiority of the methods. However, the model-based methods can be considered somewhat easier to use in practice. Anyway, this depends on the background of the user and more or less holds for simple SISO systems. At the moment, there is hardly any of this kind of application in the paper winders, so it is a promising study area.

5. Vibration control of paper winder

A survey of some basic vibration damping methods is discussed first in this chapter. Methods to actively damp vibrations are demonstrated in detail. *Vibration control* means the active control of structural vibrations in this work. For more information on active methods, see (Fuller *et al.*, 1996).

5.1. Vibrations in paper winder

Basically, paper winders suffer from the same vibration problems as the other rotating machines. Compared with basic rotating machines, the paper winding process has some special features, which make it an even more demanding process. The paper winder accelerates and decelerates from zero speed to the maximum during every set it produces. That will excite the natural frequencies of structures of a very wide frequency range. A paper winder produces smaller customer rolls from large parent reels so during the winding the diameter and mass of customer rolls increase. This situation differs from, for example, a paper machine where all the production is run with constant speed and where rotating masses stay the same (except in the reeler). Figure 43 in Section 4.3.4 shows the vibrating parts of the paper winder. Mass dampers cannot be mounted on paper rolls, so the bearing houses of the winding drums and the rider roll beam (see Figure 37) are potential places for mass dampers.

In fact, the product itself, a customer roll, is one source of vibration. Properties of paper vary very much. At least paper friction, MD (machine direction) caliper variation, hardness and thickness might cause vibration problems during winding. Paper rolls can become out-of-round in shape, which causes vibration because rolls are in touch with the drum or drums through nips. Furthermore, the core can become eccentric in the roll. This is not always a problem in a winder, but causes vibration problems later in the printing house. Small-scale variation in the MD caliper can also generate vibrating rolls.

In addition to the vibration modes mentioned above, there is a further phenomenon that has to be mentioned here: roll bouncing. This occurs only in two-drum winders. In multi-station winders, each roll is supported individually from the roll ends so rolls cannot start bouncing. In a two-drum winder, the whole set is supported only from the set ends. In a roll bouncing situation, one or more rolls become unstable and start to swing. Rolls might loose contact with one or both drums and cause quality problems in the set. In a more severe bouncing situation, the winder can throw out rolls, in which case there is a possibility of serious damage to machine components. Especially in older winders, there is also a risk of human injuries. However, it is not possible to prevent bouncing with traditional vibration damping methods. It is best to use such winders where accurate control of different winding parameters such as the rider roll and core lock forces is possible. In one winder type, it is even possible to control the gap between the rear and front drums. Besides that, great attention must be paid to the proper setting of process parameters (tension, nip load etc.) and paper web profile, which can be controlled during the earlier stages of the paper process.

5.2. Vibration damping methods

5.2.1. Overview

Damping means absorbing energy from the vibrating system, as mentioned in the previous section. On the other hand, if an external force with the opposite phase reduces vibration, it is technically not damping because there is no energy absorption. The energy from the vibration is just moved to another place in the structure. It is well known that active damping might sometimes cause undesired vibration in another part of a machine.

Vibration damping methods can be divided into three categories: passive, semi-active and active methods. Passive methods are considered as traditional damping methods. They are still very useful and are the basic approach to vibration control in machine design. If the frequencies of excitation forces are known, like rotation frequency in a paper winder, a design can be achieved so that the natural frequencies of the machine parts are out of that range. The principle is simple, but, in practice, the design procedure is far more complicated. Lowering the natural frequency of machine part can be achieved by, for example, adding more mass to the system. This is not the most cost-effective way, because of extra material costs and because a heavier machine needs more-firm foundations and its energy consumption is higher. The cost of foundations in a paper machine line forms a remarkable part of the overall expense.

The material itself, such as steel, used in paper winders and other large machines has typically very little damping. Therefore, most damping that occurs in machine parts basically happens in structural joints. A systematic use of this phenomenon in damping is

still quite rare. One major problem is that the damping properties of structural joints greatly depend on the clamping pressure (Beards, 1996). With a low clamping pressure, actual movement can occur in structural joints; friction is a phenomenon that causes damping in a joint. High clamping pressure allows no movement in a joint; higher clamping pressure typically causes less damping in joints. Most of the damping follows from the material deformation in the joint. Material technology is, however, beyond the scope of this work, so, in the following sections, only dynamic absorbers are studied more closely.

Jorkama (1996) has studied the vibrations of two-drum winders. Some targets of applications of active damping methods described in this chapter are presented in Jorkama's study.

5.2.2. Impact-damper

An impact damper is a simple aid to reducing vibrations. A hanging chain or a metal ball in a chamber are the two most typical examples of impact dampers (Figure 58). Hanging masses are also used as impact dampers, for example, in bridges (Ogava *et al.*, 1997).

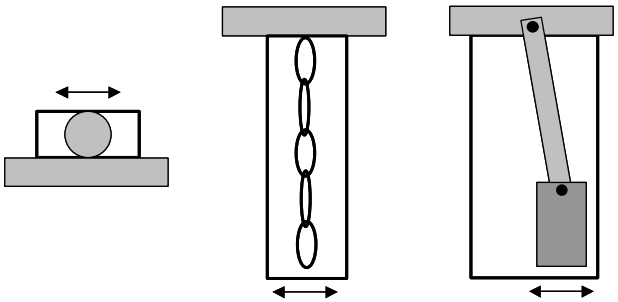

Figure 58: Three types of impact dampers: rolling ball, hanging chain and hanging mass.

The function of the impact damper is based on the phenomenon where the primary mass is vibrating and the mass inside a chamber of the impact damper is bumping against the walls of the chamber. Every collision takes out energy from the system and decreases the amplitude of the vibration. An impact damper can be used together with other types of dynamic mass dampers (Collette, 1998).

5.2.3. Tuned mass damper

A tuned mass damper is a passive damping method, which has been used for several decades. An extra-mass-spring system is added to the primary system (Beards, 1996). The natural frequency of this extra mass spring is tuned so that it is the same as the

natural/resonance frequency of the primary system, the system to be damped. Now the combined system has two resonance frequencies instead of one. These resonance frequencies are at both sides of the original resonance frequency. A mass ratio of the two masses determines how far away from the original resonance frequency those two frequencies are located.

It is also possible to add damping in the system to shape the frequency response of the whole system. A tuned mass damper is usually used to damp periodic types of disturbances. In practice, it is important that the two resonant frequencies are not too close to the resonant disturbance frequency. If the frequencies are very close to each other, it can lead to a situation where a minor inaccuracy in tuning causes the damper to increase the vibration instead of damping it. The following example demonstrates this phenomenon and the function of tuned mass dampers in general.

Example 5.1: Figure 59 presents a situation where a tuned mass damper is added to the vibrating primary system.

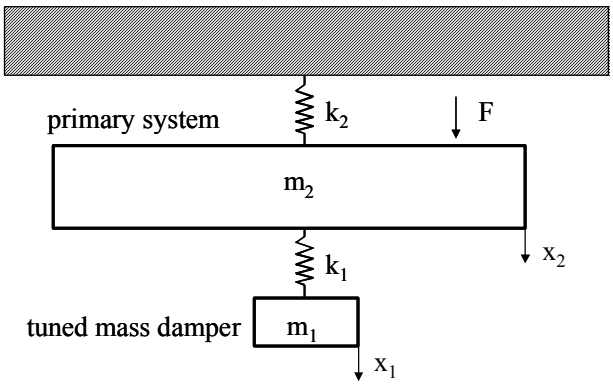

Figure 59: System with a tuned mass damper. m_1 is mass of the damper and m_2 mass of the primary mass, k_1 is the spring constant of the damper and k_2 the spring constant of the primary mass. F is the external force directed to the primary mass, and x_1 and x_2 are the positions of the masses.

The following equations of the motion can be written for the system.

$$m_2\ddot{x}_2 + k_2x_2 + k_1(x_2 - x_1) = F \tag{5.1}$$

and

$$m_1\ddot{x}_1 - k_1(x_2 - x_1) = 0 \tag{5.2}$$

Taking Laplace transform of Equations (5.1) and (5.2) and solving $X_2(s)$ gives:

$$X_2(s) = \frac{s^2 + k_1/m_1}{\left(s^2 + k_1/m_1\right)\left(m_2 s^2 + k_2 + k_1\right) - k_1^2/m_1} F(s) \tag{5.3}$$

Figure 60 shows the magnitude curves of the system with two different sizes of the tuned mass dampers. The mass of the primary system is $m_2 = 100$ kg and the spring constant $k_2 = 10000$ kg/s^2. The resonance frequency of the primary system is $\omega_2 = \sqrt{k_2/m_2} = 10\ rad/\sec$.

The basic tuning criterion is set as $\omega_2/\omega_1 = 1$. This criterion can be fulfilled with two different tuned mass dampers:

1. damper: $m_1 = 1$ kg and $k_1 = 100$ kg/s^2, (weight ratio $m_1/m_2 = 0.01$)

2. damper: $m_1 = 50$ kg and $k_1 = 5000$ kg/s^2, (weight ratio $m_1/m_2 = 0.5$)

From the magnitude curves, it can be seen that the smaller weight ratio gives a very narrow frequency band where the tuned mass damper works correctly. However, a larger weight ratio certainly gives a wider frequency band and a far more robust design against small variations in the resonance frequency.

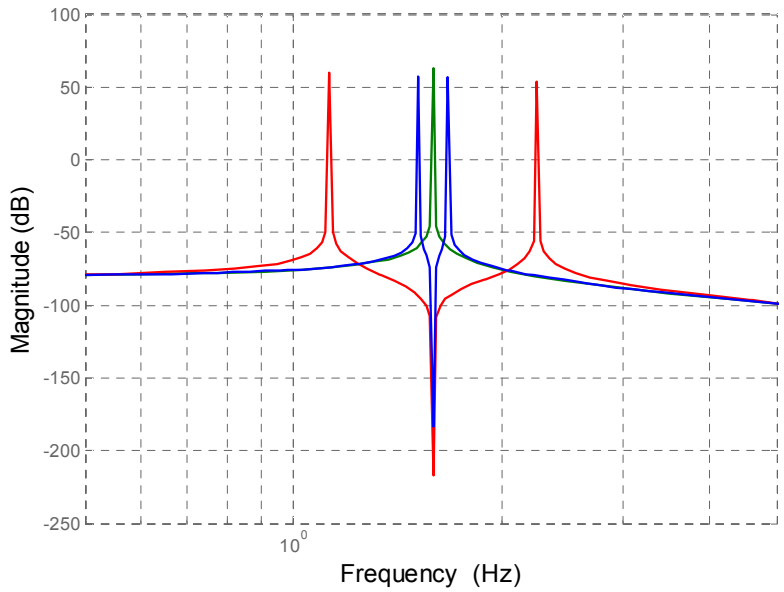

Figure 60: Magnitude diagrams with two different weight ratios: $m_1/m_2 = 0.5$ – red, $m_1/m_2 = 0.01$ blue curve and no damping – green curve.

5.3. Semi-active and active vibration absorbers

In semi-active vibration absorbers, the system characteristics of absorbers are changed with external energy. The power consumption of this type of absorbers is far less when compared to active damping absorbers. As an example, a tuned mass damper can be mentioned where the spring constant of the damper is controllable. A delayed resonator demonstrated in the next section is, in principle, this type of damper. Nevertheless, its spring constant and damping factor are controlled continuously, so it can be classified as an active damping method, too.

5.3.1. Delayed-resonator

Olgac and Holm-Hansen (1995) introduced a delayed resonator, see also (Filipovic, 1999), which is a tuned mass damper where an external force is connected to a mass of an absorber. This external force is calculated by delaying and multiplying position, speed or acceleration measurements (see Figure 61). Further information on current research can be found in (Olgac and Holm-Hansen, 1995) for design principles, (Filipovic and Schröder, 1998) and (Filipovic, 1998) for band pass absorption and (Olgac and Jalili, 1998), (Jalili and Knowles, 2004) and (Filipovic and Olgac, 1997) for a general introduction and the basics.

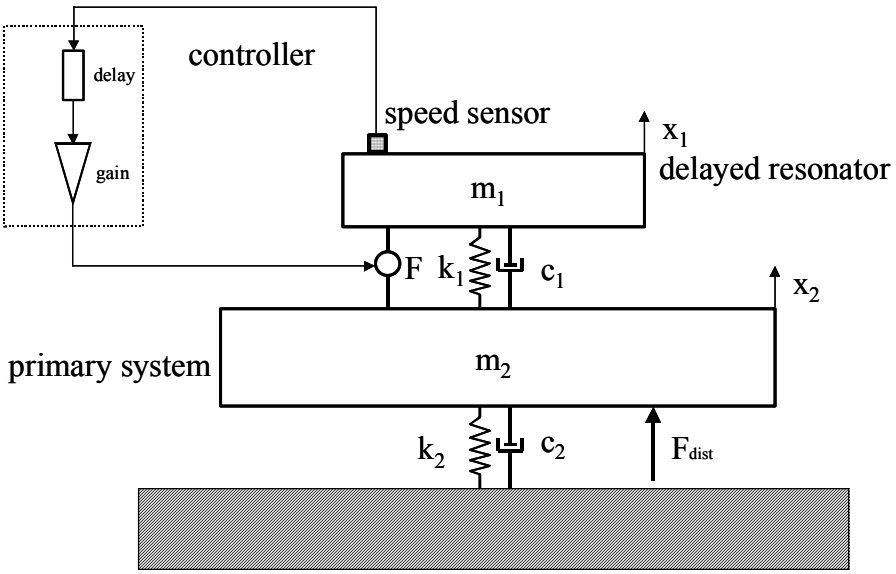

Figure 61: Delayed resonator with a speed measurement. The speed measurement is first delayed and then multiplied by gain. The result is an external force F directed on the mass of the resonator m_1. m_2 is the primary mass to be damped. k_1 and k_2 are spring constants and c_1 and c_2 damping factors.

For the system in Figure 61 above, the following equation of motion can be written:

$$m_1\ddot{x}_1(t) + c_1\dot{x}_1(t) + k_1x_1(t) - F(t) = 0 \tag{5.4}$$

where

$$F(t) = g\dot{x}_1(t-\tau) \tag{5.5}$$

External force F is a function of the delayed velocity and the multiplier gain g. The characteristic polynomial CR(s) of the system is:

$$CR(s) = m_1s^2 + c_1s + k_1 - ge^{-\tau s} \tag{5.6}$$

The roots of the system without the delayed resonator are:

$$s_{1,2} = \frac{-c_1 \pm \sqrt{c_1^2 - 4m_1k_1}}{2m_1} \tag{5.7}$$

The basic principle of the delayed resonator is to use an external force to move the two poles of the imaginary axis to the desired location.

The delay and gain, which satisfy the design principle mentioned above, can be solved from the characteristic polynomial.

By substituting

$$s = j\omega_c \tag{5.8}$$

to the characteristic equation and solving for the critical gain and the delay from

$$\Re e\{CR(j\omega_c)\} = 0 \tag{5.9}$$

$$\Im m\{CR(j\omega_c)\} = 0 \tag{5.10}$$

The delay and the critical gain derived from the equations above place the poles of the system on the imaginary axis.

$$\tau_c(\omega_c) = \frac{1}{\omega_c}\text{atan}\left(\frac{\mathrm{k}_1 - m_1\omega_c^2}{c_1\omega_c}\right) + \frac{n\pi}{\omega_c}, \quad n = 0, 1, 2, \ldots \tag{5.11}$$

$$g_c(\omega_c) = \frac{k_1 - m_1\omega_c^2}{\omega_c \sin(\tau_c\omega_c)} \tag{5.12}$$

Because of the periodic nature of the tangent function, there are infinitely many solutions.

A slight criticism of the basic idea of the delayed resonator is that it is based on the fact that the system poles are placed on the imaginary axis to make the damper a true resonator. From a mathematical point of view, a true resonator is basically unstable if the input of the system is a sinusoidal signal. From the practical point of view, there are also some risks. A system with poles on the imaginary axis or very close to it is highly sensitive to even minor changes in the system parameters. Undoubtedly, the risk that the system will become unstable is high. In fact, a true resonator is stable and also Liapunov stable, i.e., it is stable for all initial values, but it is neither asymptotically stable nor BIBO stable. The output of a BIBO-stable system is bounded for all bounded inputs, but a true resonator is unstable when the input signal is a bounded (constant amplitude) sine signal. Of course, it is probably assumed that a delayed resonator damps the vibration and this problem does not exist and/or that, in practice, the output signal is electronically or mechanically bounded. There is clearly a gap between theory and practice in this case.

A new design method to solve this problem is introduced in the next section.

5.4. Free pole placement design method for active damper

As mentioned in the previous section, robustness might be a problem in the delayed resonator. Therefore, it is possible to reduce the critical gain to improve the stability margin of the system. However, that affects the natural frequency as well as the damping so the damper does not work at the desired resonance frequency anymore.

The new free pole placement (FPP) design principle for an active damper shown in Figure 61 is introduced in this section. It makes it possible to tune the delayed resonator so that both the damping and the resonance frequency can be chosen independently.

Instead of substituting $s = j\omega_c$ use $s = a + jb$

Then the real part of the characteristic polynomial of (5.6) becomes

$$\Re e\{CR(a+jb)\} = m_1 a^2 - m_1 b^2 + c_1 a + k_1 - g_c e^{-\tau_c a}\cos(\tau_c b)a \qquad (5.13)$$

$$- g_c e^{-\tau_c a} b \sin(\tau_c b)$$

and the imaginary part

$$\Im m\{CR(a+jb)\} = 2m_1 ab + c_1 b + g_c e^{-\tau_c a}\sin(\tau_c b)a - g_c e^{-\tau_c a} b\cos(\tau_c b) \qquad (5.14)$$

By setting the right sides in (5.13) and (5.14) equal to zero, the critical gain and the delay can be solved:

$$\tau_c(\omega_c,\zeta) = \frac{-\operatorname{atan}(b(m_1 b^2 - k_1 + m_1 a^2)/(c_1 b^2 + m_1 a^3 + c_1 a^2 + a k_1 + a m_1 b^2)) + n\pi}{b} \qquad (5.15)$$

$$, n = 0, 1, 2, ...$$

$$g_c(\omega_c,\zeta) = \frac{-(m_1 a^2 + m_1 b^2 - c_1 a - k_1)}{e^{\tau_c a}(\cos(\tau_c b)a + b\sin(\tau_c b))} \qquad (5.16)$$

where $a = -\omega_c\zeta$ and $b = \omega_c\sqrt{1-\zeta^2}$

The natural frequency ω_c and damping factor ζ correspond to parameters of a second-order transfer function:

$$G(s) = \frac{\omega_c^2}{s^2 + 2\zeta\omega_c s + \omega_c^2}$$

These equations make it possible to tune the damping and the resonance frequency independently.

In Figure 62, the amplitude curves of four different systems are shown. A passively tuned mass damper has the following parameters: $m_1 = 20\,kg$ and resonance frequency $f_c = 120\,Hz$. Therefore, $k_1 = (2\pi f_c)^2 m_1 = 1.14\cdot 10^7\ N/m$. The damping factor is 5% so the damping constant c_1 becomes $c_1 = 2m_1\zeta\sqrt{k_1/m_1} = 1508\ Ns/m$.

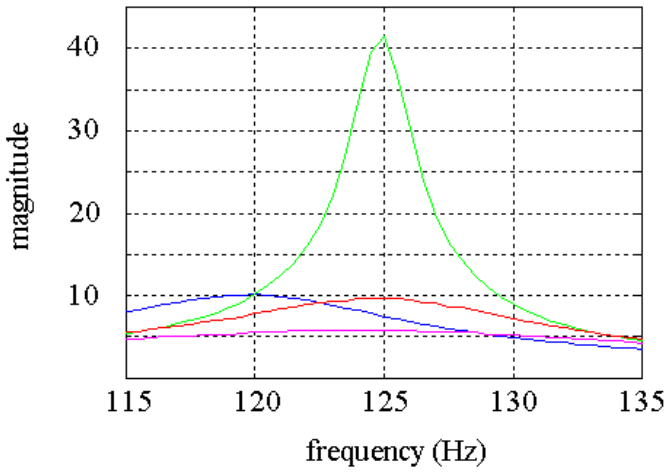

Figure 62: Magnitude curves of mass damper with different parameter values (passive damper – blue, 125 Hz resonance frequency and 1% damping – green, 125 Hz resonance frequency and 5% damping – red, 125 Hz resonance frequency and 10% damping – magenta).

An amplitude curve of the passive system is drawn in blue; it can be seen that amplification is 10 at the resonance frequency of 120 Hz. An external force element was added to a passive damper. The active damper was tuned to the resonance frequency f_c of 125 Hz at three different damping factor values ζ (see Table 5-1).

Table 5-1: Gain g_c and delay τ_c values for different damping factor values ζ .

ζ	n	f_c	g_c	τ_c
1 %	2	125 Hz	1633.7	0.00699
5 %	2	125 Hz	1001.5	0.00600
10 %	1	125 Hz	1377.8	0.00495

The amplitude curve with the damping factor ζ = 1% is drawn in green. It can be seen that the amplification is over 40 at the resonance frequency. The amplitude curve of the active damper with damping factor ζ = 5% is drawn in red. The damping factor is the same as in

the passive damper. However, the amplification is now a little lower because of the higher frequency. The amplitude curve of the system with damping factor ζ = 10% is drawn in magenta.

The required external forces for systems with ζ = 1% and ζ = 5% are displayed in Figure 63. During the 30 s period, the frequency of the chirp-signal fed to the input changed from 100 to 150 Hz. The amplitude of the signal is 0.1 mm.

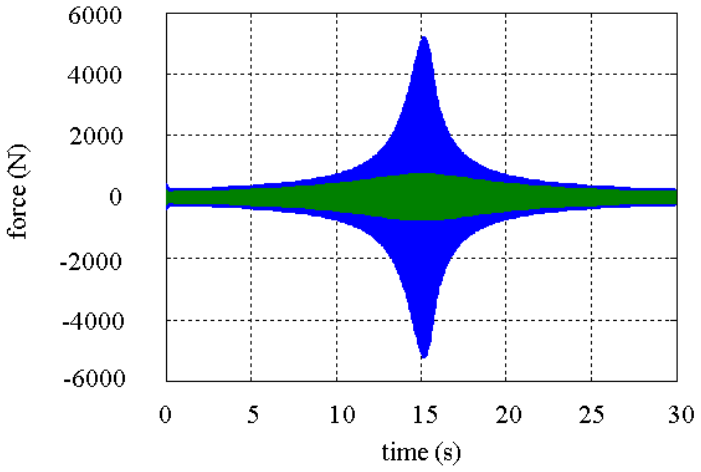

Figure 63: Required external forces, ζ = 1% (blue) and ζ = 5% (green).

In this section, a new method was introduced to calculate the delay and gain values for actively controlled mass dampers, so that both damping and resonance frequency could be controlled independently. In the earlier studies, only the resonance frequency could be adjusted and the damping factor was always zero.

5.5. Resonance frequency shift of active damper

In certain circumstances, the system might have a limited capacity to produce an external force or it is a desirable feature of the system that the controlled system has the same damping as a passive mass absorber. In the previous section, a method was introduced for the active damper of Figure 61, which made it possible to place the system poles in the desired positions in frequency domain. A new and practical method to tune the resonance frequency, but keep the damping ratio the same as the damping ratio of a passive mass damper, is introduced in this section.

The controller is based on a similar type of transfer function as that introduced in (Jalili and Knowles, 2004), where an acceleration measurement is applied.

$$F(s) = \frac{gs^2}{1+Ts} X(s) \tag{5.17}$$

F(s) is the external force in Laplace domain, *X(s)* the position, *g* is the gain, and *T* the time constant. Now, instead of an acceleration measurement, a speed measurement is applied (see Figure 64).

$$F(s) = \frac{gs}{1+Ts} X(s) \tag{5.18}$$

Taking (5.18) into account, Equation (5.4) is modified to:

$$m_1 s^2 X(s) + c_1 s X(s) + k_1 X(s) - \frac{gs}{Ts+1} X(s) = 0 \tag{5.19}$$

The characteristic polynomial takes the form:

$$CR(s) = Tm_1 s^3 + (Tc_1 + m_1)s^2 + (Tk_1 + c_1 - g)s + k_1 \tag{5.20}$$

Now the gain *g* and the time constant *T* are not used to place the system poles on the imaginary axis to create a resonator. These parameters are used instead to move the system poles from the actual passive mass absorber's poles in such a direction that the damping of the system stays the same.

The time constant is used to leave the open loop poles, which are the original mass absorber's poles, in such a position that the system's damping factor stays unchanged, but the resonance frequency changes.

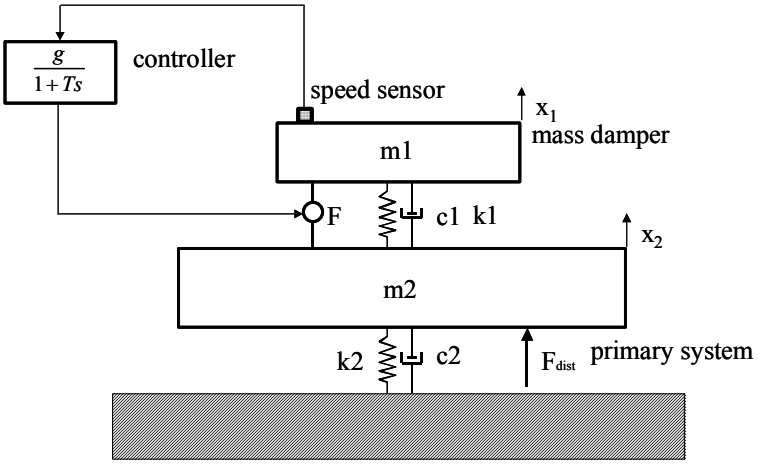

Figure 64: A first-order controller in the feedback loop.

Figure 65 demonstrates the effect of the time constant T in the controller. Two different root locus diagrams are drawn with two different time constant values T_1 and T_2. For the system with time constant T_1, the resonance frequency of the system increases, while the damping factor stays constant, when gain g increases. For the system with time constant T_2, damping decreases when g and resonance frequency increase. Both root locus diagrams start from the poles of the non-controlled mass damper (g=0). Only one pole is shown in Figure 65.

After the proper time constant value has been chosen, the resonance frequency value can be set with gain g. Figure 66 shows the results of three different simulations where three gain values are used to control the resonance frequency of the damper to 117, 120 and 122 Hz, respectively. Time constant T=0.025 s in all cases.

The following gain values are used: $g_1 = -1.0 \cdot 10^4, (f_c = 117Hz)$, $g_2 = 0.0, (f_c = 120Hz)$, and $g_3 = 1.0 \cdot 10^4, (f_c = 122Hz)$.

With gain g=0, the system behaves like a passively tuned mass damper. Gain g_3 is tuned so that the resonance frequency of the system is 122 Hz. A lower resonance frequency (117 Hz) is tuned by choosing a negative value of gain g_3.

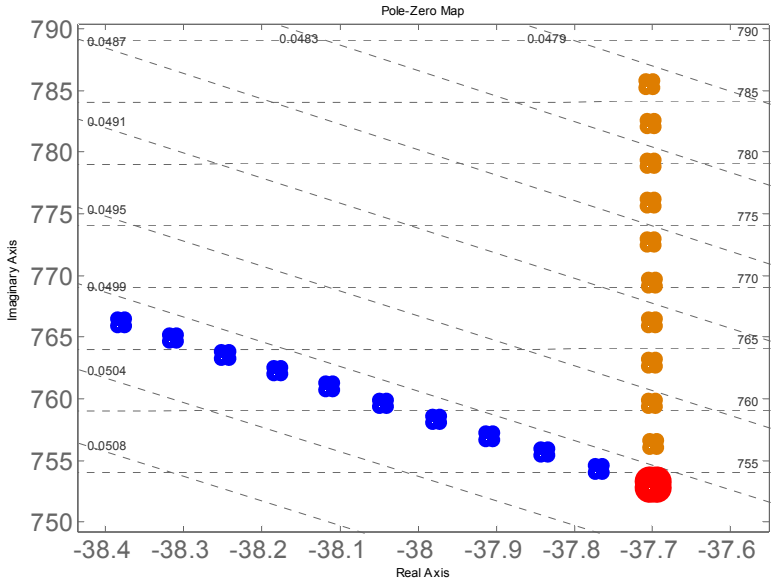

Figure 65: Parts of root locus diagrams of actively controlled mass dampers with two different time constant values T_1 = 0.025 s (blue) and T_2 = 10 s (brown). Original system pole is marked in red.

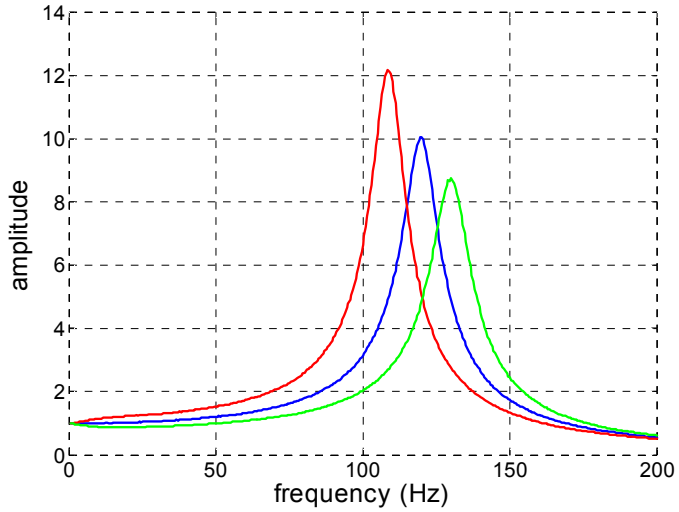

Figure 66: Bode diagrams of an actively controlled mass damper with three different tuned resonance frequencies $g_1 = -1.0 \cdot 10^4, f_c = 117Hz$ (red); $g_2 = 0.0, f_c = 120Hz$ (blue); and $g_3 = 1.0 \cdot 10^4, f_c = 122Hz$ (green) and constant damping factor. Time constant T=0.025 s in all cases.

Figure 66 shows that, when the relative damping is constant, the amplitude of the resonating signal varies with different resonance frequencies. On the other hand, amplitudes can be kept constant, if tuning parameter T is selected so that the distance of the root locus from the imaginary axis is constant. Then the relative damping changes its value when the gain varies.

5.6. Pole placement method for actively tuned mass damper

The controller introduced in the previous section can be used in another way, too. System poles can be as well located in the desired positions in the complex plane. This makes it possible to choose the system's damping factor ζ and the resonance frequency f_c. However, there are some restrictions, which are discussed later in this section.

Now, instead of the delay and the gain, the tuning parameters are the gain and the time constant. Standard pole placement methods are not suitable for systems with time delays; therefore a different method is used in Section 5.4. Actually, now it would be possible to use pole placement methods to tune the controller. Designing controllers with pole placement tools requires some system engineering background on the part of the designers. Hence a more practical method is introduced.

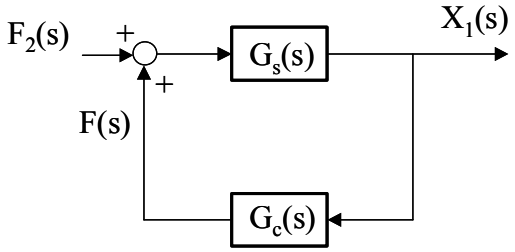

Figure 67: The block diagram of the system shown in Figure 64. $X_1(s)$ is the position of the damper mass, F(s) is the external force directed on the damper mass, $F_2(s)$ is the force created by vibration, $G_s(s)$ is the transfer function of the damper without a force element, and $G_c(s)$ is the transfer function of the controller.

The following transfer function can be derived for the mass damper shown in Figure 64. The block diagram of the system can be seen in

$$G_{damper}(s) = \frac{G_s(s)}{1 - G_s(s)G_c(s)} \tag{5.21}$$

where

$$G_s(s) = \frac{X_1(s)}{F(s)} = \frac{1}{m_1 s^2 + c_1 s + k_1} \tag{5.22}$$

and

$$G_c(s) = \frac{F(s)}{X_1(s)} = \frac{gs}{Ts + 1} \tag{5.23}$$

so

$$G_{damper} = \frac{X_1(s)}{F_2(s)} = \frac{(m_1 s^2 + c_1 s + k_1)(Ts + 1)}{Tm_1 s^3 + (Tc_1 + m_1)s^2 + (Tk_1 + c_1 - g)s + k_1} \tag{5.24}$$

where

$$F_2(s) = c_1(sX_2(s) - sX_1(s)) + k_1(X_2(s) - X_1(s))$$

The characteristic polynomial is the same as in Section 5.5, where it is used to draw the root locus of the system and to place the poles of the system along the root locus. The same idea is now used to place the system poles anywhere in the complex plane. System damping and resonance frequency can be chosen in the same way as in Section 5.4.

Substituting $s = a + jb$ into (5.20), the characteristic polynomial becomes:

$$CR(a+jb) = Tm_1(a+jb)^3 + (Tc_1 + m_1)(a+jb)^2 + (Tk_1 + c_1 - g)(a+jb) + k_1 \tag{5.25}$$

Computing the real and imaginary parts of the characteristic polynomial gives

$$\Re e\{CR(a+jb)\} = -Tb^2c_1 + k_1 + m_1a^2 + c_1a - ga - m_1b^2 + Ta^3m_1 + Ta^2c_1 + Tak_1 - 3Tam_1b^2 \tag{5.26}$$

$$\Im m\{CR(a+jb)\} = b(2m_1a - Tb^2m_1 + Tk_1 + c_1 - g + 3Ta^2m_1 + 2Tac_1) \tag{5.27}$$

Now the time constant and the gain of the forward loop controller can be solved from (5.26) and (5.27) by setting the right sides to zeros.

The final expressions for the time constant T and the gain g are:

$$T = \frac{-(m_1b^2 + m_1a^2 - k_1)}{b^2c_1 + 2m_1a^3 + c_1a^2 + 2m_1b^2a} \tag{5.28}$$

$$g = \frac{Tak_1 - m_1b^2 + Ta^3m_1 + Ta^2c_1 + k_1 - Tb^2c_1 + m_1a^2 + c_1a - 3Tam_1b^2}{a} \tag{5.29}$$

Example 5.2: Mechanical parameters of the tuned mass damper (= passive damper) are the same as in the example in Section 5.4.

$m_1 = 20$ kg, $c_1 = 1508$ Ns/m and $k_1 = 1.14 \cdot 10^7$ N/m

An active mass damper is tuned at three different operating points. Tuned damping ζ and resonance frequency f_c values and the corresponding time constant T and gain values g of the controller are shown in the following table.

Table 5-2: Gain and time constant values calculated for different damping and resonance frequency values.

ζ	f_c	g	T
1 %	115 Hz	2543	0.00146
5 %	115 Hz	2466	0.02742
5 %	125 Hz	-25573	0.02569

The system behavior is studied by simulation. A chirp signal with the frequency increased from 100 Hz to 150 Hz during 30 s is fed into the system input. The amplitude of the chirp signal is constant during that period.

Amplitude curves in the frequency domain are shown in Figure 68. The results show that, with this kind of method, it is possible to change not only the resonance frequency of the passive damper, but its damping as well. The relative damping of the passive damper is 5% and its resonance frequency 120 Hz (blue curve).

The method described above has its limitations, which are discussed next. The characteristic polynomial of the active mass damper is a third-degree polynomial. Only two poles are placed above, hence the third pole has to be investigated, too. It is enough to study whether the pole is stable or not. The Routh-Hurwitz criterion (Gantmacher, 1959) is the basis of a well-known method of studying the stability of the system. The Routh array of the characteristic polynomial of the active mass damper can be written in the following symbolic form shown in Table 5-3.

Table 5-3: Routh array of characteristic polynomial of active mass damper.

s^3	Tm_1	$Tk_1 + c_1 - g$
s^2	$m_1 + Tc_1$	k_1
s^1	$\frac{(m_1 + Tc_1)(c_1 + Tk_1 - g) - Tm_1 k_1}{m_1 + Tc_1}$	
s^0	k_1	

The Routh-Hurwitz criterion says that the system is stable, i.e., there are no poles in the right half plane, when there are no changes in the sign of the elements in the first column

of the Routh array. In fact, only the third element can be negative, so it can be used to study whether the system is stable.

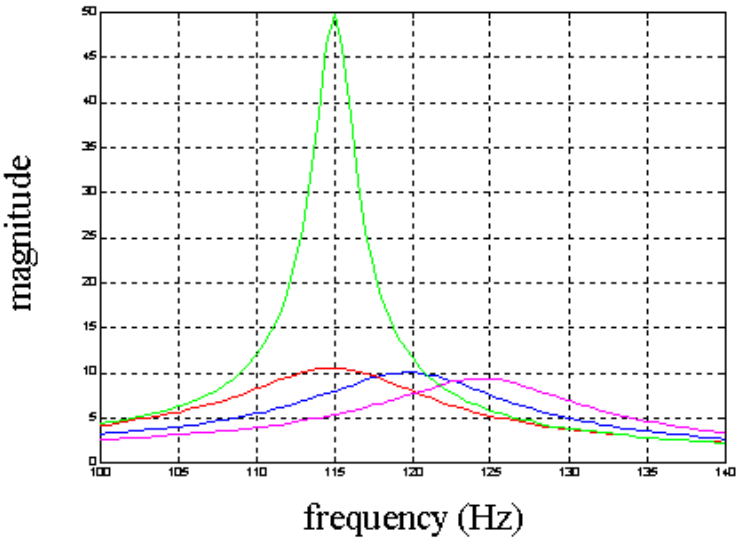

Figure 68: Amplitude curves of an active mass damper with differently tuned relative damping and resonance frequencies, ζ = 1%, f_c=115 Hz (green), ζ = 5%, f_c=115 Hz (red), ζ = 5%, f_c=120 Hz (blue), ζ = 5%, f_c=125 Hz (magenta).

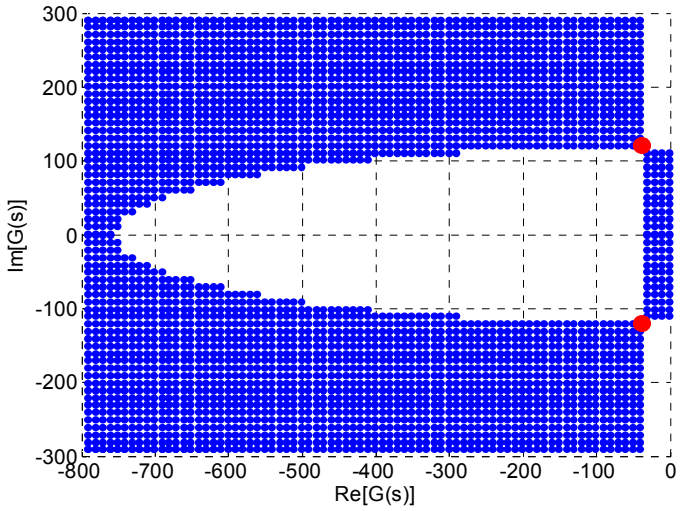

Figure 69: Stability region of the system controlled with a first-order controller. Original poles of the system are shown as red dots; the blue area is the stable region where the poles can be located.

To demonstrate the stability of an active mass damper, the stability region of the system is drawn in Figure 69. Roots shown as red dots indicate the original poles of the system without any external force and active control. The blue area is the stable area where the poles of the damper can be placed with the controller. White illustrates the area where the poles cannot be located without the third pole becoming unstable. By proper design it is, however, possible to build a damper mechanically so that the poles can be located in the desired positions. The design method is tested also by simulation; one of the simulation results is shown in Figure 70. The non-controlled system parameters are mass m= 20kg, resonance frequency f_c= 147 Hz and damping factor ζ = 2.9%.

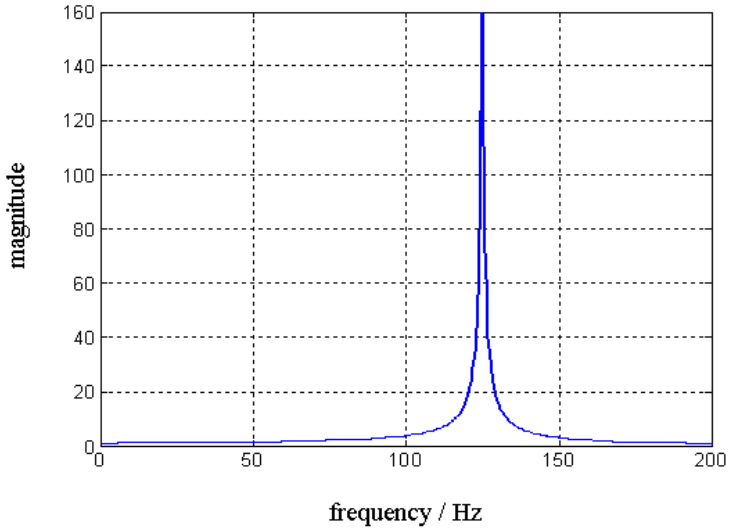

Figure 70: Magnitude curve of the system that includes the controller in Equation (5.23). The system was tuned with the pole placement method to a resonance frequency of 125 Hz with a damping factor of 0.2%. Parameter values of the controller were g=36973 and T=0.00762. Parameters were calculated with Equations (5.28) and (5.29).

5.7. Cascade control of active mass damper

In the previous sections, the force is generated in the system with an ideal force element with infinitely fast response time. In real applications, the force must be supplied to the system with some kind of actuator. The actuator has its own stiffness (spring constant), damping factor and mass, as seen in Figure 71. This section deals with active mass dampers controlled with true force actuators.

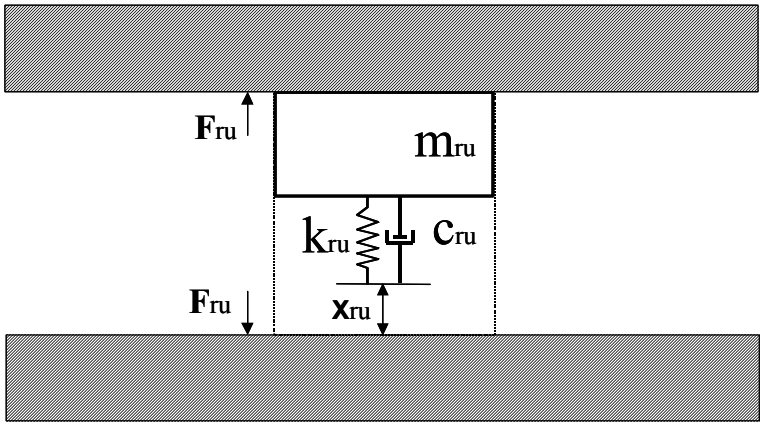

Figure 71: A model of the force element of an active mass damper.

The force element in the above figure produces force by changing the distance x_{ru}. In contrast to an ideal force element, this kind of model has dynamic behavior also. When the actuator is added to an active mass damper, it changes the system characteristics as shown in Figure 72.

Assuming that $m_{ru} << m_1$, the following motion of equations can be written for the system in Figure 72.

$$m_1\ddot{x}_1 + c_1(\dot{x}_1 - \dot{x}_2) + k_1(x_1 - x_2) + c_{ru}(-\dot{x}_1 + \dot{x}_2 + \dot{x}_{ru}) + k_{ru}(-x_1 + x_2 + x_{ru}) = 0 \tag{5.30}$$

$$m_2\ddot{x}_2 + c_2\dot{x}_2 + k_2x_2 + c_1(\dot{x}_2 - \dot{x}_1) + k_1(x_2 - x_1)$$

$$+ c_{ru}(\dot{x}_1 - \dot{x}_2 - \dot{x}_{ru}) + k_{ru}(x_1 - x_2 - x_{ru}) = 0 \tag{5.31}$$

The following transfer function relating $X_1(s)$ to $X_2(s)$ and $X_{ru}(s)$ can be derived from Equation (5.30).

$$X_1(s) = \frac{\frac{c_1}{m_1}s + \frac{k_1}{m_1} + \frac{1}{m_1}(c_{ru}s + k_{ru})}{s^2 + \frac{c_1}{m_1}s + \frac{k_1}{m_1} + \frac{1}{m_1}(c_{ru}s + k_{ru})} X_2(s) + \tag{5.32}$$

$$\frac{\frac{1}{m_1}(c_{ru}s + k_{ru})}{s^2 + \frac{c_1}{m_1}s + \frac{k_1}{m_1} + \frac{1}{m_1}(c_{ru}s + k_{ru})} X_{ru}(s)$$

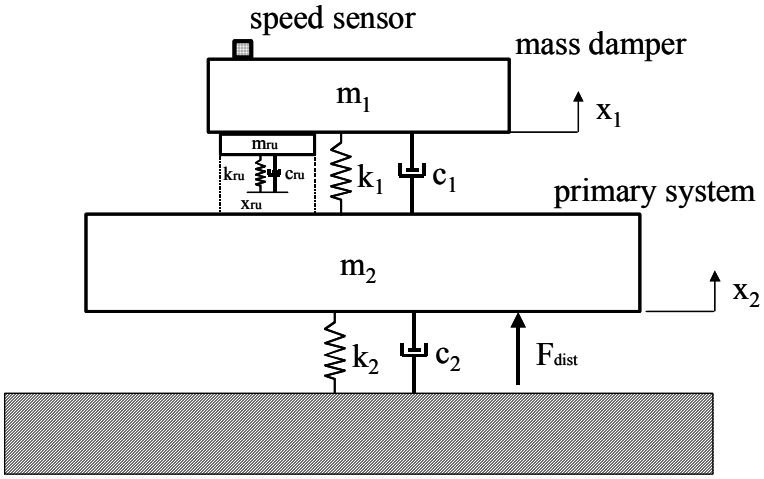

Figure 72: Active mass damper with real force actuator.

The characteristic polynomial of the mass damper without an external force element becomes:

$$CR_1(s) = m_1 s^2 + c_1 s + k_1 \tag{5.33}$$

In comparison to the equation above, the characteristic polynomial of the system with external force element is:

$$CR_2(s) = m_1 s^2 + (c_1 + c_{ru})s + (k_1 + k_{ru}) \tag{5.34}$$

Example 5.3: This example demonstrates how the force element affects the system characteristics of the damper shown in Figure 72.

In this example, it is assumed that the spring constant of the force element is 10 times larger than the spring constant of the mass damper and damping constant 5 times larger:

$k_{ru} = 10 \cdot k_1 = 1.14 \cdot 10^8 \ N/m$ and $c_{ru} = 5 \cdot c_1 = 7.54 \cdot 10^3 \ Ns/m$

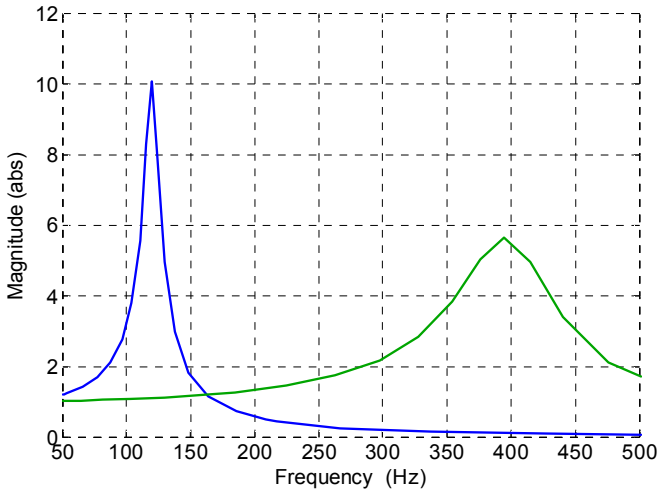

Figure 73: Magnitude curves of systems with (green line); without (blue line), external force element. Without the force element, the resonance peak is at 120 Hz, while with the force element, it is at 395 Hz.

From Figure 73, it can be seen that the uncontrolled force element strongly affects the system characteristics. The resonance frequency is raised from 120 Hz up to almost 400 Hz. It is, however, possible to use this kind of force element to control the system, as described in previous sections, but it requires a new control strategy, as explained below.

At first, it looks as if it is not possible to tune the system characteristics with this kind of external force element. However, this is not the case, as can be seen more clearly when Equation (5.30) is studied more precisely. The system characteristics can be returned back to the original value by setting:

$$F_{ru} = 0 \quad \Rightarrow \Delta x = 0 \quad \Rightarrow x_{ru} - x_1 + x_2 = 0$$

The basic control principle of the delayed resonator is that the controller output is an external force directed towards the mass of the damper. It is not always possible to feed that measurement signal straight to the external force element. However, it is possible to design another (secondary, inner) control loop and feed that delayed measurement signal as a reference value to that. This kind of setup of two control loops is commonly called a cascade controller, see e.g. (Åström and Hägglund, 1995); the whole setup can be called a cascade-controlled active mass damper.

The main reasons to use the cascade control are, in general:

- Disturbances in a secondary loop can be eliminated so that they do not disturb the primary loop.
- Non-linearities etc. can be solved in the secondary loop.

A cascade-controlled damper was tested also in practice. A test damper consisted of 20 kg mass and a spring. The resonance frequency of the passive damper was 145 Hz without an external force element. Resonance frequency is measured by the hammer-test, i.e., a short force impulse is directed onto the mass and measured with the speed sensor connected to the mass. The relative damping of the passive damper was 0.5%.

When the tests with a passive damper were performed, an external force actuator and a force sensor were mounted on the damper. The same tests were repeated for the new setup. The resonance frequency of the system is raised and it was 338 Hz. and the relative damping was 2.9%. With the traditional delayed resonator, the resonance frequency could be controlled at around 338 Hz. However, with the cascade-controlled damper, the resonance frequency can be controlled at around the original resonance frequency (145 Hz) of the passive damper.

The control system was then connected to the cascade-controlled damper according to Figure 74. In theory, the resonance frequency of the cascade-controlled damper should be the same as the resonance frequency of the passive damper without any force actuator, when force setpoint value is set to zero. This was tested in practice by setting the gain of the outer control loop to zero. The control signal of the outer loop is a reference value for the inner control loop, i.e., the force controller and the reference value is thus zero. The hammer-test showed that the resonance frequency is 147 Hz, so it is 2 Hz higher than the original resonance frequency. However, the actual force was not exactly zero, even when the reference value was zero, so that a small setpoint error explains why the resonance frequencies were not precisely the same.

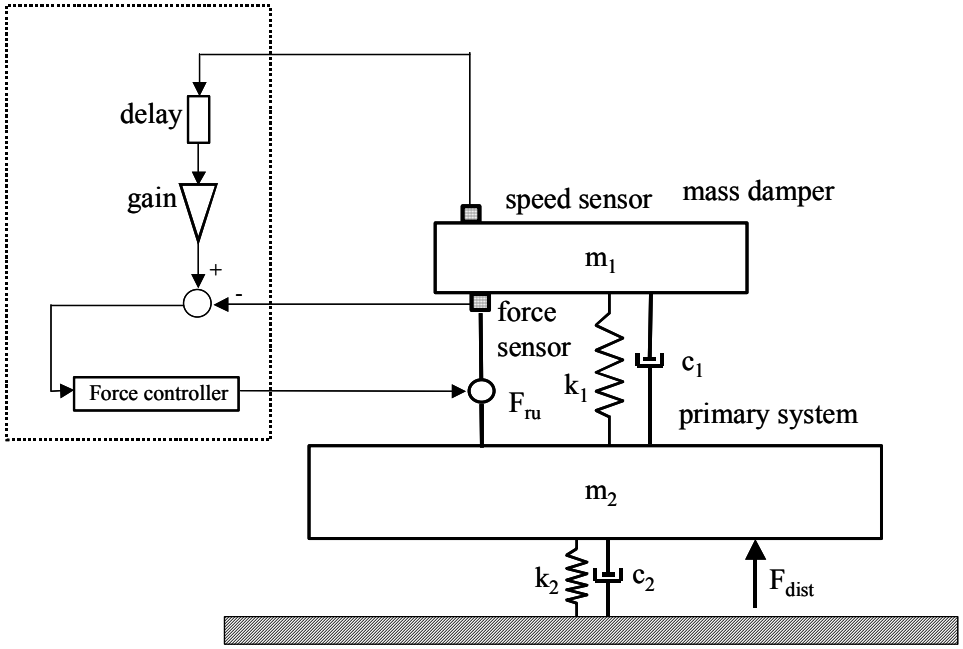

Figure 74: Cascade-controlled active mass damper.

The cascade-controlled damper is tested with different delay times τ_c and critical gain values g_c. Values used, and corresponding resonance frequencies f_c , can be seen in Table 5-4 and Table 5-5.

Table 5-4: Resonance frequencies with different delay times and positive critical gain pairs.

τ_c (ms)	g_c	f_c (Hz)	dual frequency
2.15	1.79E+04	104.5	
2.60	2.42E+04	91.5	
2.85	2.79E+04	86.0	257.5
3.10	2.63E+04	85.0	245.5
3.60	1.89E+04	216.0	
4.10	1.37E+04	194.0	
4.60	9.46E+03	177.0	
5.10	6.31E+03	165.5	
9.85	1.05E+04	120.5	182.0

Table 5-5: Resonance frequencies with different delay times and negative critical gain pairs.

τ_c (ms)	g_c	f_c (Hz)	dual frequency
2.15	-6.84E+03	162.5	
2.60	-4.73E+03	155.0	
3.10	-4.21E+03	150.0	
3.60	-3.94E+03	145.0	
4.10	-4.21E+03	140.0	
4.60	-4.73E+03	137.5	
5.10	-6.31E+03	130.0	
5.60	-7.36E+03	125.0	
6.10	-1.05E+04	117.5	
6.60	-1.26E+04	110.0	192.5
7.10	-1.16E+04	105.0	185.0
7.60	-9.46E+03	180.0	
8.10	-7.89E+03	167.5	

It can be seen from the above tables that it is possible to control the resonance frequency of a cascade-controlled damper at least from 85 Hz up to 216 Hz. Dual frequency means that, with certain delay and gain values, there were two resonance peaks in frequency response instead of one. It was shown earlier in Section 5.3.1 that the delayed resonator has infinitely many solutions, cf. (5.11) and (5.12). At certain points, two different solutions give the same delay time and gain, but a different resonance frequency. With this kind of parameter values, both frequencies start to resonate. That phenomenon can also be seen in the experiments. Dual frequency is approached in the next section also, where the stability of the active dampers is studied.

In summary, two main advantages of the cascade-controlled damper over the traditional delayed resonator can be listed.

1. Stiffness of a force actuator does not affect the resonance frequency of the damper.

2. Inner control loop (force controller) compensates possible nonlinearities or time-varying properties of the force actuator.

There are not any major disadvantages, but the control setup is more complex.

5.8. Stability of active mass dampers

When Equation (5.7) is studied more closely, it can be seen that, when the gain value is set to zero, the poles of the system are the poles of the passive mass damper. Delay time has no effect on the system characteristics at that point. With a small gain value, the system is still stable and has two poles near the poles of the original passive damper. However, the system has now infinitely many other stable poles also. When the gain value g_c starts to increase, one pair of poles reaches the imaginary axis. This is the so-called critical gain and the poles on the imaginary axis determine the resonance frequency. If the gain value is further increased, another pair of poles reaches the imaginary axis, but the previous poles are now on the right half plane, causing the system to become unstable. It is also possible that, with a certain gain and delay time, the two branches of the root locus reach the imaginary axis at different locations. This is called the dual frequency; the delayed resonator has now two resonance frequencies.

The critical frequency and the critical gain can be drawn as a function of the delay time. The cascade-controlled damper tested in practice had a 20 kg mass, 145 Hz eigenfrequency, and 2.9% relative damping. The critical frequency and corresponding gain values for 6 different (n=0..5) branches were calculated according to Equations (5.11) and (5.12). Curves for positive critical gain values can be seen in Figure 75 and for negative critical gain values in Figure 76. For example, the first critical gain value (n=0) starts to increase when the delay time increases (see blue curve in Figure 75). However, the second critical gain (green curve) starts to decrease when the delay time increases. With delay time t_c=2.8 ms, these two branches cross each other. If the critical gain is still increased

along the blue curve, the system becomes unstable because the critical gain value goes over the second curve. The point where the two curves cross is also the dual frequency point mentioned above. At that point, there is not one, but two, resonance frequencies, f_c=86 Hz and f_c=257 Hz. The second dual frequency point can be seen at the point where delay time is τ_c = 9.8 s (f_c=120 Hz and f_c=182 Hz). The values of the measured critical gain g_c and delay τ_c shown in Table 5-4 and Table 5-5 are also added to Figures 75 and 76. Measured values correspond to the calculated values well and there is only a slight difference between the actual and the calculated gain values.

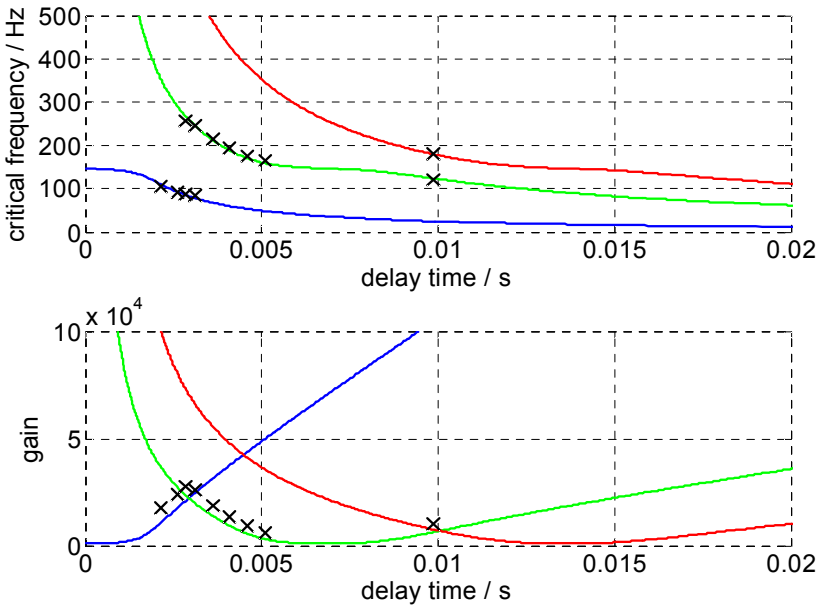

Figure 75: Stability region of the delayed resonator and corresponding frequencies with positive gain values ($g_c(\omega_c)$>0). Critical frequency f_c as a function of delay time τ_c (above) and critical gain g_c as a function of delay time τ_c (below). Dark blue curve corresponds to n=0, green curve to n=2 and red curve to n=4. Black crosses represent measured values.

In Figure 76, the negative gain values of the delayed resonator can be seen. There are also two dual frequency points and, with negative gain values, the resonance frequency can be raised to over 500 Hz. Similar types of calculation are also performed for the two-parameter damper with 20 kg mass, 147 Hz resonance frequency, 2.9% mechanical damping factor and 5% tuned damping factor. These curves are not, however, stability regions, but regions of the system with a 5% damping factor. To ensure that solutions are stable the stability regions presented above must be used. It can be seen that the first frequency-gain curve in Figure 77 cross each other. At that point, there is also a dual frequency point with delay τ_c=0.00287 s and g_c=17400. The delay value is the same as in the delayed resonator, but the gain is smaller. However, the delay value is not always the same for the same frequency. For example, the delay resonator reaches 198 Hz resonance frequency with delay τ_c=0.00134s and gain g_c=-11198, but the FPP damper reaches this with delay τ_c=0.0012 s and g_c=-10462. The simulated frequency response of the FPP damper with these dual frequency parameters can be seen in Figure 79. Stability issues of the pole placement method and dampers controlled with the first-order controller have been studied already in Section 5.6.

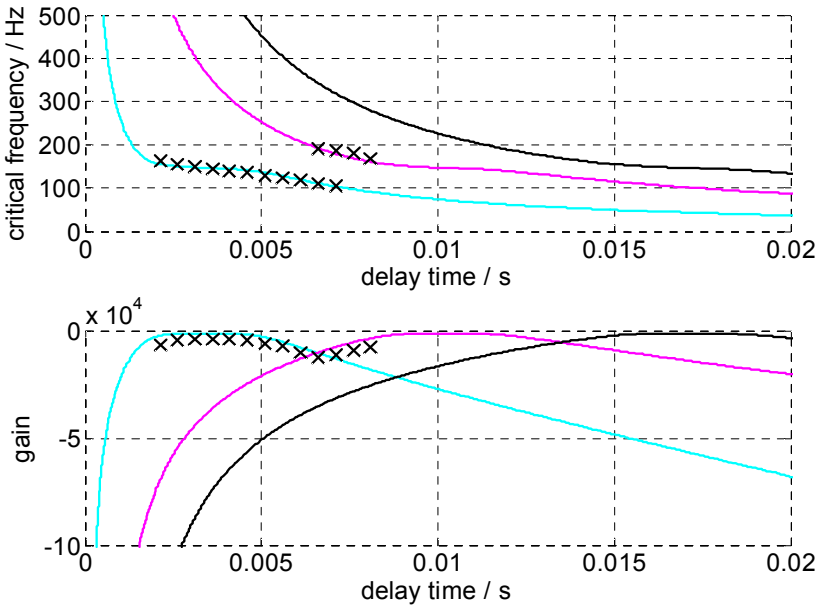

Figure 76: Stability region of the delayed resonator and corresponding frequencies with negative gain values ($g_c(\omega_c)$<0). Critical frequency f_c as a function of delay time τ_c (above) and critical gain g_c as a function of delay time τ_c (below). Light blue curve corresponds to n=1, magenta curve to n=3 and black curve to n=5. Black crosses represent measured values.

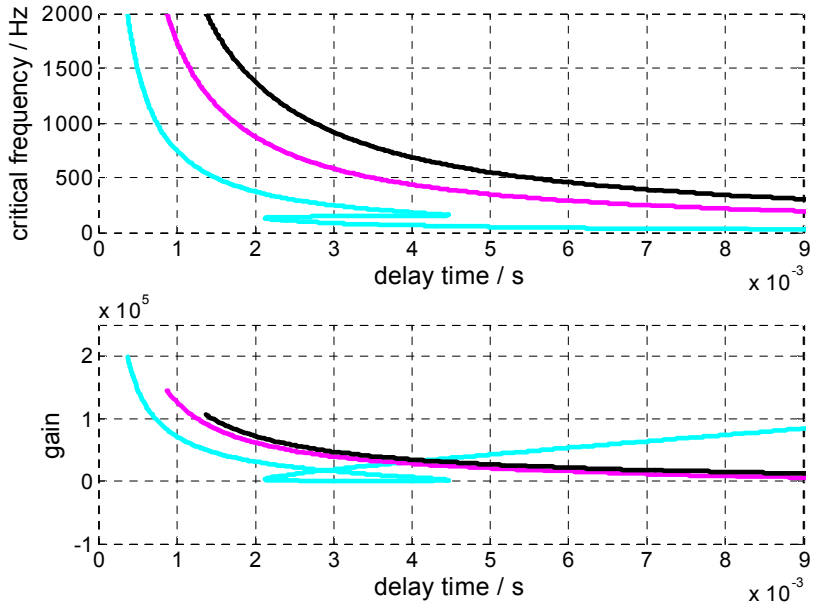

Figure 77: 5% relative damping region of the FPP damper and the corresponding frequencies with positive gain values (gc(wc)>0).

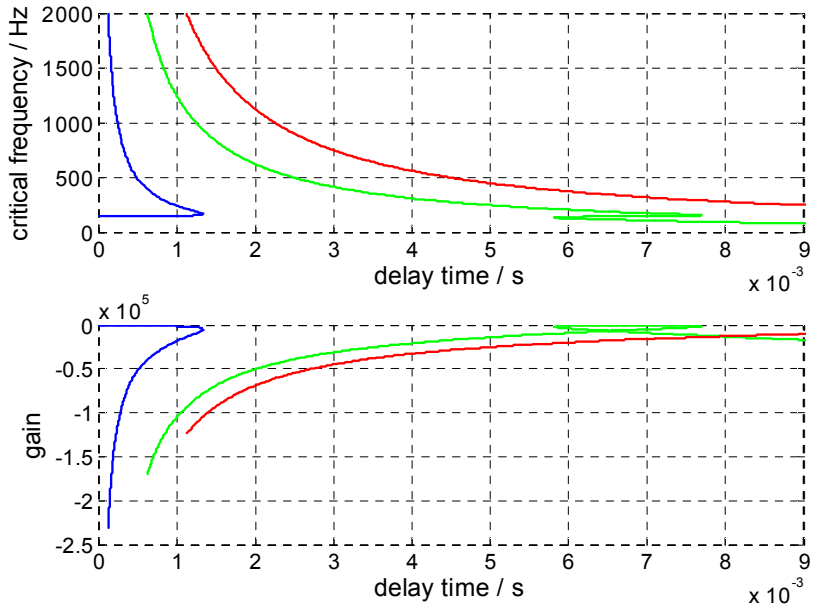

Figure 78: ζ = 5% damping factor region of the FPP damper and corresponding frequencies with negative gain values ($g_c(\omega_c)$>0). Critical frequency f_c as a function of the delay time τ_c (above) and critical gain g_c as a function of the delay time τ_c (below). Dark blue curve corresponds to n=0, green curve to n=2 and red curve to n=4.

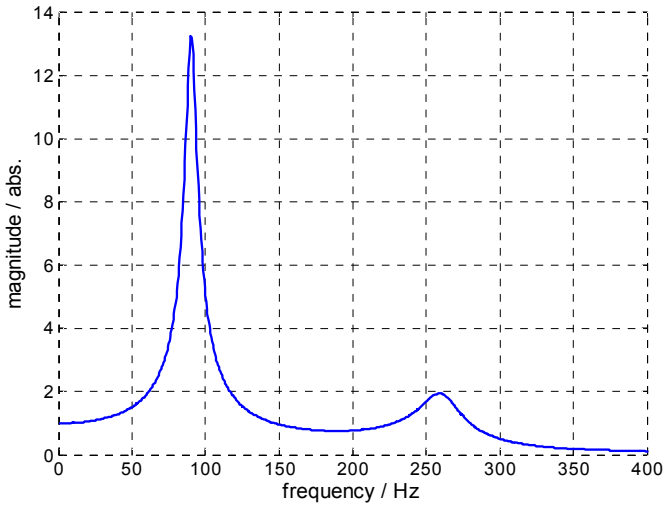

Figure 79: Magnitude diagram of the FPP damper with gc=17400 and tc=0.00287 s.

The stability of the delayed resonator is also studied with the Nyquist plot and the Nyquist stability criterion. The Nyquist plot can be used to study the stability of the closed-loop control systems (Jacobs, 1974). The Nyquist method can also be used to study the gain and phase margins of the closed-loop system.

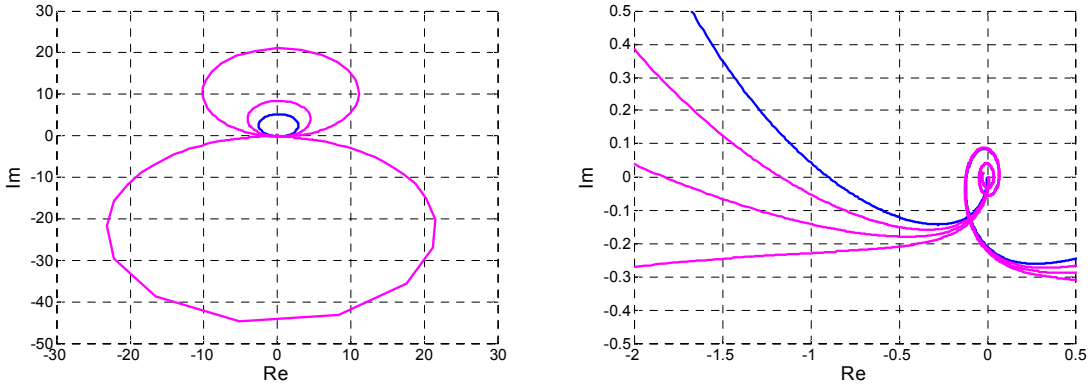

Figure 80: Nyquist diagram (blue) of a stable system with gain value of 0.9 times critical gain g_c. The whole diagram is on the left and the zoomed figure around critical point –1 on the right. Magenta contours are mappings from the stable s-plane (left half plane). The closed-loop system is stable because the Nyquist contour does not encircle point –1.

The stability of the delayed resonator used in the laboratory tests is studied with Nyquist diagrams. The system parameters are the same as above, i.e., mass m=20 kg, resonance frequency f_c = 147 Hz and damping factor ζ = 2.9 %. The delayed resonator is tuned to

125 Hz with controller parameters of delay time $\tau_c = 0.00178$ s and critical gain $g_c = 6110$. Two different Nyquist diagrams are drawn with two gain values, i.e., $g_c = 5499$ (0.9 times critical gain, a stable system) and $g_c = 6721$ (1.1 times critical gain, an unstable system). In practice, it is sometimes difficult to see whether the Nyquist contour encircles point –1 or not. Because of this, Nyquist diagrams are not only drawn by substituting $s = j\omega$, but also $s = a + j\omega$, into the open loop transfer function.

$$G(s)H(s) = \frac{-g \cdot e^{-s\tau} s}{20s^2 + 1071s + 1.7 \cdot 10^7}$$

with three different values of a, a=-10, a=-20, and a=-30.

With this substitution, the transfer function becomes:

$$G(a + j\omega)H(a + j\omega) = \frac{-ge^{-\tau a}(\cos(\tau\omega) - j\sin(\tau\omega))(a + j\omega)}{20(a + j\omega)^2 + 1071(a + j\omega) + 1.7 \cdot 10^7}$$

The Nyquist diagram of the stable system can be seen in Figure 80. The actual Nyquist contour is drawn in blue and mapped values from the left half plane in magenta. Now, the magenta contours must cover the point –1 to show that the system is stable. It is, of course, a congruent demand with the Nyquist stability criterion, so the Nyquist contour in Figure 80 does not encircle the point –1.

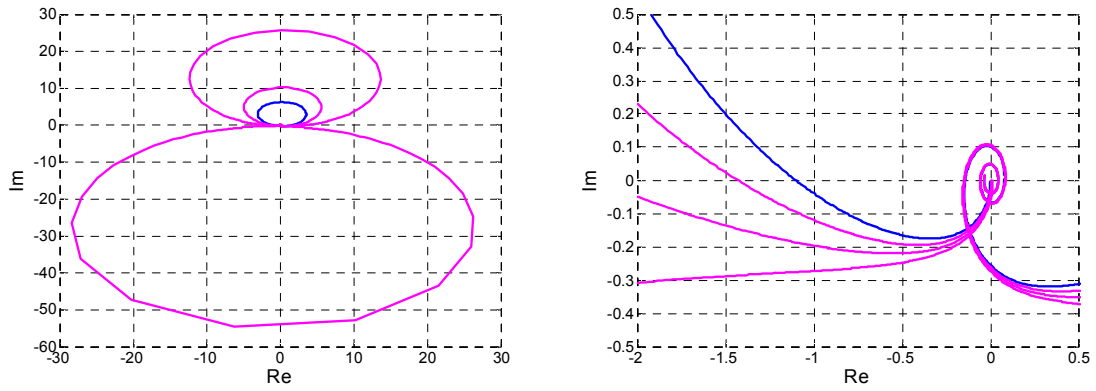

Figure 81: Nyquist diagram (blue) of an unstable system with gain value 1.1 times the critical gain g_c. The whole diagram is shown on the left and the zoomed figure around the critical point –1 on the right. The magenta contours are mappings from the stable part of the s-plane (i.e., left half plane). The closed-loop system is now unstable, because the Nyquist contour encircles the point –1.

The Nyquist diagram of the unstable system can be seen in Figure 81. Now, the stable magenta contours do not cover point –1 and the Nyquist contour also encircles point –1.

With the critical gain value g_c, the Nyquist contour goes exactly through the point –1, i.e., the closed-loop system has poles on the imaginary axis.

5.9. Active damping with hydraulic actuator

In the previous sections, methods for vibration damping are introduced. These are based on the tunable mass absorber and its variations (passive and active). In this section, a method based on the damping with a hydraulic actuator is studied. For other studies of the hydraulic vibration control of mechanical structures, see, for example, (Heiskanen *et al.*, 2003). Hydraulic actuators are also used to actively damp the vibration of the cable-stayed bridges (Helduser and Bonefeld, 2001) and, for example, in the suspensions for heavy vehicles (Kitching *et al.*, 2000).

Active vibration damping usually means producing a counterforce against vibration. In this case, the counterforce is produced with a hydraulic cylinder. It is an actuator, in which the natural frequency changes as a function of the position of the cylinder. The method is tested with the rider roll of the pilot winder located in the Winding Technology Center, Järvenpää (see Figure 33).

The frequency response of the rider roll is measured in different positions without nip contact, i.e., in the air. A chirp signal from 5 Hz to 50 Hz is fed into the system and the response measured with an acceleration transducer. Three positions that correspond to roll diameters 301 mm, 895 mm and 1200 mm (see Figure 82) are used. It can be seen that, with 301 mm and 1200 mm diameters, the natural frequency is a little higher than with an 895 mm diameter. In the hydraulic cylinder, the natural frequency is lower in the middle of the cylinder piston stroke and higher in both ends. Of course, in this measurement, all the mechanical natural frequencies must be paid attention to also, but the result supports the fact that it is the hydraulic natural frequency that can be seen in these measurements. It must also be remembered that the minimum frequency is not reached in the middle of the cylinder stroke because of the asymmetry caused by the cylinder rod diameter. The overall stroke of the hydraulic cylinder was 2.16 meters.

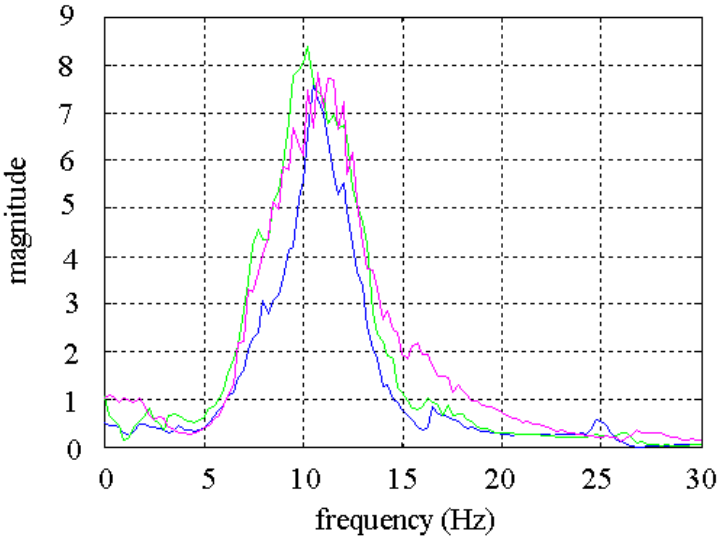

Figure 82: Amplitude curves of the rider roll in different positions without the nip contact. The position is presented as equivalent roll diameters (blue - 301 mm, green - 895 mm, magenta - 1200 mm).

The simulation model of a rider roll described in Section 4.3 calculates the hydraulic natural frequency of the rider roll also. The calculated natural frequency as a function of cylinder stroke is shown in Figure 83. It can be seen that the minimum value of the natural frequency is reached in the same region as in the measurements.

The same types of measurement are also repeated with the nip closed, i.e., the rider roll is pressing against the paper roll as in the normal operation. It must be kept in mind that the properties of the paper roll (stiffness and damping) are changing as a function of the roll diameter. A usual situation is that stiffness is lowering and damping properties are increasing when the roll diameter increases. Test results in Figure 84 must be interpreted with this in mind.

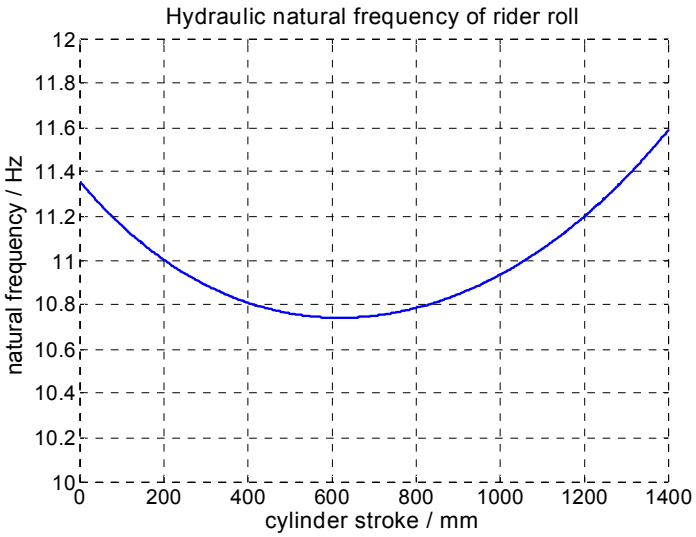

Figure 83: Calculated hydraulic natural frequency of the rider roll as a function of the rider roll position.

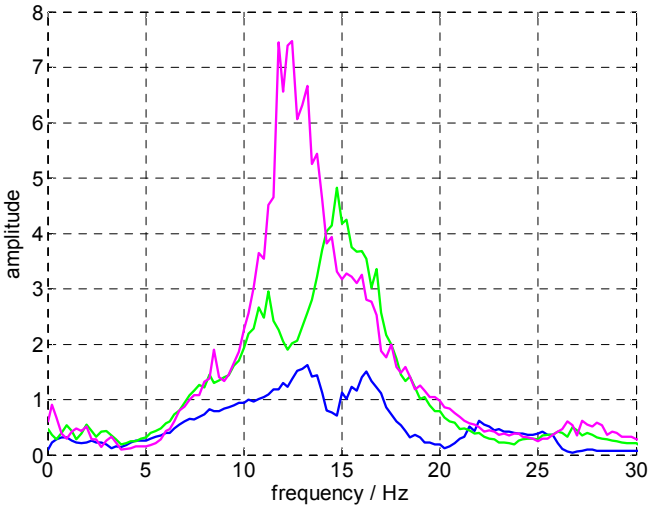

Figure 84: Frequency responses of the rider roll with different roll diameters with the nip contact (blue – 310 mm, green – 591 mm, red – 1159 mm).

It can be seen that, with the two smallest diameters, frequency responses have two peaks. It is possible that the paper roll works as a damper in these cases (compared with the results with mass dampers) and cuts the maximum peaks. However, another possibility is that, with smaller diameters, two different resonance frequencies can be observed. Overall, it can be seen that the natural frequencies are higher when the rider roll is in contact with the paper roll.

Vibration control is first tested in a non-rotating winder. In this test, a 12.5 Hz vibration excitation is fed into the rider roll. Vibration is then measured with and without the controller (see Figure 85). The test is performed so that the rider roll is lying normally on the core. The controller is a feedback controller from the speed measurement of the acceleration transducer shown in (5.35). The controller parameters are calculated with the pole placement method. Input u is the vibration measurement and y the control signal to the hydraulic valve. The tests proved that the active hydraulic vibration damper could decrease vibration of the rider roll over some frequency range.

$$\dot{x} = \begin{bmatrix} 0.12 & -0.0447 \\ 0.0447 & 0.0 \end{bmatrix} x + \begin{bmatrix} 1.0 \\ 0.0 \end{bmatrix} u \tag{5.35}$$

$$y = \begin{bmatrix} -0.693 & 4.58 \end{bmatrix} x + 0.7\,u$$

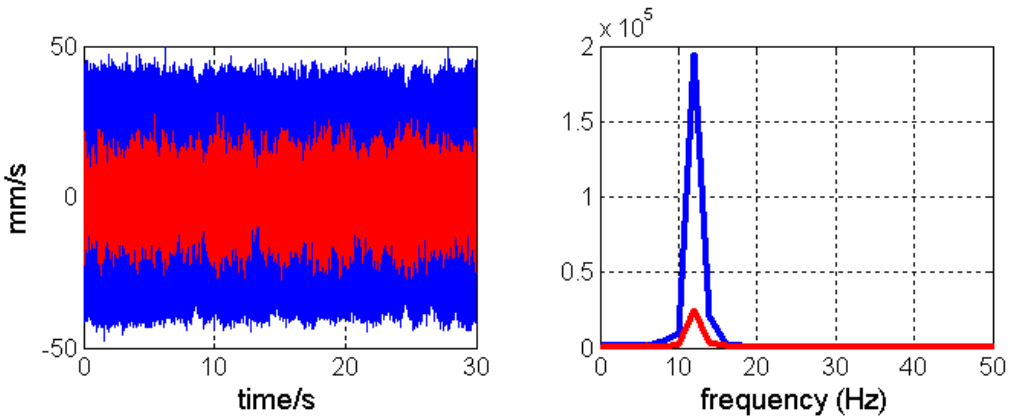

Figure 85: Rider roll vibration with a controller (red) and without (blue) in time and frequency domains.

Vibration control is tested under normal running conditions also. Results of eight different test runs are represented in Table 5-6. The same roll is used over and over again. Because the vibration property of a paper roll depends on the direction of the run, the tests had to be organized so that the results were comparable (see numbers in set-column in the table below).

It can be seen that the RMS (Root Mean Square) values drop roughly to half when the vibration control is used (see Figure 86). This type of controller is, however, tuned to damp a particular frequency range, and it increases the vibration at some other frequencies. Because of this, the controller is switched off when the rotating speed of the paper roll is outside of the operating range of the controller. As mentioned earlier, this kind of active damping method based on the counterforce does not actually absorb any energy from the vibrating system. Vibration energy must be absorbed in structures, so noise and other

issues must be considered carefully. It is also typical for hydraulic systems that their natural frequencies are quite low, which limit their use in vibration damping.

Table 5-6: Maximum RMS values with and without controller.

set	max. RMS	controller
1	26.78	OFF
3	14.40	ON
4	22.47	OFF
2	12.46	ON
5	25.58	OFF
7	14.00	ON
8	23.84	OFF
6	13.88	ON

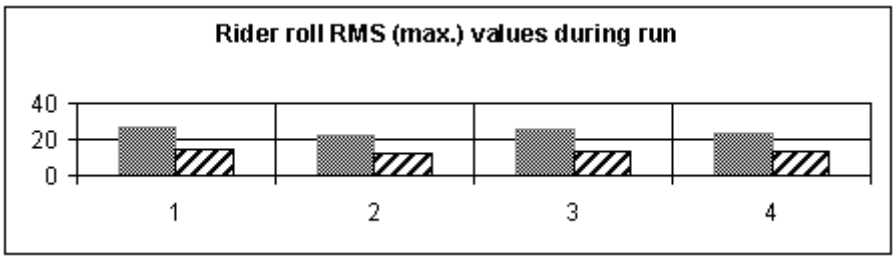

Figure 86: Maximum RMS values of the rider roll during the test run. Results without the vibration controller are shown on the left side and with the controller on the right side.

5.10. Summary

Two different active damping structures are studied in this section. The first type of dampers is based on a passive damper, a tunable mass absorber. Tunable mass absorbers have been used over a hundred years, but they can be changed to active dampers by directing additional force on the mass. There are several possibilities to calculate this control force.

The delayed resonator is the basic setup where the external force is calculated from acceleration, speed or position measurement of mass. The force is a delayed measurement multiplied by a gain. The gain and delay values are calculated by setting one pair of poles

on the imaginary axis on the desired location. Other poles must also be in the left half plane to guarantee that the system is stable.

With Equations (5.15) and (5.16), it is, however, possible to locate dominant system poles anywhere in the left half plane. By means of these equations, it is not only possible to control the resonance frequency, but also the damping of the system.

It is also possible to control the additional force by substituting the delay and gain of the delayed resonator with the first-order transfer function. Other types of transfer functions have been studied as well in literature. In those papers, poles of the system have been located on the imaginary axis. Equations (5.28) and (5.29) enable, however, the poles to be located anywhere in the left half plane, with certain restrictions discussed in Section 5.6.

In the earlier papers, the resonance frequency is controlled around the natural frequency of the whole system. In that case, the stiffness of the force actuator affects the operation range of the damper. A new cascade-controlled damper is introduced in Section 5.7. This algorithm makes it possible to design the passive part of the damper with the desired natural frequency. Now, regardless of the stiffness of the force actuator, it can be added onto the system and the damper can still operate around the same original natural frequency. Actuators with different stiffness can also be used without having an effect on the resonance frequency. It is also possible that the force actuator has certain nonlinearities or that its properties change due to some external conditions, i.e., temperature etc. These factors can be compensated, however, with an inner control loop of a cascade controller. The method is also verified with tests of an actual damper; the results can be seen in Sections 5.7 and 5.8.

The active damping method based on a hydraulic actuator is also introduced. The method is tested with a full-scale pilot winder; it decreased the vibrations during winding considerably. The main disadvantage of the system is its low natural frequency, which limits its use to disturbances with frequencies lower than 10-15 Hz.

6. Conclusions

Designing a paper winder is very much an interdisciplinary process. It requires state-of-art competence in the fields of mechanics, hydraulics, pneumatics, electronics, paper technology, winding processes, control engineering and servo control, fault diagnostics, maintenance, and low- and high-level programming. In this thesis, new methods are introduced for controllability of a paper winder, especially in the fields of vibration control and fault diagnostics.

One of the main contributions of this thesis is the method to automatically modify the control programs of a paper winder to be used in a fault diagnostic system. Until now, there have been no such methods available, because, in practice, the problem becomes unmanageable. The PLC programs contain thousands of lines of code, and, with traditional methods, the computing time needed is so large that they cannot be used. On the other hand, the work can be performed manually, but this is very expensive, time-consuming, and it has other disadvantages, as discussed in Chapter 3. The developed method has been tested in practice and it has saved expenses of the fault diagnostic systems to be used in paper winders. The quality of the diagnostic system has become better, too. After the PLC programs have been changed, it is easy to update the diagnostic system so the new method reduces the risk of faulty alarms also. This is really a win-win situation for paper-winder manufacturers and for their customers (paper mills).

Conditioning monitoring and maintenance are under constant research in the paper industry. The developed fault diagnostic methods are closely related to this field. The binary part presented a method for the operator and maintenance people. The analog part describes a model-based fault detection and isolation method that can be used as a basis for conditioning monitoring. At some point, it is possible to raise the productivity of a paper winder by increasing the maximum speed of the winder. It is, however, important to bear in mind that the reliability and usability of a paper winder are important factors, too. An issue not included in this thesis, but having a great impact on the productivity of paper winders, is the servo-controlled movement of the winder. Paper winding is a batch process and a winder is stopped after every set for a set change. Every second, when a paper

winder is not running, has an influence on productivity, so fast servo-controlled movements are important.

The running speed of a paper winder has increased remarkably during the last few years. An increased running speed and acceleration excites resonance frequencies over a very wide range. The vibration control part of this thesis deals with active vibration control methods. Mass dampers are separate devices that can be attached to the structure to damp its vibration. The resonance frequency of a mass damper has to be the same as the resonance frequency of a structure, so the traditional tuned mass damper, also called a passive damper, can be used to damp only one frequency. In this thesis, a delayed resonator and other damping methods have been developed further. Now, it is not only possible to control the resonance frequency of a damper, but its damping as well. A simple method to shift a resonance frequency of a damper is also introduced. It does not require as much external energy when the operating point is near the damper's own physical properties, i.e., its resonance frequency and damping. The frequency can also be tuned with one linear parameter, so its use is very simple in practice.

Besides actively controlled mass dampers, another active damping method is studied. This method is based on a hydraulic actuator. It is used to damp the vibration of a rider roll. The system directed a counter force against the vibrating roll by means of an acceleration measurement. This active vibration control method is tested with a full-scale pilot winder. One problem concerning such a system is the phenomenon that vibrating energy from rolls is transformed into structures of the paper winder through the rider roll. A method to eliminate that energy needs to be developed.

This thesis covers several fields of research. A future theme of interest is the further development of vibration control. The actively controlled mass dampers ought to be tested in practice with the full-scale paper winders. There are also several possibilities of applying active methods to damp structural vibrations in winders. Another interesting subject would be to bind the fault diagnosis of the binary and analog signals more closely together. It was not possible to test analog fault diagnostic methods in practice within the limits of this work. Long-term tests in paper mills would throw light on the concept of the functionality of these methods.

Bibliography

Bartlett, K.A., Brayton, R.K., Hachtel, G.D., Jacoby, R.M., Morrison, C.R., Rudell, R.L., Sangiovanni-Vincentelli, A. and Wang, A. (1988). Multi-level Logic Minimization Using Implicit Don't Cares. *Computer-Aided Design of Integrated Circuits and Systems*, IEEE Transactions on Computer-Aided Design, Vol. 7, Issue: 6, pp. 723–740.

Beards, C. F. (1996). *Structural Vibration: Analysis and Damping*. Arnold, London, Great Britain.

Berger, H. (1998). *Automating with STEP7 in STL*. MCD Verlag, Erlangen and Munich, Germany.

Boole, G. (1854). *An investigation into the Laws of Thought on Which are Founded the Mathematical Theories of Logic and Probabilities*. Dover Publications. (published 1958, originally published 1854).

Brayton, R., Hachtel, G., McMullen, C. and Sangiovanni-Vincentelli, A. (1984). *Logic Minimization Algorithms for VLSI Synthesis*. Kluwer Ac. Pub., Boston, Massachusetts, USA.

Brayton, R.K., Rudell, R., Sangiovanni-Vincentelli, A. and Wang, A.R. (1987). MIS: A Multiple-Level Logic Optimization System. *Computer-Aided Design of Integrated Circuits and Systems*, IEEE Transactions on Computer-Aided Design, Vol. 6, Issue: 6, pp. 1062-1081.

Chang, S., Cheng, D. I. and Yeh, C. (2002). Removing Multiple Redundancies in Combinational Circuits. *IEE Proceedings - Computers and Digital Techniques*, Vol. 149, No. 1.

Chen, J. and Patton, R. (1999). *Robust Model-Based Fault Diagnosis for Dynamic Systems*. Kluwer Academic Publishers, Norwell, Massachusetts, USA.

Collette, F. S. (1998). A Combined Tuned Absorber and Pendulum Impact Damper Under Random Excitation. *Journal of Sound and Vibration*, Vol. 216, No 2, pp. 199-213.

Colon-Bonet, G.; Schwarz, E.M.; Bostick, D.G.; Hachtel, G.D. and Lightner, M.R. (1989). On Optimal Extraction of Combinational Logic and Don't Care Sets from Hardware Description Languages. *Computer-Aided Design,* ICCAD-89, Digest of Technical Papers, IEEE International Conference on Computer-Aided Design, November 6-9, Santa Clara, CA, USA.

Coudert, O. (1995). Doing Two-Level Logic Minimization 100 Times Faster. *Proceedings of Symposium on Discrete Algorithms (SODA)*. January 22-24, San Francisco CA, USA.

Coudert, O., Madre, J.C. and Fraisse, H. (1993). A New Viewpoint on Two-Level Logic Minimization. *Proceedings of the 30th Design Automation Conference*. June 14-18, Dallas, Texas, USA.

Filipovic, D. and Schröder, D. (1998). Vibration Suppression with Bandpass Absorber. *Movic '98*, August 25-28, Zurich, Switzerland.

Filipovic, D. (1999). *Resonating and Bandpass Vibration Absorbers with Local Dynamic Feedback*. Shaker Verlag, Munich, Germany, (Doctoral thesis).

Filipovic, D. and Olgac, N. (1997). Delayed Resonator with Speed Feedback Including Dual Frequency – Theory and Experiments. *Proceedings of the 36th Conference on Decicion & Control*, December 10-12, San Diego, CA, USA.

Filipovic, D. and Schröder, D. (1998). Bandpass Vibration Absorber. *Journal of Sound and Vibration*, Vol. 214, No. 3, pp. 553-566.

Fuller, C. R., Elliot, S. J., Nelson, P. A. (1996). *Active Control of Vibration*. Academic Press, London, Great Britain.

Gantmacher, F.R. (1959). *Applications of the theory of matrices*. Intersience Publishers Inc, NY., USA.

Hackworth, J. R. and Hackworth F. D. (2004). *Programmable logic controllers: programming methods and applications*. Pearson, USA.

Hasan, K., Ramsay, B., Ranade, S. and Ozveren, C. S. (1994). An object-oriented expert system for power system alarm processing and fault identification. *7th Mediterranean Electrotechnical Conference*, Proceedings (Cat. No.94CH3388-6). IEEE, New York, USA, pp. 909-912.

Heiskanen K., Hakola J., Laitinen L. and Pietola M. (2003). Vibration Suppression with Hydraulic Actuator. *The Eight Scandinavian International Conference on Fluid Power (SICFP'03)*, May 7-9, Tampere, Finland.

Helduser, S.; Bonefeld, R. (2001). Active Damping in Civil Engineering Using Hydraulic Actuators. *Proceedings of the Fifth International Conference on Fluid Power Transmission and Control*, Hangzhou, China, pp. 259-263.

Hill, F. J. and Peterson, G. R. (1968). *Introduction to Switching Theory and Logical design*. John Wiley &Sons, Inc., New York, USA.

Hlavicka, J. and Fiser, P. (2001). BOOM – a Heuristic Boolean Minimizer. *IEEE/ACM International Conference on Computer-Aided Design (ICCAD –01)*. November 4-8, San Jose, CA, USA.

Hong, S., Cain, R. and Ostapko, D. (1974). MINI: A Heuristic Approach for Logic Minimization. *IBM Jour. R&D*, Vol. 18, No. 5, pp. 443-458.

Hong, S., Muroga, S. (1991). Absolute Minimization of Completely Switching Functions, *IEEE Trans. on Comp.*, Vol. 40, pp. 53-65.

Honkanen, T. (2004). *Modelling Industrial Maintenance Systems and the Effects of Automatic Condition Monitoring*. Helsinki University of Technology, Helsinki, Finland. (Doctoral thesis).

Huuskonen, P. J. (1997). *Model-base explanation of plant knowledge*. Technical Research Centre of Finland, VTT Publications 308, Espoo. (Doctoral thesis).

Huuskonen, P., Kaarela, K., Okkonen, J. and Vaisanen, *A*. (1995). Explaining Control Logic to Process Operators. *8th Conf. On Industrial & Engineering Applications of AI & Expert Systems*, Melbourne, Australia.

Idhammar, C. (1997). Less Time for Maintenance. *Pulp & Paper*, Vol. 71, Issue 2.

Isermann, R. and Balle, P. (1997). Trends in the Application of Model-Based Fault Detection and Diagnosis of Technical Process. *Control Eng. Practice*, Vol. 5, No. 5, pp. 709-719.

Jacobs, O. (1974), *Introduction to Control Theory*, Clarendon Press, New York, NY, USA.

Jalili, N. and Knowles, D. (2004). Structural Vibration Control Using an Active Resonator Absorber: Modelling and Control Implementation. *Smart Materials and Structures*, Vol. 13, pp. 998-1005.

Jokio, M. (editor). (1999). Papermaking, Part 3: Finishing. *Papermaking Science and Technology Series*, Fabet Oy, Helsinki, Finland.

Jorkama, M. (1996). *On the Winder Vibration Analysis*. Helsinki University of Technology, Espoo, Finland (Licentiate's Thesis).

Jorkama, M. (2001). *Contact Mechanical Model for Winding Nip*. Acta Polytechnica Scandinavica, Mechanical Engineering Series No. 146, Espoo, Finland. (Doctoral thesis).

Kaistinen, S. (2001). *Automated database configuration for winder's diagnostics*. Helsinki University of Technology, Espoo, Finland. (Master's Thesis).

Kajaste, J., Kauranne, H., Ellman, A. and Pietola, M. (2005). Experimental Validation of Different Models for Effective Bulk Modulus of Hydraulic Oil. *9th International Conference on Fluid Power SICFP'05*, June 1-3, Linköping, Sweden.

Karnaugh, M. (1953). The Map Method for Synthesis of Combinational Logic Circuits. *Trans. AIEE*, Vol. 72, pp. 593-598.

Keskinen, E.K., Saarinen, H. and Tuokko R.O. (1993). Mechanics of Seal Friction with Special Reference to Hydraulic Cylinder Applications. *The Third Scandinavian International Conference on Fluid Power*, May 25-26, Linköping, Sweden.

Kitching, K. J., Cole, D. J., Cebon, D. (2000). Performance of a Semi-Active Damper for Heavy Vehicles. *Journal of Dynamic Systems, Measurement, and Control*, Vol. 122, Issue 3, pp. 498-506.

Kuhmonen, M. (1997). *The Effect of Operational Disturbances on Reliability and Operation Time Distribution of NC-machine Tools in FMS*. Research Papers 59, Lappeenranta University of Technology, Lappeenranta, Finland. (Doctoral thesis).

Leask, A. (1987). *Pulp and Paper Manufacture. Mechanical Pulping, Volume 2.,* Published by The Joint Textbook Committee of the Paper Industry, Third Edition, Tappi, CPPA, Atlanta, USA.

Lehtinen, E. (editor) (2000). Pigment Coating and Surface Sizing of Paper. *Papermaking Science and Technology Series*, Fabet Oy, Helsinki, Finland.

McCluskey, E. (1959). Minimization of Boolean Functions. *Bell System Technical Journal*, Vol. 35, pp.1417-1444.

McGeer, P., Sanghavi, R., Brayton, R. and Sangiovanni-Vincentelli, A. (1993). ESPRESSO SIGNATURE: A new Exact Minimizer for Logic Functions, *IEEE Trans on VLSI*, Vol. 1-4, pp.432-440.

McMullen, C. and Shearer, J. (1986). Prime Implicants, Minimum Covers, and the Complexity of Logic Simplification. *IEEE Transactions on Computers*, Vol. 35, pp. 761-762.

Merrit, H. E. (1967). *Hydraulic Control Systems*. John Wiley & Sons, Inc., New York, USA.

Mohamed, S., Perkowski, M. and Jozwiak, L. (1997). Fast Minimization of Multi-Output Boolean Functions in Sum-Of-Condition-Decoders Structures. *Proceedings of the 23rd EUROMICRO Conference*, September 1-4, Budapest, Hungary.

Nam, G., Aloul, F., Sakallah, K. A. and Rutenbar, R. A. (2004). A Comparative Study of Two Boolean Formulations of FPGA Detailed Routing Constraints. *IEEE Transactions on Computers*, Vol. 53, No. 6, pp. 688-696..

Nevalainen, S. J. (1988). *Minimization of Boolean sum of products with applications to the computation of reliability of general networks*. Technical Research Centre of Finland, Espoo, Finland. (Doctoral thesis).

Norvelle, F. D. (2000). *Electrohydraulic Control Systems*. Prentice Hall, New Jersey, USA.

Nyberg, M. (1999). *Model Based Fault Diagnosis, Methods, Theory, and Automotive Engine Applications*. Linköping Studies in Science and Technology, No. 591, Sweden. (Doctoral thesis).

Nykänen, T., Esque, S. and Ellman, A. (2000). Comparison of Different Fluid Models. *Bath Workshop on Power Transmission and Motion Control PTMC'00*, September 13-15, Bath, UK.

Ogava, K., Ide, T. and Saitou, T. (1997). Application of Impact Mass Damper to a Cable-Stayed Bridge Pylon. *Journal of Wind Engineering and Industrial Aerodynamics*, Vol. 72, No 1-3, pp. 301-312.

Olgac, N. and Holm-Hansen, B. (1995). Design Considerations for Delayed-Resonator Vibration Absorbers. *Journal of Engineering Mechanics*, Vol. 121, No. 1, pp. 80-89

Olgac, N. and Jalili, N. (1998). Modal Analysis of Flexible Beams with Delayed Resonator Vibration Absorber: Theory and Experiments. *Journal of Sound and Vibration*, Vol. 218, No. 2, pp. 307-331.

Olsson, H., Åström K.J., Canudas de Wit C., Gäfvert M. and Lischinsky P., Friction Models and Friction Compensation. *European Journal of Control*, Dec. 1998, No.4, pp.176-195.

Paanasalo, J. (2005), *Modelling and Control of Printing Paper Surface Winding*, Control Engineering Laboratory report 146, Helsinki University of Technology. (Doctoral thesis).

Parr, A. (1997). Fault Diagnosis - a Users View. *IEE Colloquium on Fault Diagnosis in Process Systems*.

Paunonen, H. (1997). *Roles of Informating Process Control Systems*. Publication 225, Tampere University of Technology, Tampere, Finland. (Doctoral thesis).

Perkowski, M., Csanky, L., Sarabi, A. and Schäfer, I. (1992). Fast Minimization of Mixed-Polarity AND/XOR Canonical Networks. *IEEE International Conference on Computer Design: VLSI in Computer & Processors, (ICCD '92)*, October 11-14, Cambridge, MA, USA.

Plomp, J. (1997). Logic Explanation to Process Operators. *Final report of LEPO project*. VTT Electronics, Oulu, Finland.

Plomp, J., Huuskonen, P., Malm, E. and Paanasalo, J. (1996). An Object-Oriented Approach to PLC Explanation. *SteP '96*, Vaasa, Finland.

Quine, W. (1952). The Problem of simplifying Truth Functions. *Am. Math. Month.*, Vol. 59, pp. 521-531.

Rivin, E.I. (1987). *Mechanical Design of Robots*. McGraw-Hill Book Company, USA

Roberts, J.C. (1991). *Paper Chemistry*. Chapman and Hall, New York, USA.

Rollo, M., Novak, P., Kubalík, J. and Pěchouček, M. (2004). Alarm Root Cause Detection System. *Emerging Solutions for Future Manufacturing Systems*, USA, Springer, Vol. 1.

Rudell, R. and Sangiovanni-Vincentelli, A. (1987). Multiple Valued Minimization for PLA Optimization. *IEEE Transactions on Computer-Aided Design of Integrated Circuits and Systems*, Vol. 6, No. 5, pp. 727-750.

Seong, P.H. and Kim, J.H. (2000). A Methodology for the Quantitative Evaluation of NPP Fault Diagnostic Systems' Dynamic Aspects. *Annals of Nuclear Energy*, Vol. 27, pp. 1459-1481.

Simani, S., Fantuzzi, C. and Patton, R. (2003). *Model-Based Fault Diagnosis in Dynamic Systems Using Identification Techniques*, Springer, London, Great Britain.

Sloan, H., Szörenyi, B. and Turan, G. (2005). On k-term DNF with the Largest Number of Prime Implicants. *Electronic Colloquium on Computational Complexity*, Vol. 12, 23rd Report.

Smook, G.A. (1992). *Handbook for Pulp and Paper Technologists*. Agnus Wilde Publications Inc., Vancouver, Canada.

Sorsa T., Koivo H. N. and Koivisto H. (1991). Neural Networks in Process Fault Diagnosis. *IEEE Transactions on Systems, Man and Cybernetics*, Vol. 21, No. 4, pp. 815-825.

Thorp, B.A. (1991). *Pulp and Paper Manufacture. Paper Machine Operations. Volume 7*. Published by The Joint Textbook Committee of the Paper Industry, Third Edition, Tappi, CPPA, Atlanta, USA.

Tonyan, M. J. (1985). *Electronically Controlled Proportional Valves*. Rexroth Worldwide Hydraulics, Marcel Dekker Inc., New York, USA.

Whitesitt, J.E. (1961). *Boolean algebra and its applications*. Addison-Wesley, Reading, MA, USA.

Wiatrowski, C., House C. (1984). *Logic Circuits and Microcomputer Systems*. McGraw-Hill, New York, NY, USA.

Virtanen, T. (2004). Logic Code Transformation and Minimization Algorithm for Fault Diagnostic Systems. *IEEE International Conference on Mechatronics 2004 (ICM '04)*. Proceedings of the IEEE International Conference, June 3-5, Istanbul, Turkey.

Virtanen, T. and Paanasalo, J. (2000). Fault Diagnosis of Paper Winders. *2000 TAPPI PCE & I ISA-PUPID 39th Annual Symposium*, March 26-30, Williamsburg, VA, USA.

Yuwono, B. and Lee, D. (1996). Search and Ranking Algorithms for Locating Resources on the World Wide Web. *Proceedings of the 1996 IEEE 12th International Conference on Data Engineering*, February 26 - March 01, New Orleans, LA, USA.

Åström, K. J., Hägglund, T. (1995). *PID Controllers: Theory, Design, and Tuning*. Instrument Society of America, USA.

Appendix 1

Results of the questionnaire study introduced in Section 3.1.3.

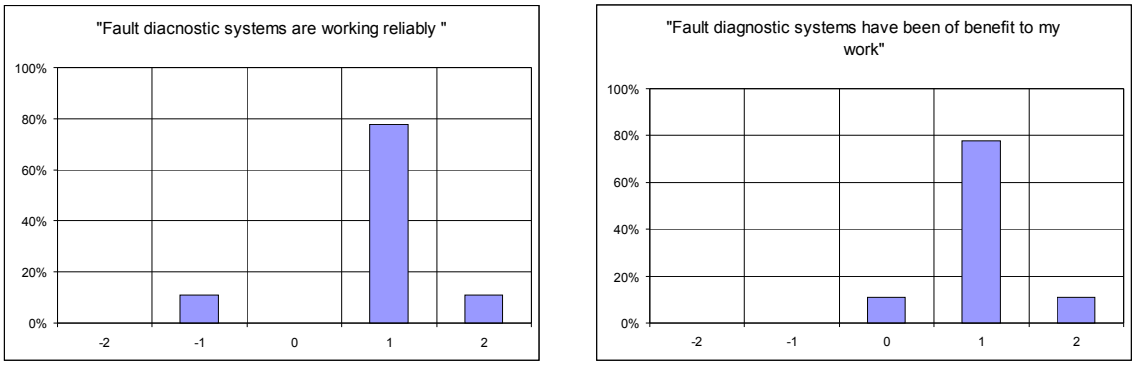

Figure A 1: Statements concerning the usefulness and reliability of fault diagnostic systems.

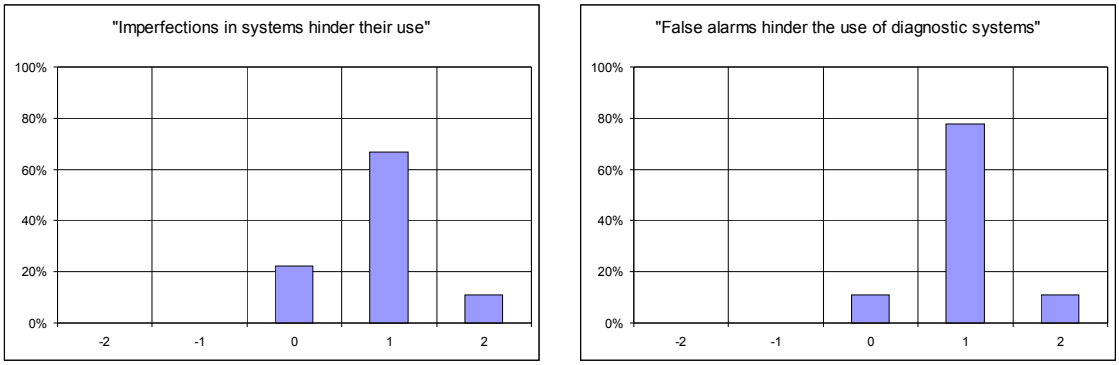

Figure A 2: Influence of false alarms on the usability of systems.

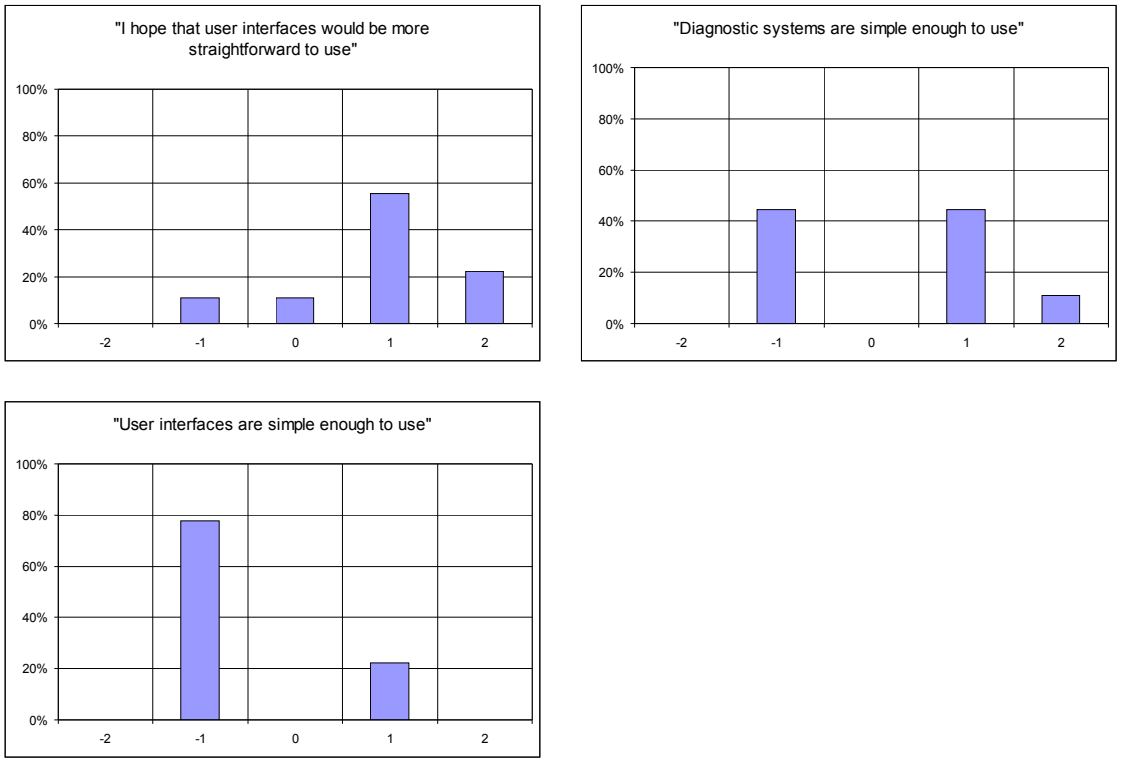

Figure A 3: Simplicity and usability of diagnostic systems and their user interfaces.

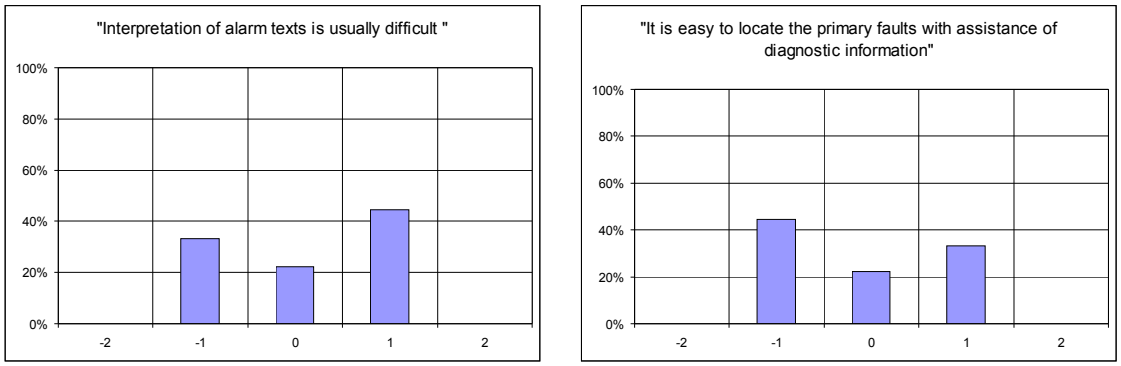

Figure A 4: Quality of information given by fault diagnostic systems.

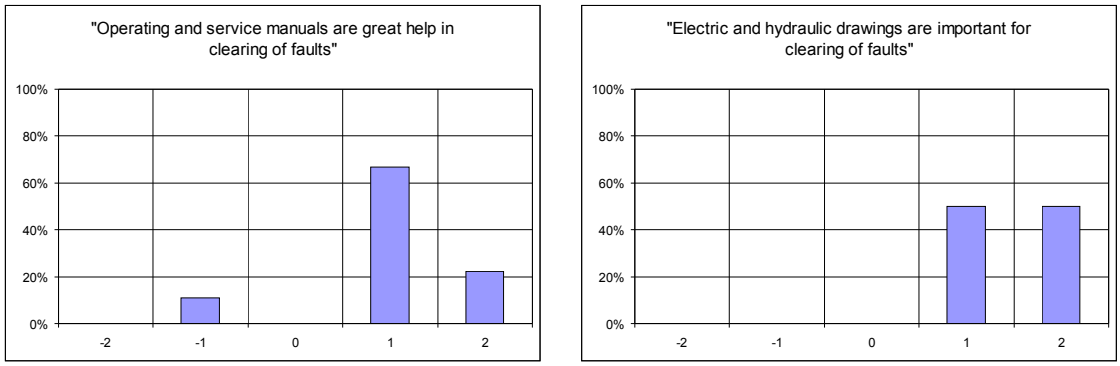

Figure A 5: Importance of written material.

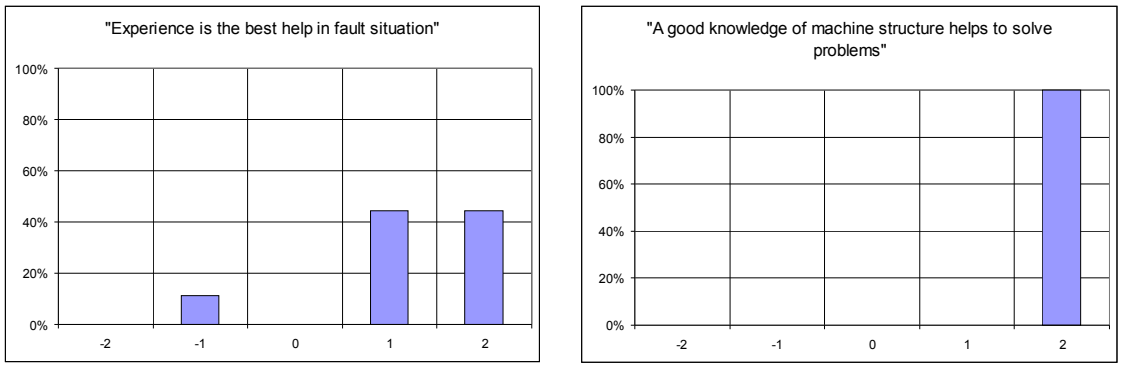

Figure A 6: Importance of experience and good knowledge of machine.

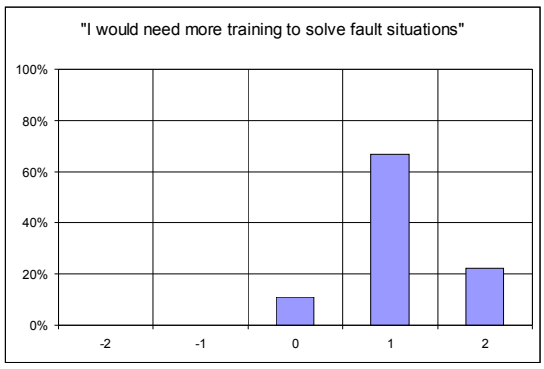

Figure A 7: Need for training.

Appendix 2

Table A 1: Basic laws of Boolean algebra.

BOOLEAN IDENTITIES	
Complement Laws	
A*~A = 0	A+~A = 1
Law of double complement	
~(~A) = A	
Idempotent laws	
A*A = A	A+A = A
Identity laws	
A*1 = A	A+0 = A
Dominance laws	
A*0 = 0	A+1 = 1
Commutative laws	
A*B = B*A	A+B = B+A
Associative laws	
A*(B*C) = (A*B)*C	A+(B+C) = (A+B)+C
Distributive laws	
A*(B+C) = (A*B)+(A*C)	A+(B*C) = (A+B)*(A+C)
DeMorgan's laws	
~(A+B) = ~A*~B	~(A*B) = ~A+~B
Absorption laws	
A*(A+B) = A	A+(A*B) = A

Table A 2: Other Boolean identities (Wiatrowski, 1984).

OTHER IDENTITIES	
(A*~B)+B = A+B	(A+~B)*B = A*B
(A+B)*(~A+C)*(B+C) = (A+B)*(~A+C)	A*B+~A*C+B*C = A*B+~A*C

Appendix 3

This appendix contains Boolean function test cases used in Chapter 3.

Case 1

This test case is designed to study minimization of the Boolean function where the same literals appear in different places in the function.

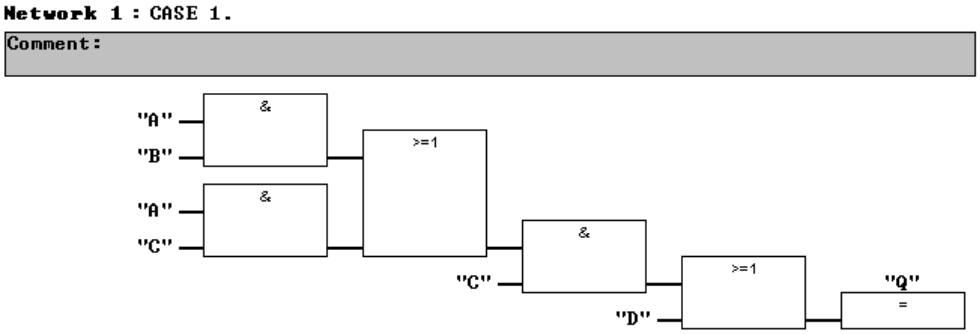

Figure A.8: FBD format representation for test case 1.

Table A.3: Truth table (maxterms) of case 1.

A	B	C	D	Q=D+(C(AB+AC))
0	0	0	0	0
0	0	1	0	0
0	1	0	0	0
0	1	1	0	0
1	0	0	0	0
1	1	0	0	0

Case 2

This test case is designed to study the minimization of the Boolean function with the same, but inverted, literals in different terms.

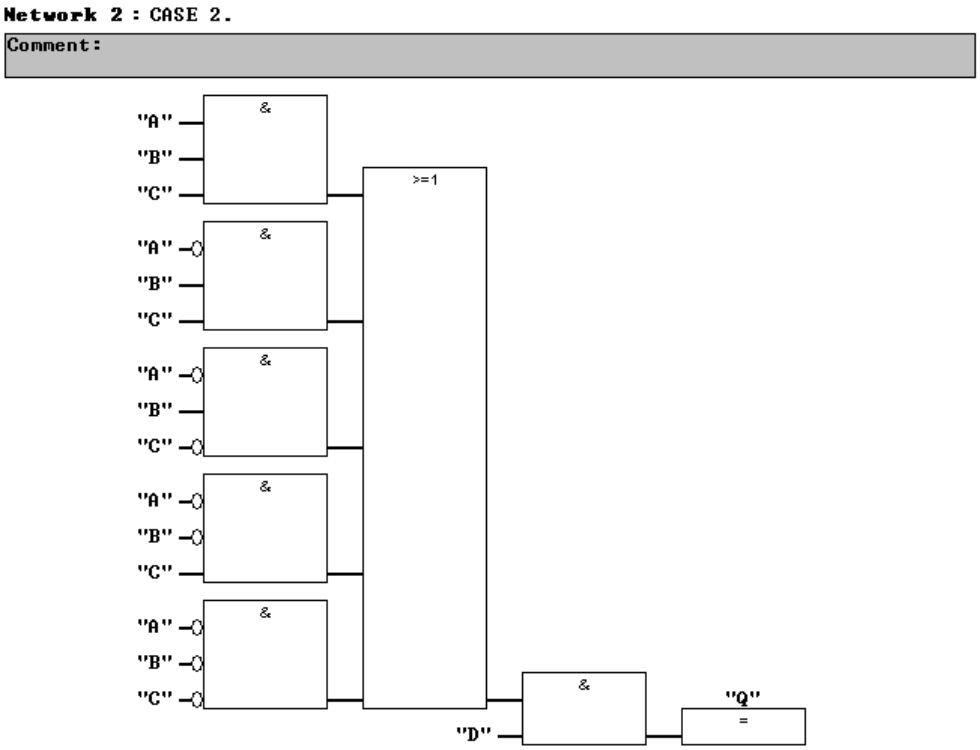

Figure A.9: FBD format representation for test case 2.

Table A.4: Truth table (maxterms) of case 2.

A	B	C	D	Q=D(ABC+~ABC+~AB~C+~A~BC+~A~B~C)
0	0	0	0	0
0	0	1	0	0
0	1	0	0	0
0	1	1	0	0
1	0	0	0	0
1	0	0	1	0
1	0	1	0	0
1	0	1	1	0
1	1	0	0	0
1	1	0	1	0
1	1	1	0	0

Case 3

This test case is designed to study the minimization of the Boolean function where there are near-similar terms in different branches.

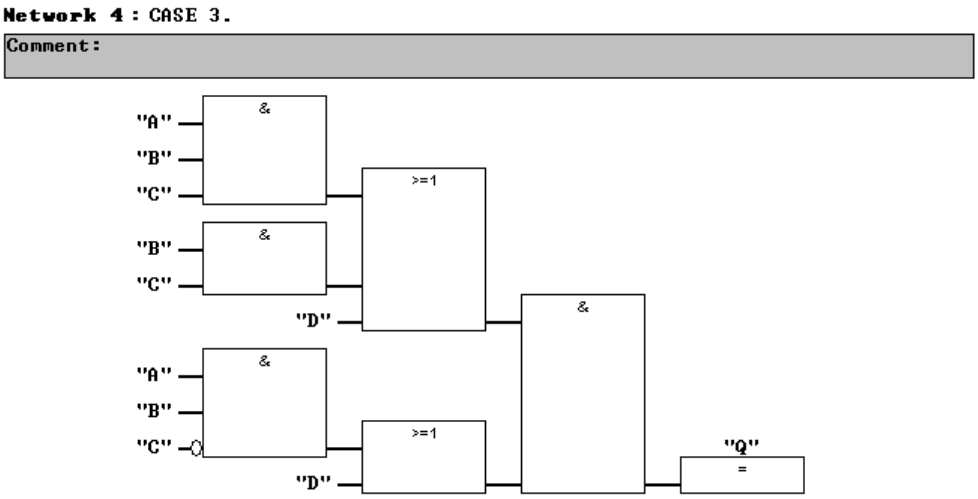

Figure A.10: FBD format representation for test case 3.

Table A.5: Truth table (maxterms) of case 3.

A	B	C	D	Q=(D+AB~C)(D+BC+ABC)
0	0	0	0	0
0	0	1	0	0
0	1	0	0	0
0	1	1	0	0
1	0	0	0	0
1	0	1	0	0
1	1	0	0	0
1	1	1	0	0

Case 4

This test case is designed to study the minimization of the Boolean function that includes the term A*B+~A*C+B*C (see table A3-2).

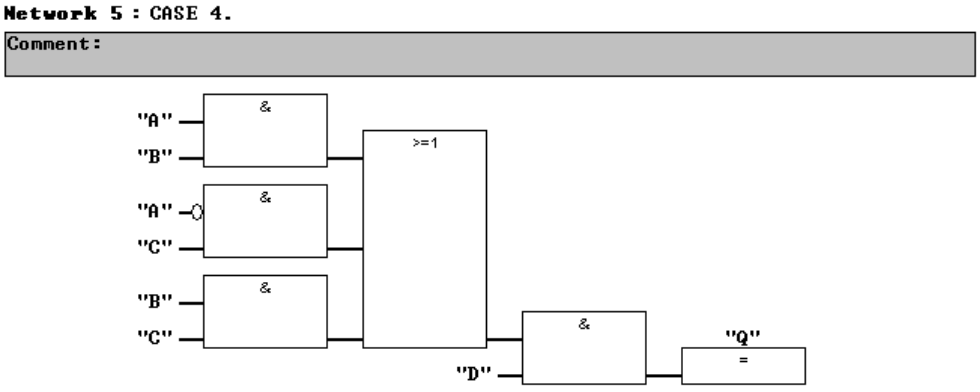

Figure A.11: FBD format representation for test case 4.

Table A.6: Truth table (maxterms) of case 4.

A	B	C	D	O=D(BC+~AC+AB)
0	0	0	0	0
0	0	0	1	0
0	0	1	0	0
0	1	0	0	0
0	1	0	1	0
0	1	1	0	0
1	0	0	0	0
1	0	0	1	0
1	0	1	0	0
1	0	1	1	0
1	1	0	0	0
1	1	1	0	0

Case 5

This test case is designed to study the minimization of the Boolean function that includes the term (A*~B)+B (see Table A 2 in Appendix 2).

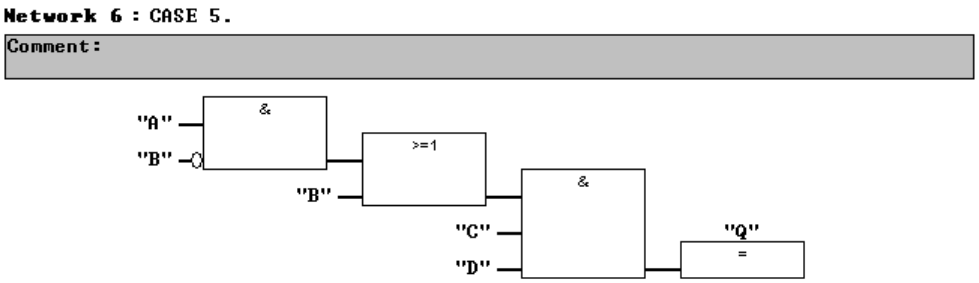

Figure A.12: FBD format representation for test case 5.

Table A.7: Truth table (maxterms) of case 5.

A	B	C	D	Q=DC(B+(A~B))
0	0	0	0	0
0	0	0	1	0
0	0	1	0	0
0	0	1	1	0
0	1	0	0	0
0	1	0	1	0
0	1	1	0	0
1	0	0	0	0
1	0	0	1	0
1	0	1	0	0
1	1	0	0	0
1	1	0	1	0
1	1	1	0	0

Appendix 4

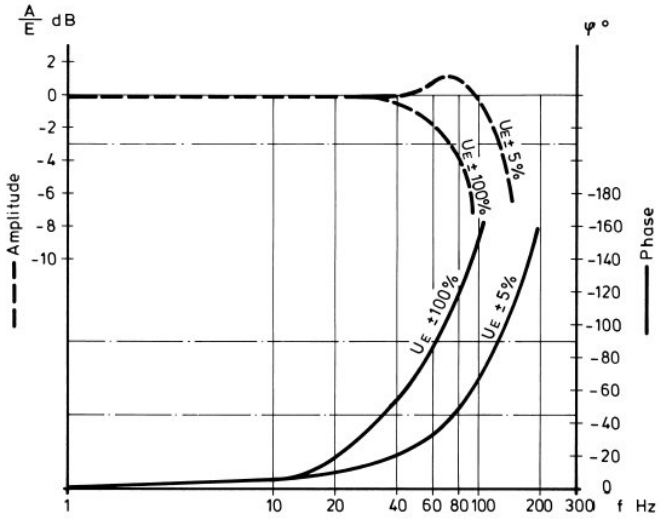

Figure A 13: Manufacture's datasheet of a hydraulic valve (Bosch).

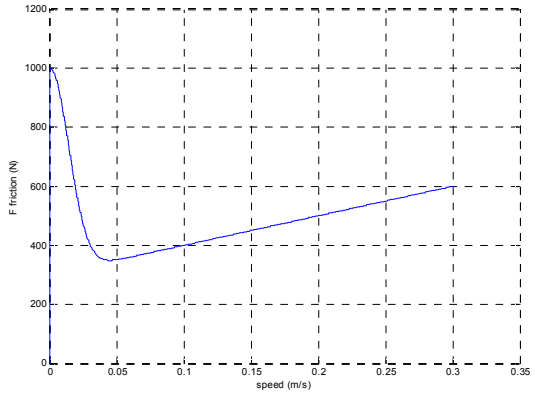

Figure A 14: A friction force of a hydraulic cylinder.

HELSINKI UNIVERSITY OF TECHNOLOGY CONTROL ENGINEERING LABORATORY

Editor: H. Koivo

Report 137 Hasu, V.
Adaptive Beamforming and Power Control in Wireless Communication Systems. August 2003.

Report 138 Haavisto, O., Hyötyniemi, H.
Simulation Tool of a Biped Walking Robot Model. March 2004.

Report 139 Halmevaara, K., Hyötyniemi, H.
Process Performance Optimization Using Iterative Regression Tuning. April 2004.

Report 140 Viitamäki, P.
Hybrid Modeling of Paper Machine Grade Changes. May 2004.

Report 141 Pöyhönen, S.
Support Vector Machine Based Classification in Condition Monitoring of Induction Motors. June 2004.

Report 142 Elmusrati, M. S.
Radio Resource Scheduling and Smart Antennas in Cellular CDMA Communication Systems. August 2004.

Report 143 Tenno, A.
Modelling and Evaluation of Valve-Regulated Lead-Acid Batteries. September 2004.

Report 144 Hyötyniemi, H.
Hebbian Neuron Grids: System Theoretic Approach. September 2004.

Report 145 Hyötyniemi, H. (ed.)
Complex Systems: Science at the Edge of Chaos - Collected papers of the Spring 2003 postgraduate seminar. October 2004.

Report 146 Paanasalo, J.
Modelling and Control of Printing Paper Surface Winding. June 2005.

Report 147 Mohamed, F.
Microgrid Modelling and Simulation. March 2006.

Report 148 Mäenpää, T.
Robust Model Predictive Control for Cross-Directional Processes. May 2006.

Report 149 Kantola, K.
Modelling, Estimation and Control of Electroless Nickel Plating Process of Printed Circuit Board Manufacturing. March 2006.

Report 150 Virtanen, T.
Fault Diagnostics and Vibration Control of Paper Winders. June 2006.

ISBN-13 978-951-22-8467-2

ISBN-10 951-22-8467-7

ISSN 0356-0872

Picaset Oy, Helsinki 2006